THE EFFECT OF FRAGMENTATION ON THE ENGINEERING PROPERTIES OF GRANULAR MATERIALS: LABORATORY AND FRACTAL ANALYSES

by

Zamri Chik

BS, University of Aberdeen, 1983

MS, University of Pittsburgh, 1993

Submitted to the Graduate Faculty of

the School of Engineering in partial fulfillment

of the requirements for the degree of

Doctor of Philosophy

University of Pittsburgh

2004

UNIVERSITY OF PITTSBURGH

SCHOOL OF ENGINEERING

This dissertation was presented

by

Zamri Chik

It was defended on

April 16, 2004

and approved by

Jeen-Shang Lin, Ph.D., Associate Professor, Civil and Environmental Engineering

Tin K. Hung, Ph.D., Professor, Civil and Environmental Engineering

Ian Nettleship, Ph.D., Associate Professor, Materials Science and Engineering

Luis E. Vallejo, Ph.D., Associate Professor, Civil and Environmental Engineering
Dissertation Director

THE EFFECT OF FRAGMENTATION ON THE ENGINEERING PROPERTIES OF GRANULAR MATERIALS; LABORATORY AND FRACTAL ANALYSES

Zamri Chik, Ph.D.

University of Pittsburgh, 2004

Granular materials forming part of engineering structures such as rockfill dams, embankments, the base of flexible pavements and foundations are constantly subjected to harsh environmental conditions and external forces including static and dynamic loads. As a result, these materials experience various levels of fragmentation.

In this study, the levels of fragmentation were analyzed from particle/grain size distribution (PSD) plots before and after fragmentation as well as the fractal dimension concept from fractal theory. The fractal dimension concept was found to evaluate well the fragmentation induced in specimens of sands, gravels and glass beads.

Tests on abrasion as a result of peripheral fragmentation of gravels (5.5 mm.) were produced in the laboratory using the Jar mill apparatus. Applying the area-perimeter method of fractal analysis, it was found that as the profile of the particles becomes more rounded the fractal dimension reduces in value.

Total fragmentation and crushing of granular specimens induced in test apparatus such as the Bromhead Ring Shear, Universal Testing machine and Standard Proctor produces the PSD that evolves from a uniform to a well-graded condition. As a result, the fragmentation fractal dimension increases.

Changes in the engineering properties such as the elastic moduli, hydraulic conductivity and the shear strength were also studied. Tests on the elastic moduli of the fragmented gravels using an ultrasonic velocity Pundit apparatus indicated an increase in the elastic moduli as the levels of fragmentation were increased. Hydraulic conductivity tests indicated that the permeability of the samples decreased as the levels of fragmentation increased. Shearing of Quartz sand (1.6 mm.) in the Ring Shear apparatus indicated a decrease in the angle of internal friction as the fragmentation was increased.

An investigation on the angle of repose of binary mixtures of coarse and fine materials on a smooth glass base as compared to that on rough surface porous stone base was also conducted. A theoretical relationship between the angle of repose, the angle of internal friction and the interface basal friction was developed. It was found that the different compositions of the binary mixture and the basal friction significantly influenced the angle of repose.

TABLE OF CONTENTS

Page

LIST OF TABLES

Page

LIST OF FIGURES

Page

PREFACE

The study presented herein was performed under the supervision of Professor Luis E. Vallejo whom I was very fortunate and honored to be working with. For his gifts of overwhelming support, impeccable logic and knowledgeable direction, I am perpetually indebted. I would like to express my gratitude to Dr. Ian Nettleship for his keen support and for the provision of material science laboratory facilities necessary in the research project.

I would like to thank Dr. Jeen-Shang Lin and Professor Tin K. Hung for serving on my Ph.D. committee and for their valuable comments that has resulted in considerable improvement of the quality of the work.

To the others who have been constantly supportive especially in my laboratory works, they include Dan Urban, my colleagues Sebastian Loboguerrero and Luis Vesga, I thank you for your kind assistance.

I would like to dedicate this dissertation to my wife Rohana Katan for her sacrifices and help, to my children Azra-Elia, Fariq-Aqim, Azra-Eshreen, Heiqal-Aqim and Izet-Aqim and to the loving memory of my parents.

1.0 INTRODUCTION

1.1 BACKGROUND OF THE STUDY

Through natural processes such as physical and chemical weathering large rocks disintegrate into smaller sized granular materials. When the entire physical representation is completely altered from the initial outlook, a set of new conditions is in place in order to solve the problem in hand. Soils are continuously worked on in all engineering construction projects. As they are constantly subjected to increasingly greater loads in the field, the process of disintegration is accelerated as the larger sized rocks are crushed into smaller elements.

Particle crushing involving particles communition, has been a subject of common interest in various fields of engineering in the recent years. In conjunction with the popular construction concept of rock fills in dams and embankments in the sixties and seventies, a number of studies have been carried out to investigate the strength characteristics of rock particles in contact to each other in the fills[(1)].

It is said that even the hardest rock suffers considerable crushing. Terzaghi[(2)] showed that this phenomenon occurred at the points of contact of large pieces of rocks in a dumped rockfill causing substantial settlement. Rocks samples with irregular shapes as well as those with

[(1)] Numeric references placed superior to the line of text refer to the bibliography.

machine–shaped points were tested in the laboratory by Clements[3]. The included-angles of the points were measured and the loads at which crushing damage took place were observed as illustrated in Figure 1.

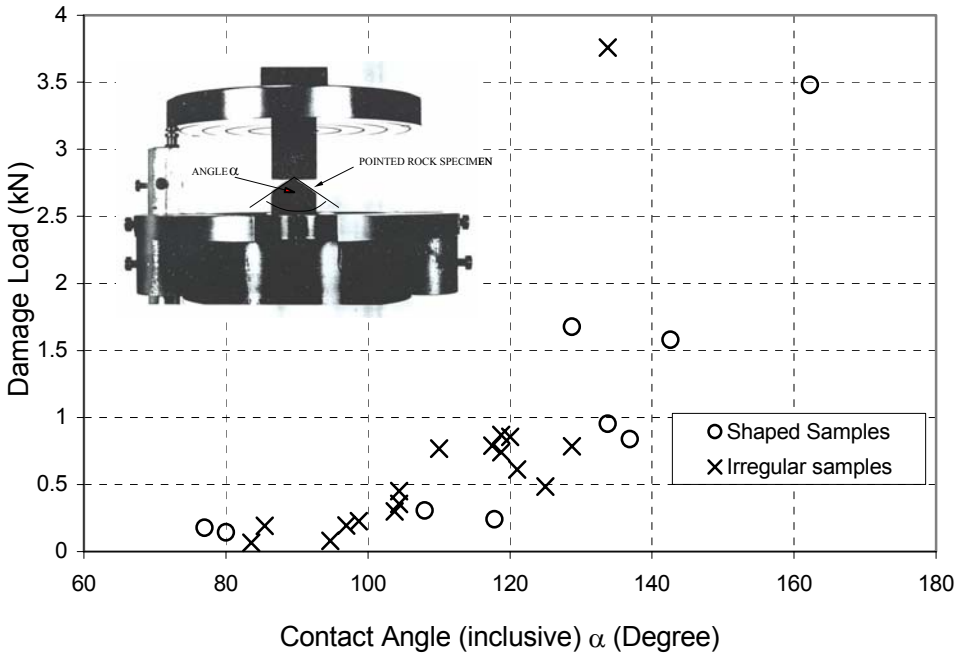

Figure 1 Damage Load versus Contact Angle α (Clements)[3]

The load at which fragmentation first occurs is of particular interest, because it amounts to failure at the contacts of adjacent rock particles causing deformation settlement. It is interesting to note from Figure 1 that fragmentation takes place almost immediately at every instance as the contact points are generally crushed at amazingly low loads. The behavior of the soils within the working condition should be carefully studied with respect to the crushing event due to the fact that this may very well alter the basic geo-materials response to load. And when crushing occurs the common experience with granular materials such as the effects of angularity, density, grain size etc. need not be valid and hence, needs reexamination[4].

1.1.1 Problem Statement

Much of part of the world where man chooses to live is covered by fine-grained soils, however these do not always form the desired fill. With the advancements in the arts and science of soil mechanics almost all fills can be used with considerable success given the appropriate technology and construction method. However, because it is more costly to install drainage layers in a wet clayey fill, importing granular fill may be the better option. The final choice in most cases is dependent on the issue of cost.

Many natural slopes and rockfill structures are made of a mixture of rock fragments and sand-sized particles[5]. Although historically the use of stones and other granular materials in an engineering structure has been more common, a great deal has been written about problems encountered in the use of clayey materials than in granular materials[6].

However, it is acknowledged that there have been serious problems related by geotechnical engineers in their numerous encounters with granular materials. For example, calcareous sands were said to complicate even site investigation and laboratory testing procedures due to their brittle and crushable nature[7]. We have also described earlier that whenever in particle-to-particle contact, crushing will occur in even the hardest material. Figure 2 shows a typical soil profile found in many parts of the world.

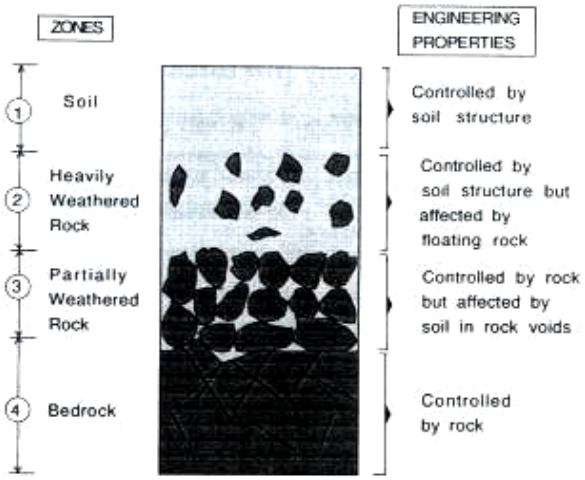

Figure 2 Rock- Soil Mixtures Resulting From Weathering[8]

The diagram shows particle breakage and fragmentation that is occurring in a natural environment. It is suggested that the strength and stress-strain behavior of an element of soil is greatly affected by the degree to which crushing or particle breakage takes place during loading and deformation[9]. Marsal further stated that the most important factor affecting both shear strength and compressibility is the phenomenon of fragmentation undergone by a granular body when subjected to changes in its state of stresses both during the uniform compression stage and during deviator load application[10].

Although fragmentation and crushing of granular materials are common phenomena in many engineering activities and engineering structures, there have been limited studies in particular in the civil engineering discipline on what effect these may have on the engineering properties of the construction materials after they were fragmented or crushed and hence the effects they have on the construction design of an engineering project as a whole. On the same

note with regard to fragmentation of granular materials, it was also observed that, failures involving steep slopes often leads to crushing and spreading of the failed material upon impacting the toe of the slopes. As this particular phenomenon and potent behavior of crushing increases the risk of destruction to properties and livelihood, therefore it is also important to investigate the factors that influence this type of geotechnical failures.

Granular materials forming not only part of the designed structural members of civil engineering structures such as highway embankments, rockfill dams and the base of flexible pavements and foundations, but also together constituted a crucial drainage component in numerous geotechnical engineering projects. Other structural members such as sand drains and stone columns experienced crushing when and as they are subjected to static and dynamic loads.

Because of sustained crushing, the initial engineering properties such as the hydraulic conductivity, shear strength and elastic modulus, by which a structure was designed for will change during its engineering life. There are numerous engineering structures that had failed to outlast their engineering life with the expected performance, and indeed the change in the original engineering properties of some, might have contributed to their instability and caused eventual weaknesses in the structures.

It is only natural therefore to carryout exploratory investigations on the fragmentation phenomenon of granular materials because there is obviously a need to a better understanding of the behavior of this most abundantly used type of construction material and to provide more information on the evolution of fragmentation and crushing for the benefit of improving the design of related engineering structures.

1.2 LITERATURE REVIEW

In many engineering structures such as rockfill dams, highway embankment, the base of pavements and foundations and in other soil stabilization systems, granular materials can be found to form a contiguous as well as a permanent part within the overall structural system.

When subjected to static or dynamic loads materials are stressed, and at stresses reaching to a critical point, particle breakage occurs. Virtually in all soils tested above normal geotechnical pressures and for some even under low pressures breakage takes place[4, 11]. In fact, particle breakage or crushing seems to be a general feature observed in all granular materials [12].

1.2.1 Factors Contributing to Crushing

Grain angularity, grain size, uniformity of gradation, low particle strength, high porosity and the stress level and anisotropy are found to influence the extent of crushing in the grains[13]. However, it is observed that one of the most important factors influencing the crushing of a mass of granular materials is the crushing-resistance property of the grains[12].

From previous works, it was found that the magnitude of the load leading to crushing in granular medium is illustrated from the examples as follows; coarse granitic sand particles with an average diameter of 2.8mm experienced breakage at pressures equal to 2 MPa while calcareous shells begin to crush at 0.5 to 0.2 MPa[12, 13] and under ordinary pressures (about 0.98MPa), angular particles of freshly quarried materials undergo fragmentation due to breakdown of sharp angularities[14].

When a granular mass is subjected to a compressive load, the particles resist the load through a series of contacts between the grains[15, 16]. Some particles that may have more contacts than the others therefore carry greater load and thus implying that the particles do not share equally in the bearing of the applied load. These highly loaded contacts are also usually aligned in chains[17, 18] and as such, as in the illustration in Figure 3, the mechanical equilibrium of the packing may not rely on every one particle present but rather on part of those that fall within the band of the chains.

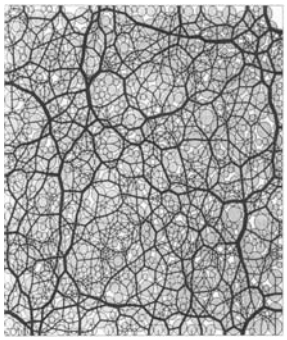

Figure 3 Force Chains in 2-Dimensional Static Assembly of Discs in a Horizontal Container with Three Fixed Walls and One piston, on which a Fixed Vertical Force is Applied[18]

1.2.2 Mechanics of Crushing

Fragmentation and crushing begins when highly loaded particles stressed to a critical point fail and break into smaller pieces. As some these broken pieces displace and move into the voids of the original material, the force chains in the particle assemblage change in their intensity and direction. When more crushing takes place the amount of finer particles increases and the curve of the grain size distribution becomes gentler indicating a departure from a poorly graded condition to a better graded mixture. It was suggested that the extent of crushing could suitably be measured by carrying out the grain size distribution tests on the materials[9, 11].

(a) Physical changes of crushed packing: With increasing finer materials content, the volume of the voids consequently decreases and making the soil less permeable. The broken materials are more difficult to be crushed further and the soil becomes increasingly more resistant to crushing. When a uniform granular material is crushed the resulting particle/grain size distribution approaches that of a well-graded soil for very large compressive loads[11]. The number of broken grains will be a function of the level of compressive force acting on the granular assembly. The larger this compressive force the larger will be the number of broken grains.

Crushing induced granular material, such as in the unbound granular base under an asphalt pavement, causes a decrease in volume of the original assembly. A settlement can be detected if the material is laterally confined. This settlement varies according to the level of crushing and the type of breakage that has taken place. The compressive force acting on the small broken pieces that are produced aids their migration inside the granular mass. If the breakage produces multiple small pieces that are small enough to migrate to the adjacent voids then the decrease in volume of the material packing will be substantial. However, if the breakage consists a few broken pieces large enough to replace the space of the original particles than the reduction in the volume the will be insignificant.

It was established that the grain size distribution of a granular assembly that had been crushed under large comprehensive loads was a fractal distribution[19]. Depending on the magnitude of the compressive load applied to it, the granular structure will experience gradual changes in particle sizes before it reaches a well graded or a fractal particle size distribution. A well-graded particle distribution or, particles with a fractal distribution represent a granular

structure that is made of grains of all sizes including the original unbroken grains. According to Lade et. al.[11] these original large grains did not break because with more small size particles surrounding them the average contact stress acting on these large grains tends to decrease. It was also suggested that the amount of crushing produced by a given breakage effective stress may be expected to decrease with increasing particle concentration because the contact forces will be reduced by increased concentration.

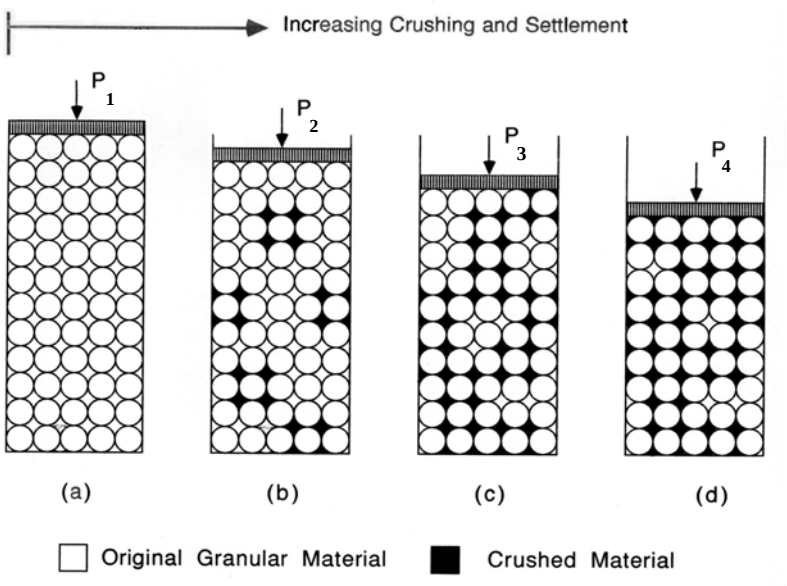

Figure 4 Evolution of Crushing in a Confined Granular Material under Compression

(b) Crushing process in a laterally confined assembly: A simplified representation of crushing process of a granular assembly subjected to a vertical load P_i similar to those experienced by the granular base under an asphalt pavement shown in Figure 4 illustrates the evolution of the crushing in four stages[20]. Discs stacked in a cubical arrangement as in Figure 4(a) represents the original loose unbroken granular particles packing. Small isolated dense zones of broken

particles were then formed as a few particles started to break under low compressive loads. As shown in Figure 4(b), the amount of voids that is filled constitutes 31% of the total volume of the voids.

As more particles are crushed under increasing loads, the number of pockets of dense zones of broken materials increases and becomes connected and in turn, the loose packing zones of intact particles becomes isolated. The Figure 4(c) indicates that the percentage of voids filled with crushed particles has increased to 64.5%. And with much higher compaction load P_4 applied to the packing, a high level of crushing is attained with 82% of the voids occupied by the crushed materials as observed in Figure 4(d).

(c) Stability and drainage in flexible pavements: Drainage in many geotechnical structures as well as structure such as the road pavement forms a very crucial component in the overall design. In most cases, the stability and the safety of such structure depends greatly on the efficiency of the drainage system constructed within the structure. According to Cedergreen[21] unless the pavements are well drained under their full width, because of their relative flatness water that may enter through their tops, bottoms and sides exit the structures very slowly. And waterlogged pavements due to the inability of the base to drain water efficiently often caused numerous problems to the asphalt.

Assuming drainage goes vertically or horizontally, Figure 4(a) illustrates a well-drained granular base and Figure 4(b) displays interconnected pockets of loose particles that may still provide an adequate drainage system. However, in Figure 4(c) and Figure 4(d) the loose grain zones are disconnected and the dense crushed particles zones on the other hand are interconnected thus denying free passage of water to the outside via connected voids. A closed

hydraulic system such as this in a flexible pavement developing excess pore water pressures under traffic loads will result in the failure of the granular base as well as the pavement[21]. Therefore as the crushing process approaches the latter condition, serious problems will develop in the pavement.

(d) Innovative usage of granular material: Under relentless loading due to traffic granular base for flexible pavement structure requires very durable rock particles that do not crush in order to provide the required solution to the drainage problem. Unfortunately such materials are not always easily available and if they are, the high cost of obtaining them may render a project economically unfavorable.

The solution of a granular material that crushes and somewhat allows water to drain points to the conditions illustrated in Figure 4(b). In addition, the crushing could be designed to produce adequate fine materials in the mixture to help reduce the point-to-point contacts between the large particles. If such grain size distribution is achieved detrimental settlement could also be avoided because reduction of point-to-point contacts prevents rotations and reorientation of the larger particles, which is one of the causes to the long-term settlement in rockfills[22].

As crushed materials are expected to acquire increased resistance to further crushing with the reduction in point-to-point contacts of the larger particles, the required size distribution could be achieved in the field using heavier compaction equipment. Such positive effects of crushing on the granular materials are highly warranted. And only after the targeted distribution is achieved, the flexible pavement could be laid on the optimally engineered granular base that will now enhance the performance of the structure.

1.3 THE NEED OF RESEARCH ON FRAGMENTATION OF GRANULAR MATERIALS

Fragmentation or crushing occurs when slow failed material comes to rest on the stable ground and when soil materials are subjected to static and dynamic loads. To date there is not much research being conducted on the effect of varying levels of crushing of granular materials have on their engineering properties namely, the hydraulic conductivity, the shear strength and the elastic moduli.

Fragmentation of granular materials produces fines. The contribution of these fines in changing the engineering properties of the material's use in an engineering structure may be substantial and has been the subject of keen research for many years. Because of grain fragmentation, several different features of geo-material behavior maybe produced for example dense sands start to behave like loose sands. Changes in the geo-materials' response to load may have serious consequences in an engineering structure that have been constructed. Understanding the effect of fragmentation on the engineering properties of the material is therefore highly desirable to a designer to produce a well-designed structure especially for those that have components of granular materials.

For the sake of simplicity, fragmentation can be defined into two types, namely total fragmentation and peripheral fragmentation, also known as abrasion. In most cases these forms of fragmentation are related to the intensity or level of loading that they are subjected to. The diagram in Figure 5 illustrates the two types of fragmentation that may take place as granular materials respond to loading.

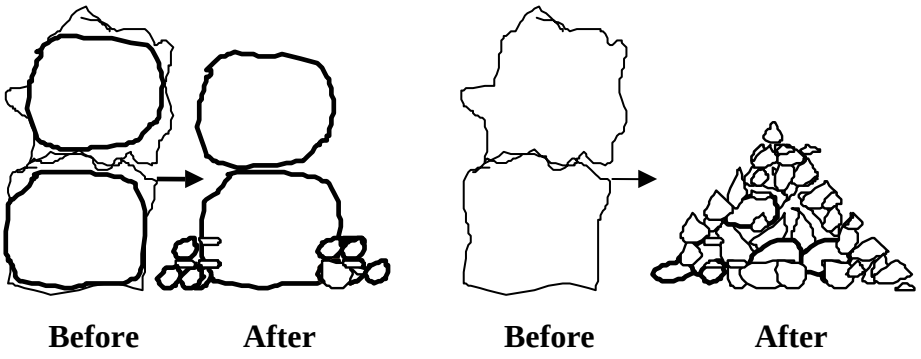

Figure 5 An Illustration for the Before and After Conditions in (a) Peripheral Fragmentation (Abrasion) and (b) Total Fragmentation

Abrasion takes place when the sharp corners and edges of the granular particles are removed as a result of compressive and shear loads while the bulk masses of the grains are left intact as indicated in the Figure 5 (a). And as the particles become more rounded, a lot of fines are produced. Total fragmentation on the other hand produces fragments of various sizes as indicated in Figure 5 (b). The particles completely disintegrate after being subjected to load. A laboratory exercise on abrasion will draw the distinction between total and peripheral fragmentation. An analysis on the fractal dimension of the materials will also be performed.

The key measure of the strength of a granular material is its inter-granular friction angle, also known as angle of internal friction. And the angle of internal friction of a material is akin to the angle of repose. In the beginning of this research the importance of the relationship between the angle of repose as the material property and its internal friction angle will be investigated. For this purpose, a simple angle of repose funnel' laboratory test is performed. A relationship

between basal friction, internal friction and angle of repose is then developed and examined through a simulated fragmentation model in an attempt to relate the effects in the strength properties of the material.

Initial information to grain crushing using the ring shear apparatus is referred to in formulating a simplified simulated model for testing the phenomenon of fragmentation due to slow continuous failures. In addition, a comprehensive investigation on the changes in the elastic modulus and the hydraulic conductivity before and after crushing is conducted on various levels of fragmentation due to static and dynamic loading. The relevance of introduction of fractal theory to enhance the understanding of grain crushing and encouraging the application of the fractal dimensional number in the future related works is an important feature of the research.

1.4 THE OBJECTIVES AND SCOPE OF THE STUDY

The principle objective of this study is to investigate fragmentation and the effects it has on the engineering properties of granular materials in relation to hydraulic conductivity, shear strength characteristics and elastic modulus. To achieve this, the investigations on the materials are carried out at an initial stage before the crushing, and proceed to the later stages after crushing in order to provide a better understanding of the changes caused by each event. A comprehensive evaluation at those stages on the shear strength characteristics, the elastic modulus of the materials and their hydraulic conductivities is carried out by experimental simulation in the laboratory. The other part of the investigation involves a theoretical evaluation of the experimental results and the application of the fractal theory based models.

The scope of the investigation focuses basically on crushing fragmentation phenomenon in the laboratory including, fragmentation as a result of slowly shearing mode, fragmentation due to static loading and fragmentation due to dynamic forces. To satisfy these objectives the following explorative studies are performed.

1.4.1 An Investigation on Fragmentation of Sand: The Effect on Angle of Repose

(a) Crushing of Sand with Shear Apparatus: As an introduction to the investigation on the crushing, the behavior of coarse sand under gradually increasing uniaxial loads were carried out initially using The Ring Shear apparatus. The shear strength characteristics as well as the different levels of crushing in an extended duration of stress were observed to understand the properties and the limitations involving the respective granular material. Following this, a comparative study is conducted on the fragmentation of coarse Quartz sand, Calcareous and Ottawa sand.

(b) Angle of Repose: When fragmentation takes place as a result of slow evolution of failed materials in slope failures, the heap of disintegrated material formed at the toe of the slope spreads out in a manner related to the shear strength properties of the material as well as the interfacial friction forces developed in the event between the failed material and the impacted surface. For the fragmented heap of granular material, the extent over which the quantity of the failed material is distributed on the contact surface depends on among other factors, the angle at which the heap makes with the horizontal surface known as the angle of repose.

Presently, the angle of repose of a granular material is commonly implied as a close resemblance of the measure of the angle of internal friction of a granular material and to a certain

extent they are considered the same. In many cases the concepts in relation to both of the characteristic properties of the granular material has not been clearly defined and the understanding that they are both the same is left very much uncontested. The study seeks to clearly distinguish the unique relationship between the angle of repose and angle of internal friction. An investigation on the angle of repose, friction angle and interface angle was conducted in the laboratory using different proportion of the coarse Quartz sand (average diameter of 1.6 mm) and the very fine of the sand of size smaller than 0.104mm in diameter.

(c) Rankine Active Earth Pressure–Wedge Theory: This was employed to describe the mechanics of the formation of the heap from which the angle of repose of the granular material was observed. The theoretical values were then compared to the ones obtained in the laboratory in an attempt to define the relationships involving the internal friction angle and the angle of repose of the granular material with the basal interface friction between the granular material and the material forming the supporting base of the heap.

1.4.2 An investigation on Fragmentation of Gravels: The Phenomenon of Abrasion

An important product of granular fragmentation is fines particles. A material may be found unsuitable for use in road construction due to excess in the fines content of the material since fines is said to increase the possibility of a number of failures in flexible as well as rigid road pavement. It is therefore important to investigate the conditions relating to abrasion in gravels and to carry out analytical study in order to add to the understanding of this subject.

1.4.3 Investigations on Fragmentation due to Static and Dynamic Loads

For the crushing of glass beads and small-sized gravels these larger sized granular materials were crushed under constant stress apparatus simulating the static loading conditions and also under repeated falling hammer loading simulating the dynamic loading conditions. The important characteristic properties of the materials investigated include the hydraulic conductivity, and the elastic modulus. Static and dynamic compression tests generating crushing evolutions are carried out in the laboratory to simulate the confined conditions such as those found in parts of structures such as in the rockfill dams, highway embankments, stone columns, sand drains, flexible pavements and in the bases of foundations.

The exploratory investigations carried out over a series of tests intended to acquire a comprehensive understanding regarding the changes experienced by granular materials under simulated static and dynamic loading conditions. The objective is therefore to study and analyze the changes in the hydraulic conductivity, the shear strength characteristic specifically, the friction angle, and the elastic modulus of a sample before and after each crushing event.

1.4.4 The Fractal Theory

As the result of crushing of the coarse sand in the Ring Shear apparatus, the strength of the granular material on different level of loading is obtained. The grain-size distribution for every level of crushing is computed and simultaneously using the mass-based approach of the fractal particle-size distributions[23], dimension number can be assigned for each one evolution of crushing.

Similar exercise of fractal analysis was performed for the other laboratory-tested materials. Before and after every crushing of the glass beads or the small-sized gravels, they are mechanically sieved and a fractal analysis is then carried out for each sample. The objective of the exercise is to relate the fractal number to the engineering properties as described in the earlier discussions.

1.5 ORGANIZATION OF THE DISSERTATION

Chapter 1 introduces the topic of the research. A description on fragmentation process was detailed including the importance and the need of the present study. A thorough literature review was included focusing into the scope of the study. An outline of the overall research contents is described.

Chapter 2 describes the engineering properties of the granular soil that the study is focused on. The factors affecting the strength characteristics, Elastic modulus, permeability and their uses are discussed.

Chapter 3 introduces fractal theory and. discusses statistical distributions involving fragmentation of rocks and soil particles. Mathematical relationships in relation to the development of fractal distributions are presented in brief to appreciate important aspects of fractal dimensioning.

Chapter 4 describes fragmentation and crushing processes in sand due to gradual shearing. The Ring Shear apparatus employed in the laboratory were used to measure and investigate fragmentation characteristics in sands that have different structures namely, Quartz, Calcareous

and Ottawa sand. Particle size distribution analysis was performed. Fractal fragmentation relationships to the strength and the hydraulic properties of the material are demonstrated and compared analytically.

Chapter 5 introduces binary mixture in the simulation of fragmentation and focuses on the important effect of fragmentation on the angle of repose. A theoretical formulation was developed from a statically determinate problem to arrive at a general equation as well as the one implied as the equation for the special conditions. Intensive experimental exercises related to the angle of repose of binary granular mixtures were carried out. The data were processed and compared to the theoretical values.

Chapter 6 introduces fragmentation involving the larger sized granular materials. The chapter presents exploratory investigations on peripheral fragmentation (abrasion). The distinction of the phenomenon is demonstrated by experimenting on angular as well as round structured gravels. Fractal analyses using both area-perimeter method and mass-based method were employed in order to quantify the abrasion effects in both cases.

Chapter 7 describes and analyzes the laboratory data with respect to the crushing characteristics of glass beads and small gravels using the Universal Testing Machine (UTM). Laboratory tests on elastic moduli of a granular specimen before and after crushing were performed to relate the effect of fragmentation to the values of the elastic constants

Chapter 8 describes tests on the permeability of the granular soil before and after the fragmentation process due to static and dynamic load. Cells where the granular materials was crushed was used as a Constant head permeameter to measure hydraulic conductivity. To have a

clearer understanding of the effect of different physical shapes of particles on hydraulic conductivity, round and angular-shaped gravels are used in the exercise to explore the effect of the shape on their engineering properties and to relate the result to fractal dimension.

Chapter 9 is the summary and the conclusion of the research works in the thesis.

2.0 ENGINEERING PROPERTIES OF GRANULAR SOIL

2.1 PERFORMANCE AND CHARACTERISTICS

The performance of the granular soil as a particulate system in an engineering structure is very much dependent on the properties of the granular materials involved. A granular material is often a preferred option to a clayey material with a large percentage of fines because it provides the necessary features or elements required to successfully make a designed structure functions efficiently.

For example, in both flexible and rigid pavements, it is found that poor performance of unbound granular layers contributes to reduced life and costly maintenance. In flexible pavements, failures of the bases are manifested as rutting, fatigue cracking, longitudinal cracking, depressions, corrugation and frost heave. Whilst in rigid pavements their failure contributed to pumping, faulting, cracking and corner breaks[24].

The use of the granular base appeals because the inclusion of the granular layer to support the traffic load provided the additional strength to the system. Ideally, we would want to get materials with the highest strength and durability in a construction project. However, this shall not be realistic in most cases. Because most granular materials failed at point-to-point contacts fragmentation and breakage is expected in materials with a lesser strength.

In relation to the strength and durability of the material, the characteristic property of the particulate such as the elastic modulus is important. With the elastic modulus of the material known it will provide the very important information regarding the extent of settlement that may take place under imposition of vertical loading.

As soil is inherently a multiphase system it is important to assess the property of the granular soil and predicts its reaction when interfacing with the water regime. As the presence of water could cause problems, the presence of a granular regime provides the necessary drainage to keep the structural members dry. The permeability of the soil is therefore the other very important factor that will be investigated in this research.

2.1.1 Strength Characteristics

A soil engineer equates soil strength to the soil shear strength. The strength characteristics that influence the shear strength of granular materials is defined by the internal frictional force developed within the soil skeleton as a result of an external load acting on them. Coulomb[25] the French engineer, proposed that the normal stress across a potential shear plane tends to press the two parts together, giving an internal friction that opposed their movement. Coulomb's failure criterion that relates the critical shear stress τ_c at failure on an arbitrary failure plane in a material to the normal stress σ_n acting perpendicular to the plane is expressed as follows.

$$\tau_c = \sigma_n \tan \phi + \tau_0 \qquad (2.1)$$

Where ϕ is called the angle of internal friction, τ_c and σ_n are the shear and normal stresses respectively at failure and τ_0 is the cohesion.

According to some earlier researchers shear strength of granular material is, to a large extent, influenced by the initial void ratio and to some extent by the particle shape, the surface roughness, and the grain size distribution[26]. However since particle shape, the surface roughness, and the grain size distribution are characteristics of a specific soil deposit, their effect leads to the differences in the strength characteristics of various deposits.

(a) Angle of Internal Friction: The internal friction angle is a characteristic property of a specific material. The term cohesion τ_0 which was in fact defined as the shear stress necessary to overcome the initial strength of the material when σ_n is zero, for a granular material is considered negligible[27]. And thus in accordance to the empirical equation given, the ratio of the shear stress with respect to the normal stress at failure is approximately constant for the material.

As we know, the friction between the particles in a granular form is dependent on the nature of contacts between the grains. Therefore in the study, factors that influence the characteristics of the contacts will be investigated during the process of fragmentation-evolution of the granular soil. The determination of angle of internal friction is to be accomplished mainly by the ring shear apparatus and in some instances by direct shear box test.

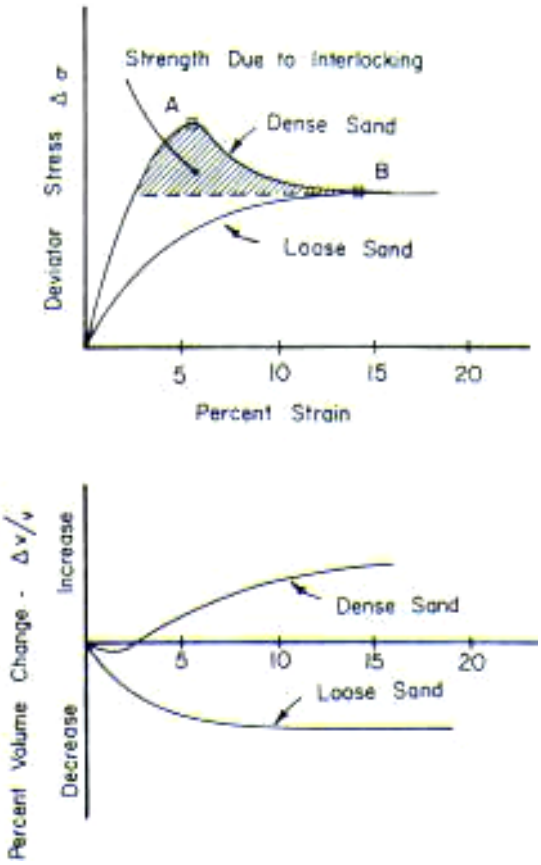

Figure 6 Stress-Strain and 'Volume Change'-Strain Relationships for Samples of Dense and Loose Sands[28]

There are two major factors that determine the soil friction angle in the laboratory test. The energy applied by the external load used both to overcome the frictional resistance between the soil particles and also to expand the soil against the confining pressure. In a study of stress dilatency theory presented by Rowe[29] it was explained that in order for sliding to occur soil grains which were highly irregular in shape have to be lifted over one another in the behavior called dilatency. Hence, the angle of friction ϕ can be expressed as,

$$\phi = \phi_u + \lambda \qquad (2.2)$$

Where, ϕ_u is the angle of sliding friction between the mineral surfaces and λ is the effect of the interlocking phenomenon.

The effect of the interlocking component of shear strength is realized especially in the dense sand by the peak in the stress-strain plot[28] as illustrated in Figure 6. At greater strains in the plot as the interlocking stress is overcome, the curve for the dense samples at high strain tends to arrive to the same level as the loose samples.

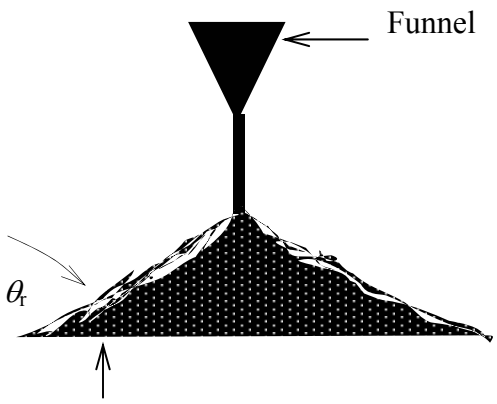

Figure 7 The Measurement of Angle of Repose, θ_r of Free-Flowing Granular Material

(b) Angle of Repose: Free-flowing granular materials are easily employed in tests for angle of repose. It is the particle size, shape and bulk density that will affect the flow ability of the materials[30]. As shown in Figure 7 granular materials are dropped through a funnel to form a heap of soil in the form of a cone on a horizontal plane and the angle at which the slope of the stable cone made with plane is called the angle of repose.

Slopes in homogeneous and cohesionless soils do not exhibit deep circular failures instead they fail by shallow sliding motions parallel to the slopes. Assuming each grain of sand acts like a block lying on an inclined plane, when the slope angle exceeds the angle of friction of sand on sand (angle of internal friction), the sand grain will slide down the plane. The steepest slope that sand can attain hence represents the angle of internal friction of the sand[20]. It could in fact be the minimum value because near the surface the sand is very likely to be found in a loose condition.

Since the measure of Angle of Repose is easily performed without too many restrictions, it has been used to estimate the value of the angle of internal friction ϕ for a dry granular material. Such is not the case for tests using the direct shear equipment. Because of its generally rather small size, the container shearbox restricts that only small diameter granular materials (such as sands) should be used to ensure a higher degree of accuracy in the test results.

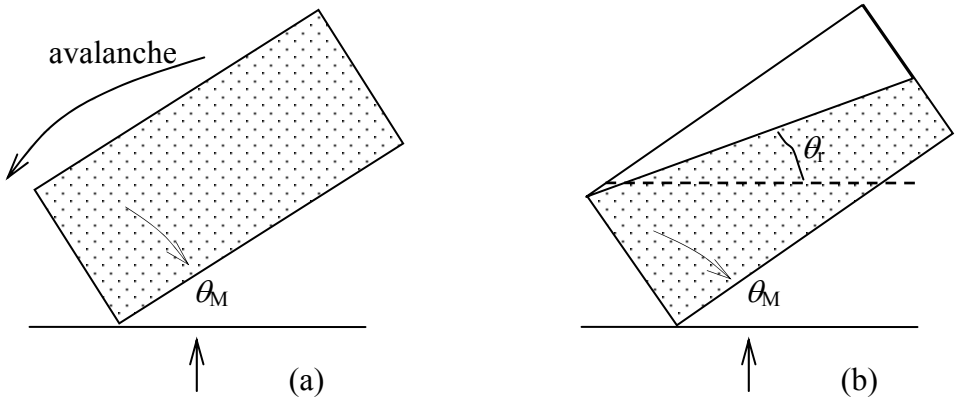

Figure 8 (a) Scheme of Packing Before the Avalanche Begins at θ_M, The Maximum Angle of Stability. (b) θ_r is the Angle of Repose When the Avalanche Stops[31]

It is found however that measurement of angle of repose has also been conducted in a slightly different manner than the one illustrated in Figure 8. A granular material packed in a box

is tilted to an angle θ_M, which is the maximum angle of stability at which avalanche takes place. As the large sliding decreases the slope of the free surface, the slope of the second critical angle[31] that is the angle of repose is obtained.

(c) Grain Size Distribution: The measure of grain size distributions is a very important aspect of the study. As the particle size seems to affect the flow ability of the granular material it will be interesting to see what effect this would also have on the internal friction angle measured using the ring shear as well as the shear box apparatus.

By conducting the sieve analysis before and after fragmentation of the granular material, Breakage index[(32)] as well as Fractal dimensional analysis could be performed[(33)] to facilitate the understanding of their influence with respect to the strength characteristics of the materials tested.

2.1.2 Elastic Modulus

Soils and granular materials in completed pavements are subjected to large numbers of load applications at stress levels well below their shear strength. However, under partially completed pavements, when construction traffic is applied directly to the granular layer, the number of load applications is fewer but the stress levels are much higher[(34)]. Moreover although under a single application of a moving wheel the pavement response is essentially resilient, under repeated loading, plastic and viscous strains can accumulate. The following plots in Figure 9 indicate the large difference in the magnitude of vertical stress subjected to the granular layer of the pavement foundation.

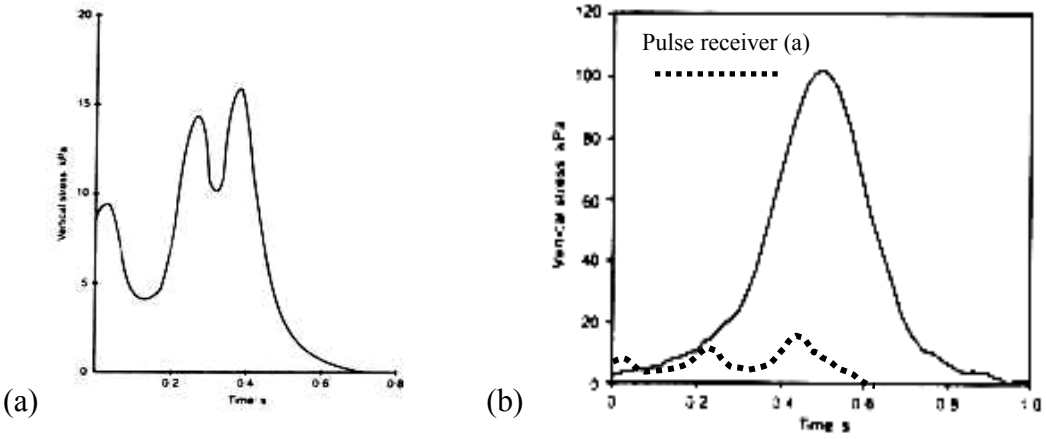

Figure 9 In Situ Vertical Stress in Sub-Grades (a) Below 165mm. Asphalt Construction at Wakefield, England (b) Below 350mm. Granular Layer at Bothkennar, Scotland[34]

In an embankment forming a water-retaining dam for example, settlements and deformations are often observed during the placement of the granular fill. These settlements and deformations may be of much greater concern compared to a road pavement settlement in terms of the magnitude of settlement. In both cases it is clear that the evaluation regarding elastic response of the granular material is necessary in the design of these structures so that their performance can be well predicted and assessed.

For the calculation of the elastic deformation experienced by soil when subjected to either static or dynamic loads the values of the elastic moduli comprising Young's modulus of elasticity, E, Poisson's ratio, υ and the shear modulus, G are required. Although it is arguable that the theoretical analysis of the stress-strain response of the soils may be more akin to an elasto-plastic or elasto-visco-plastic analysis rather than elastic, solutions based on linear elastic behavior are also commonly used for the estimations of stresses or strains in the field.

The laboratory testing equipment used to measure the elastic moduli of the materials includes an ultra sonic pundit apparatus that measures the progressive P waves and the shear S waves distance traveled in a given time across a sample, hence the velocities V_p and V_s respectively. The equations employed are similar to that used in the recent research by Loboguerrero[35]. The equations for the Young's modulus of elasticity, E, Poisson's ratio, υ and the shear modulus, G are as follows.

$$\text{Young's modulus of elasticity, } E = \frac{V_s^2\left(3V_p^2 - 4V_s^2\right)\rho}{V_p^2 - V_s^2} \tag{2.3}$$

$$\text{Poisson's ratio, } v = \frac{1}{2}\left(\frac{V_p^2 - 2V_s^2}{V_p^2 - V_s^2}\right) \tag{2.4}$$

$$\text{Shear modulus, } G = \rho V_s^2 \tag{2.5}$$

where, ρ is the density of the particulate system through which the waves passes

V_s is the shear velocity wave, and

V_p is the compression or progressive velocity wave.

2.1.3 Hydraulic Conductivity

Soils and granular materials in pavements exist above the water table but beneath a sealed surface though this may not completely inhibit ingress of water. Therefore because of such arrangement both saturated and partially saturated conditions can be present at one time or the

other in the system[34]. Granular materials forming part of highway embankments, rockfills, rigid and flexible pavements and bases of foundations are all introduced into a system with the common criteria that water that enters the system will immediately be drained away.

However when the granular materials are subjected to static and dynamic loads crushing and fragmentation will increase the fine fragment component of the system and hence increasing the tendency of a closed system[21] as described earlier. Although with the increase of finer fragments the strength of the granular system is expected to improve as the system acquired greater resistance to further crushing, the tendency to reduce their hydraulic conductivity at the same time will take away their favorable contribution if in the long run the system is rendered less efficient.

The permeability of the granular materials is to be monitored before and after every fragmentation stage to understand this relationship. In hydrogeologic practice, methods based on empirical formulas are often used to determine hydraulic conductivity. Some of these equations are presented in Table 1. One of the reasons for the existing variations in these equations is that often the conditions and the domain of applicability under which the proposed empirical formulas were derived differ. To complicate matter more, there are also a number of variations for a particular equation under an author in deferent texts[36, 37]. Kozeny-Carman equation that was proven to give a good fit to laboratory test data[36] for coarse-grained soils will be used along with Hazen equation which is always found to be popular partly due to the simplicity of the formula.

Table 1 Empirical and Analytical Solutions for the Hydraulic Conductivity

EQUATIONS	AUTHORS	SYMBOLS
$K = C(d_{10})^2$ $K = 0.35(d_{15})^2$	Hazen : Loose sands Dense sands	Permeability K (cm/s) Empirical Factor C=100 $d_{10}(d_{15})$= particle dia.(mm) at 10% (or15%) on Grain Size Distribution plot.
$K = 0.05\left(\frac{n^2}{(1-n)^2}\right)(d_{15})^2$	Terzaghi	n = porosity of soil
$K = \frac{n^3}{2S^2}$	Darcy-Poisville	S = surface area exposed to the fluid per unit volume of solid
$K = \frac{n^3}{k_0 T^2 S^2}$	Carman	k_0 = empirical constant T = tortuosity
$K = \left(\frac{g}{v}\right)\frac{d^2 n^3}{180(1-n)^2}$ $K = \left(\frac{g}{v}\right)\frac{n^3}{C_0 S^2(1-n^2)}$ $K = \left(\frac{g}{v}\right)\frac{n^3}{(C_t T S^2)}$	Kozeny-Carman (modified) (modified by Collins)	d = grain diameter v = dynamic viscosity C_0= factor reflecting pore shape and packing C_t= coefficient for pore shape and packing
$K = \frac{n^3}{45(1-n)^2(V_s/R_s + V_c/R_c)^2}$	Yin	V_s,V_c = volume of sand and clay respectively V_s,V_c = radius of sand and clay particles respectively

3.0 FRACTAL THEORY AND FRAGMENTATION OF ROCK

With a scale a map will be able to indicate if it covers 10 meters or it is in fact covering 10 km. In the discipline of Geology, an object with a characteristic dimension, such as, a coin, a rock hammer or a person is often included in a photograph in order to provide an appreciation in the sense measurement in size. It is in this context, Mendelbrot[38] introduced the concept of fractals. It is for the same reason of scale invariance that the length of a coastline increases as the length of the measuring rod decreases in accordance to a power law. The fractal dimension of the coastline is thus determined by the magnitude of the power.

The word "fractal" originated from the Latin word "fractus" means broken, irregular fragments was used to introduce the concept of fractional dimensions, a concept in specialized areas of physics and mathematics developed by Hausdorff[39] in 1919. The concepts introduced by Mandelbrot[38] in 1967 were generally associated with describing irregular and random phenomena in nature.

3.1 FRACTAL THEORY

The shapes of forms have been viewed dimensionally in the Euclidean sense. Euclidean geometry describes objects by points, lines, planes and cubes using dimensional numbers of 0, 1, 2 and 3 respectively. A measure that is established in a dimension such as length for a line, area

for a plane or volume for a cube remains invariant with respect to the unit of measure. Whether feet or inches is used the length of a line remains the same. On contrary, an object found in nature, rough surfaces that appear irregular and disordered for example, are scale-dependent in their measures of length, area and volume. This relatively new mathematical concept in fractals is used in describing the geometry of these irregular shaped objects suggests that their dimensions are not limited to integers but rather in terms of a continuous real number in the form of a fraction. For the Euclidean or topographic dimension, a line of any shape is one and two for a surface. The fractal dimension for a line of any shape varies between 1 and 2, and for a surface between 2 and 3. The rougher or more irregular is the fractal, the larger is its fractal dimension.

3.1.1 Fractal Dimension Concept

By decreasing the unit of measurement Mandebrot[38] found that the length of a coastal line, L does not converge but instead increases. A relationship in the form of $L \propto \varepsilon^{(1-D)}$ was developed when the increasing values of L were plotted against the decreasing unit of measurement ε on a log-log plot. What he concluded then was that the real number D was in fact the dimension of the coastline. It was this concept that marked the origins of fractal geometry related to self-similar and self-affined fractals that have thereon unearthed numerous applications in characterizing and describing disordered and chaotic phenomena in science and engineering.

(a) Self-Similar Fractals: Self–similar fractals includes exactly self-similar as well as statistically self-similar fractals. As an example, the coastline problem discussed earlier is a statistically self-similar fractal as compared to exactly self-similar fractal which according to mathematicians includes the likes of Cantor dust, Sierpinski carpet and Koch curve[42] that strictly prescribe to certain mathematical forms.

In the similarity transformation, points $X = (x_1, x_2, ..., x_N)$ in the Euclidean space are transformed into new points $X' = (r_1x_1, r_2x_2, .., r_Nx_N)$ where the scaling ratios are equal ($r_1 = r_2 = \ldots, = r_N = r$). If the points X' are identical to the original points X then they are exactly self – similar. They are statistically self similar if the transformed points of X' are identical in all statistical respects to the original points X.

(b) Self-Affined Fractals: The definition of self-affined fractals includes self-mapping, self-squaring and self-inverse fractals. This involves cases where the sets are not clearly defined as self-similar due to the fact that the different physical quantities cannot be scaled with a same scaling ratio. For instance in the study related to the motion of a Brownian particle, the different physical quantities of time and position cannot be scaled with the same scaling ratio. The self-affined transformation therefore provides for a general form for the self-similar transformation where the scaling ratios $r_1, r_2, .. r_N$, are not all equal.

3.2 FRAGMENTATION OF ROCK

As the most abundant building material on earth, rocks has been the object of keen research and interesting innovations since the early history of mankind. Rocks of different sizes provide different uses and have been utilized in many different ways. From our early encounters with the material, it has been recognized that larger size rocks break down into smaller fragments through fracturing. The magnitude of force that is needed to break rock materials comes in various forms.

Fragmentation of the earth crust is by tectonic processes involving faults, fractures and join sets. On the other hand, rock fragments can be produced in many different ways and may involve natural or manmade activities such as weathering or by explosion, and impact.

Relatively little progress that has been made in developing comprehensive theories of fragmentation has been attributed to the fact that fragmentation involves the initiation and propagation of cracks. The highly nonlinear process of fracture propagation requires complex models for even the simplest configuration. Fragmentation also involves the interaction between fractures over a wide range of scale. If fragments are produced with a wide range of sizes and if natural scales are not associated with either the fragmented material or the fragmentation process, fractal distributions of number versus size would seem to be expected[40].

3.2.1 Statistical Distributions and Rock Fragments

Fragment sizes distribution is clearly a statistical problem. Masses of n fragments represent discrete data that can generally be characterized by a set of n data points $\{x_1, x_2, \ldots x_i, \ldots x_n\}$. Following the standard practice of describing the statistical properties of a discrete data, the mean and moments of deviations from the mean can be obtained as follows. The mean value of x_i, $\bar{x}$ is given by,

$$\bar{x} = \frac{1}{n}\sum_{i=1}^{n} x_i \qquad (3.1)$$

and the second-order moment of distribution which is the variance V is given by,

$$V = \frac{1}{n}\sum_{i=1}^{n}(x_i - \bar{x})^2 \qquad (3.2)$$

the standard deviation σ is related to variance as such, $\sigma = \sqrt{V}$

The common practice of fitting an empirical statistical distribution to a discrete set of data is often done by equating the mean $\bar{x}$, variance V and skew γ of the distribution to that of the data. Where the third-order moment skew γ representing the asymmetry of the data is given as,

$$\gamma = \frac{1}{n\sigma^3}\sum_{i=1}^{n}(x_i - \bar{x})^3 \qquad (3.3)$$

A variety of statistical relationships are used to correlate data on the size distribution of rock fragments. According to Turcotte[41]; two of the most widely used distributions are the log normal and the power law. Korčak once stated that only two fundamental types of statistical distribution exist and that they are the normal and the power law distribution[42]. However other statistical distributions have also been used to approximate particles size distributions of rock fragmentations[40, 43,44].

3.2.2 The Common Distribution Functions

Gaussian distribution or the normal distribution also simply known as the bell curve is one of the most widely used statistical distributions. The wide applicability of the distribution is attributed to the central limit theorem. The theorem states that if the distribution is the sum of a large

number of independent random distributions, the distribution will approach a normal distribution as the number approaches infinity. As it is symmetrical about its mean, the coefficient of skew for a normal distribution is zero and the independent variable x takes on all values from - ∞ to $+\infty$.

In many applications however, a distribution of only positive values is required. In such cases the log-normal distribution hence become the more popular distribution and is found skewed to the right giving equal probability of ratios of sizes rather than differences of sizes. The log-normal distribution can be obtained directly from the normal distribution simply by taking the logarithm of the normally distributed values. The probability distribution of both of these functions are indicated as follows,

The normal distribution : $$f(x) = \frac{1}{\sigma(2\pi)^{1/2}} \exp\left[-\frac{(x-\bar{x})^2}{2\sigma^2} \right] \qquad (3.4)$$

The log-normal distribution : $$f(x) = \frac{1}{x\sigma_y(2\pi)^{1/2}} \exp\left[-\frac{(\ln x - \bar{y})^2}{2\sigma_y{}^2} \right] \qquad (3.5)$$

where, $y = \ln x$

Whilst the normal distribution function is a two-parameter function, referring to the arithmetic mean $\bar{x}$ (which is also the mode and the median of the distribution) and the standard deviation σ, the log-normal distribution is basically depending on one parameter and that is the coefficient of variation c_v. The coefficient of variation is the ratio of standard deviation and mean. And having both as positive numbers, the ratio of the two quantities is a measure of the spread of the distribution.

In 1956 as proposed by Gardner[45] a two-parameter, log-normal distribution was used to fit soil grain-size distribution data. However, because the equation often failed to provide a close fit of the grain size distributions, improvements were later made upon the log-normal equation by introducing three-parameter and four-parameter log-normal equations.

According to Fredlund[44] who discussed extensively on numerous mathematical representations of soil grain-size distributions, the limitation associated with using a log-normal type of equation is the assumption that the grain size distribution is symmetric when in reality it is not. Secondly, for soils that are gap-graded or bimodal as in many cases of fragmentation[46] application of the four-parameter log-normal equation does not render satisfactory results.

3.2.3 The Fractal Distributions

In his own word Mendelbrot described that a fractal is the shape that is formed by part that is the same as the whole. The fractal dimension D provides a measure of the relative importance of large versus small objects. Long before the concepts of fractals were conceived it was recognized that there were empirical applicability of power-law statistics to geological phenomena[47]. Other distributions that have been used also include the normal (Gaussian) distribution and the log-normal distribution which were described earlier. A fractal distribution requires that the number of objects larger than a specified size have a power-law dependence on the size. Evidently, the power-law distribution is the only distribution that does not include a characteristic length scale and thus making it applicable to scale-invariant phenomena. To the many geological phenomena including frequency-size distribution of rock fragments and mineral deposits scale invariance provides a rational basis for the applicability of power-law, fractal distribution[38], just as central-limit theorem provides a basis for the usage of Gaussian distribution.

Fractal sets such as Sierpinski carpet, Cantor set, the triadid Koch island which are deterministic fractals can be defined quantitatively using a mathematical equation similar to the one given below[48]. In fragmentation however, using Korčak's empirical relationship of size distribution of areas of islands, Mandelbrot suggested that fractal fragmentation could be quantified by developing fractal dimension from the equation[33].

$$N(R > r) = \frac{C}{r^{D_F}} \qquad (3.6)$$

For the distribution to be fractal, the number of objects N (fragments) with a characteristic linear dimension greater than r should satisfy the above relation given C as a constant of proportionality and D_F as the fractal dimension. Statistical number–size distribution for a large number of objects such as rock fragments can also be fractal. They are commonly recognized as statistical fractals. In soil particle-size distribution the concept of fractal scaling suggests that across a wide range of scales, the solid phase of the soil appears self-similar[23].

3.2.4 Associated Statistical Distributions

(a) Pareto distribution.

Probability distribution function; $f(x) = \frac{ak^a}{(k+x)^{a+1}} \qquad x \geq 0 \qquad (3.7)$

Cumulative distribution function; $F(x) = \left(\frac{k}{k+x}\right)^a \qquad x \geq 0 \qquad (3.8)$

The standard form of the distribution is obtained when $k = 1$. Plotting the probability distribution function for the standard form of the Pareto with positive values of a shows that the power-law tail of the Pareto distribution dies off more gradually than the tails of the normal or log-normal distributions, a characteristic of fractal distributions. A close association between statistical fractals and Pareto distribution can be demonstrated as follows;

Standard form of Pareto cumulative distribution ; $F(y) = \dfrac{1}{(1+y)^a} \qquad y \geq 0 \qquad (3.9)$

For $y >> 1$, equation (3.9) becomes, $F(y) = \dfrac{1}{y^a}$ indicating similarity to the statistical fractal equation (3.6) that lead many to believe that fractals are a trivial function of the Pareto distribution. However, a very important distinction that exists between the two can be shown as follows,

As $x \to 0$, the Pareto function $F(x) = \left(\dfrac{k}{k+x}\right)^a$ is finite.

As $r \to 0$, the fractal function $N = \dfrac{C}{r^D}$ is diverged. And this divergence is required by scale invariance of the fractals.

(b) Exponential distribution.

Probability distribution function; $f(x) = \dfrac{vx^{v-1}}{x_0^v} \exp\left[-\left(\dfrac{x}{x_0}\right)^v\right] \qquad x \geq 0 \qquad (3.10)$

Cumulative distribution function; $F(x) = \exp\left[-\left(\frac{x}{x_0}\right)^v\right]$ (3.11)

Equation (3.11) known as the Rosin and Rammler (Rosin-Rammler-Bennett)[49] distributions is also used extensively in geostatistical applications. The equation can also be written as the following and known as the Weibull distribution[50].

$$1 - F(x) = 1 - \exp\left[-\left(\frac{x}{x_0}\right)^v\right] \tag{3.12}$$

If $(x/x_0)^v$ is small, then the exponential in equation (3.12) can be expanded in a Taylor series to give,

$$\exp\left[-\left(\frac{x}{x_0}\right)^v\right] = 1 - \left(\frac{x}{x_0}\right)^v + \text{.....} \tag{3.13}$$

Neglecting the higher powers $(x/x_0)^v$ and substitute (3.13) into (3.12), it is seen that for small x the Weibull distribution reduces to a power-law (fractal) distribution[50] as follows,

$$1 - F(x) = \left(\frac{x}{x_0}\right)^v \tag{3.14}$$

3.2.5 The Sieve Analysis Application: Particle(Grain) Size Distribution (PSD)

Civil engineers and other soil scientists commonly use sieve and hydrometer test data to present the particle-size distributions (PSD). In the analysis, using a semi logarithmic graph paper as suggested by The American Society for Testing and Materials standards D1140-54 and D422-63 (ASTM 1964a, 1964b) the cumulative percentage finer by mass is plotted against the respective sieve openings representing the grain sizes. Due to its simplicity and informative nature the PSD is very much favored when performing routine soil classification works. Through the PSD researchers are attempting to estimate other soil properties such as the soil-water characteristics. The existence of such prospect makes mathematically represented PSD becomes even more appealing.

In the sieve analysis the mass of fragments passing through a sieve with a specified aperture r is $M(<r)$ and the remaining mass is $M(>r)$. Thus we have the total mass M_T as,

$$M(<r) + M(>r) = M_T \tag{3.15}$$

The power-law approximation to the Weibull distribution as demonstrated in equation (3.14) can be used to approximate sieve analyses in the form,

$$\frac{M(R < r)}{M_T} = \left(\frac{r}{r_L}\right)^m \tag{3.16}$$

where $M(R < r)$ is the cumulative mass of particles with size R smaller than a given comparative size r ; M_T is the total mass of particles (introduced for normalization); r is the sieve size opening; r_L is the maximum particle size as defined by the largest sieve size opening.

Fractal number relation can be related to the power-law mass relation of equation (3.16) by taking incremental values. Rewriting equation (3.6) we have,

$$N(> r) = Cr^{-D} \tag{3.17}$$

the derivative of equation (3.16) gives, $dM \sim r^{m-1}dr$ (3.18)

the derivative of equation (3.17) gives, $dN \sim r^{-D-1}dr$ (3.19)

Since fragments occur in a variety of shapes, the linear dimension r is defined as the cube root of volume ($r = V^{1/3}$) and assuming constant density, mass of a fragment $m \sim r^3$. The incremental number in relation to incremental mass is therefore given by,

$$dN \sim r^{-3}dM \tag{3.20}$$

Substituting (3.18) and (3.19) into (3.20) gives, $r^{-D-1}dr \sim r^{-3}.r^{m-1}dr$ and we have, $r^{-D-1} \sim r^{m-4}$. So that,

$$D_F = 3 - m \tag{3.21}$$

Data obtained by sieve analyses can thereby used to convert number-based distributions to mass-based distribution to specify a fractal dimension D using equations (3.16) and (3.21). Accordingly these are the two most frequently used equations in most parts of the study of fractal dimension analysis of the granular mass as a consequence of the PSD[33].

3.2.6 Why Fractal?

Some of the advantages of using of a mathematical equation to fit the PSD[44] are;

(1) Soils can be identified on the basis of PSD by equations that are best fit the data. It is a classification method using best–fit parameters.

(2) The equations provide a consistent method for determining physical indices such as percent clay, percent sand, percent silt and particle-diameter variables such as d_{10}, d_{20}, d_{30}, d_{40} and d_{60}.

(3) The mathematical equation can provide a method of representing the entire curve between measured data points.

(4) Representing the soil as a mathematical equation increase the flexibility in searching for similar soils in databases.

It has been shown thus far it is plausible to carry out fitting an empirical statistical distribution to a discrete set of data of fragmented rock. However, since grain–size distribution is theoretically a continuous curve representing the amount of various particle sizes, there exists some limitations when applying these equations. In most cases accuracy of curve fitting of statistical equations are dependent on the required parameters.

Based on the laboratory observation that the failure of the rock is a consequence of fractures which are preceded by the concentration of a swarm of microfissures which are themselves the result of an accumulation of microcracks, the distribution of fragments of rock has been proved to be statistically fractal[40, 51]. Therefore fractal dimensioning can be used to quantify the size distribution[24] of the fragmented material. Not surprising that as an answer to the question of which one of the three size distributions (when referring to the exponential, the log-normal and the power law) is right for presenting the fragmentation. Korvin stated that very likely all of them[43].

Graphical presentation of grain-size distribution has been very useful in characterizing the soil by detailing the distribution attributes into predefined categories. Further descriptive refinement for soils classified by The Unified Soil Classification system can be added from such numerical quantities as the uniformity coefficient, C_u and coefficient of curvature C_c. from the cumulative distributions Fractal fragmentation theory on the other hand provides a means by which the entire size distribution of material can be quantified through specific and exact values[33].

To be able to quantify the description of ruggedness of a system according to Kaye[50] is desirable as if not more, it is absolutely an elegant descriptive technique in the science of mathematics. Due to the scope of this research, the focus will be therefore to use the power-law plots as the basis of the measure of the fractal distributions. An analysis of the fractal dimensions of the crushed rocks is performed in the light of establishing a relationship to a particular engineering characteristic of the tested material.

4.0 FRAGMENTATION AND CRUSHING OF SAND

A series of testing consisting of different experimental packages is being carried out in the "Geotechnical/Construction" Material Engineering and Transportation Engineering Laboratories University of Pittsburgh in order to meet the research objectives mention earlier. However, it is very important to observe especially in the early stage of the study, the processes involved in the characteristic fragmentation and crushing in order to understand such occurrences in practice. In the field, often a very slow process of soil fragmentation and crushing takes place for example in slopes wherever there exists instability in the system.

To simulate the field conditions, a general observation regarding fragmentation and crushing behavior of coarse sand was first carried out using The Bromhead Ring Shear apparatus. As a result of the observation from the tests a representative of crushed granular material could be modeled for future investigations.

In the following tests small samples of coarse sand of 31.3 g of weight retained in sieve number 16 (-2.0+1.18mm.) was sheared in dry condition to a complete 360 degrees rotation in 5 hours. Each sample was sieved before and after shearing in order to observe the difference in the grain distribution characteristics as increasing normal loads were applied. A total of 15 samples were tested with normal loads ranging from 14.96 kPa to the maximum at 1374.30 kPa.

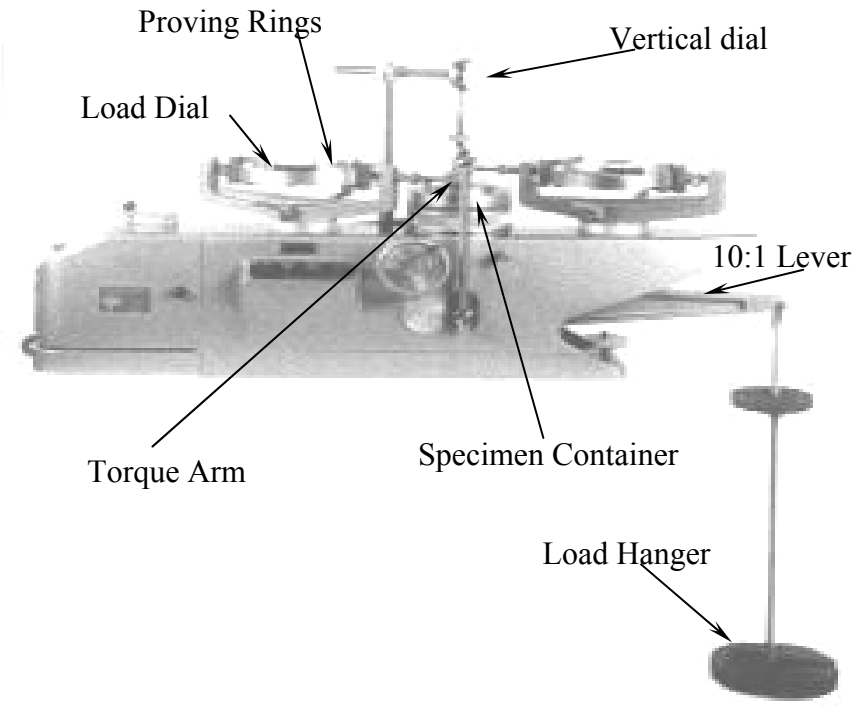

Figure 10 The Bromhead Ring Shear Apparatus

4.1 TEST METHOD AND PROCEDURE

The tests were carried out using The Standard Test Method described in ASTM D 6467-99. The procedure consists of placing the specimen in the annular specimen container and applying a normal stress as determined. As load is applied to the hanger, the force is transferred through a lever arm at a ratio of 10:1 to the top platen of the container. The specimen of 5 mm. thick is thus, confined in radial between two concentric rings with the inner diameter and outer diameter measuring 70 mm. and 100 mm. respectively and compressed vertically between porous bronze loading platens via a counterbalanced 10:1 ratio lever loading system.

The base plate and lower platen are rotated at a speed of 1.2 degrees per minutes via a speed motor and worm-drive gear box, causing the sample to shear close to the upper platen which is roughened to prevent slip. Settlement of the upper platen during shear is monitored via a sensitive dial gauge on the top load hanger. A pair of matched load rings assembled to the brackets that can be swung horizontally is locked in right angle to the outer bearing stops of the torque arm assembly that is attached to the top platen. The measurement of the shear stress is manipulated from the proving ring gages that in fact record the magnitude of the torque delivered by the torque assembly.

4.1.1 Calculations

Bishop[53] detailed the interpretation of the results obtained and the discussion on the influence of a variety of distributions of shear stress across the sample in the ring shear device. Since the sample is narrow with respect to the diameter a uniform stress distribution is assumed. The torque transmitted through the sample is given by:

$$T = \frac{2}{3}\pi\left(R_2^3 - R_1^3\right)\tau \qquad (4.1)$$

Where R_1 and R_2 are respectively inner and outer sample radii in mm. (or in.). τ is the shear stress in MPa (or lbf/in^2).

Since the torque is given by the average load on the proving rings denoted by F Newton (or lbf) multiplied by the distance L mm. (or in.) between them, then the equation is as follows.

$$T = \frac{(F_1 + F_2)L}{2} \qquad (4.2)$$

Manipulating the equations (4.1) and (4.2), we have,

$$\text{Shear Stress, } \tau = \frac{3(F_1 + F_2)L}{4\pi(R_2^3 - R_1^3)} \tag{4.3}$$

The normal stress acting on the failure plane is given by,

$$\text{Normal Stress } \sigma_n = \frac{P}{\pi(R_2^2 - R_1^2)} \tag{4.4}$$

Where, P is the normal vertical force Newton (or lbf) acting on the specimen.

The actual shear displacement rate d_r mm./min (or inch/min) is equal to the shear displacement d_h mm (or inch) divided by the elapse time t_e min.

$$d_r = \frac{d_h}{t_e} \tag{4.5}$$

and,
$$d_h = [\text{degree of rotation}] \left(\frac{\pi}{180^\circ}\right)\left(\frac{R_1 + R_2}{2}\right) \tag{4.6}$$

4.2 OBSERVATION

The oven dried sand specimens of specific gravity of 2.6 contained sands of uniform diameter size passing standard sieve no. 10 (2.0 mm.) and retained on no. 16 (1.18 mm.). As the soil was sheared three readings were taken manually at a specific time throughout the duration of each 5-hour test. It was observed that in general in the initial stage of the tests, readings for both of the

load dials were very unsteady with many sudden ‘jumps and falls’ and the effect that this had on the load dial was more pronounced at lower normal loads than at higher loads. However as the particular test proceeded, the readings then became steadier with the reduction and finally the absence of the erratic ‘jumps and falls’. It was also evident that during the ‘jumps and falls’ cracking sounds were heard coming from the container of the sand specimen indicating the process of fragmentation and crushing of the grains was taking place. Samples of the data collected for one of the tests are tabulated in the appendix A including the manipulation of the related calculations.

4.2.1 Crushing Effects on Friction Angle of Coarse Sand

The collected data provides the following observations for the samples in terms of the strength of the sheared granular material. At stress value of 15 kPa the granular specimen in Figure 11(b) shows a distinct interlocking peak characteristic similar to those observed in a dense sand laboratory testing at the earliest stage of shearing. The peak friction angle was 37.6 degrees. However for the plot in Figure 11(a), the interlocking feature as illustrated earlier in Figure 6 was absent when a very high value of normal stress of 1374.3 kPa was applied. The plot seems to characterize identical feature to those laboratory direct shear tests of loose sands. In the actual case however the interlocking action continues until the shear force becomes constant. The friction angle obtained from the plot at this point provided a lower value of 28.6 degrees. The values of the calculated angle of friction for each of the test are shown in Table 2.

(a)

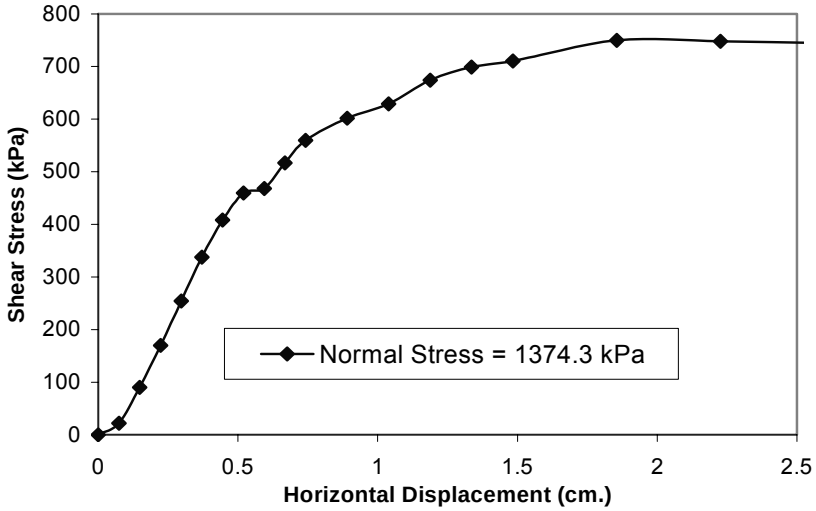

(b)

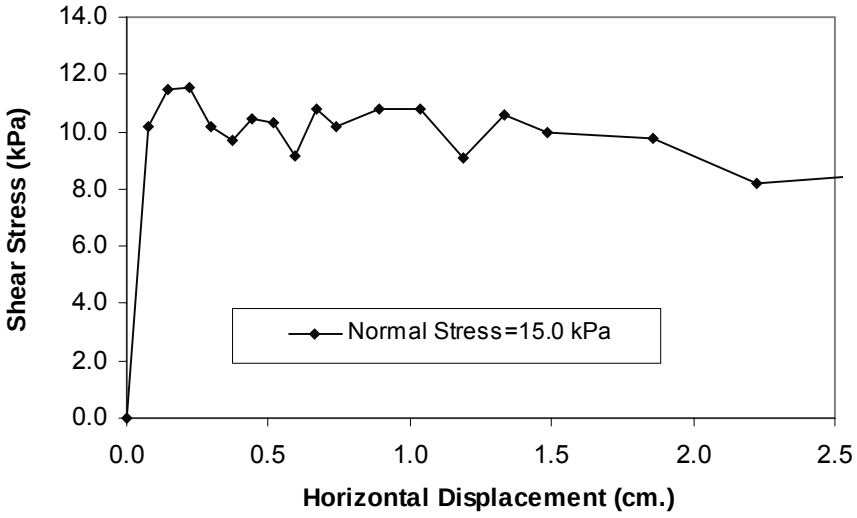

Figure 11 Shear Stress–Displacement Relationship For (a) Maximum and (b) Minimum Normal Stress in the Ring Shear for Coarse Sand (1.6 mm.)

Table 2 Variation of Angle of Internal Friction ϕ with the Confining Normal Stress in the Ring Shear Tests

Test	N (kg)	σ (kPa)	τ_{max} (kPa)	ϕ_{max} (degree)	Ave.ϕ (degree)
0	0.00	0.00	0.00	0.0	0.0
1	6.11	14.96	11.53	37.6	37.6
2	23.76	58.19	35.89	31.7	32.1
3	41.12	100.71	58.35	30.1	30.6
4	81.12	198.68	107.24	28.4	29.0
5	103.76	254.13	167.33	33.4	31.4
6	121.12	296.65	156.55	27.8	29.9
7	143.76	352.09	201.72	29.8	29.9
8	161.12	394.61	205.62	27.5	29.1
9	183.76	450.06	227.49	26.8	28.5
10	201.12	492.58	268.75	28.6	28.5
11	223.76	548.03	283.39	27.3	28.2
12	321.12	786.48	408.86	27.5	28.0
13	401.12	982.42	506.39	27.3	27.7
14	481.12	1178.35	634.40	28.3	27.9
15	561.12	1374.30	749.80	28.6	28.1

The Data displayed in Table 2 shows that the angle of internal friction decreases with the increase in normal stress. At lower values of normal stresses at which condition the study is more relevant, the plots in Figure 12 show the difference between the internal friction angles at various normal stresses, indicating a curved Mohr failure envelope. Similar observations were also recorded by Clements[3] in his earlier Casagrande shear box tests related to rock fragments as shown in the following Table 3.

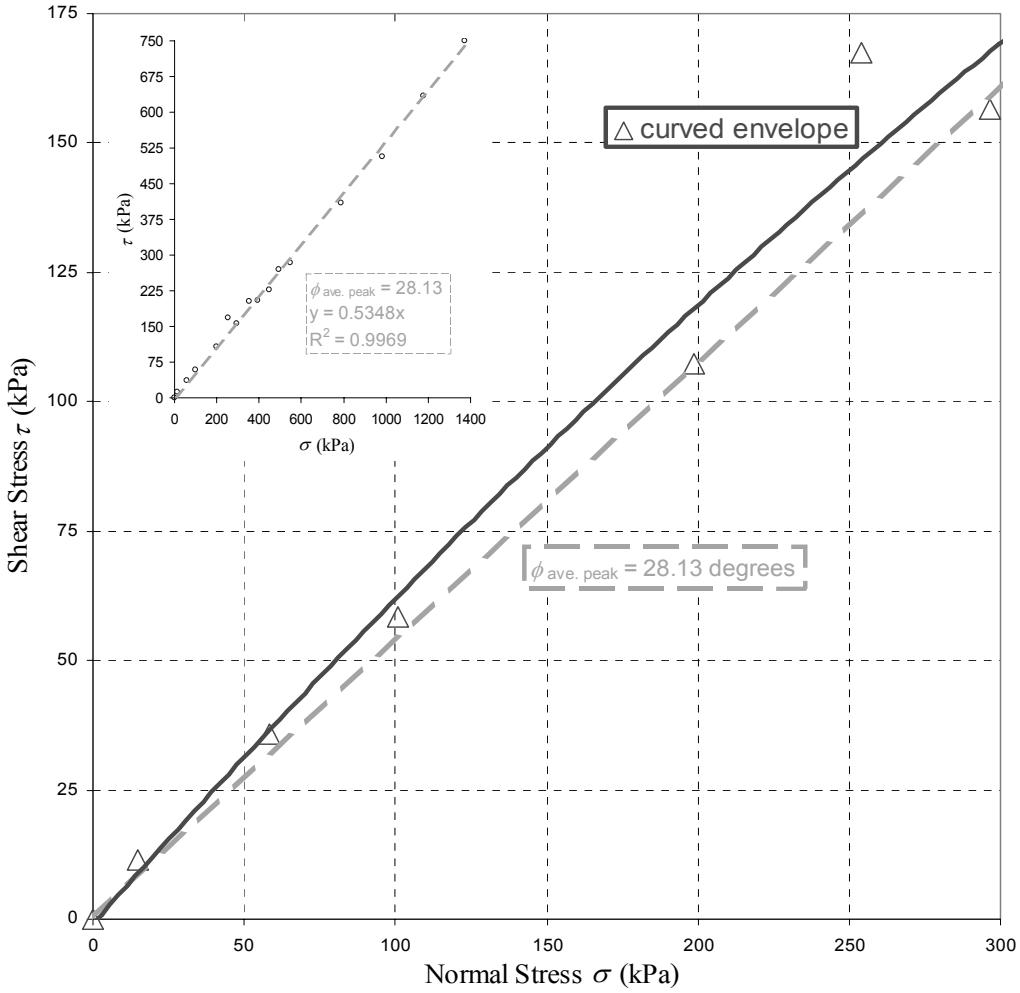

Figure 12 A Curved Mohr Failure Envelope for Shallow Foundation Condition from Torsional Ring Shear Tests

Table 3 Shear Box Test Results on Internal Friction Angle ϕ [From Ph.D. Dissertation by Clements[3]]

	Normal Stress 39.12 kPa	
Fraction	Shear Strength (kPa)	Internal Friction ϕ
-1.18+0.6	40.43	45.94°
-0.6+0.3	35.19	41.97°
-0.3+0.15	34.44	41.36°
-0.15	36.98	43.39°

4.2.2 Grain Size Distributions

In all the tests, the samples initially placed in the shear box are made up of one size granular material. After a specimen has undergone the shearing failure they were taken out and sorted by mechanical sieving apparatus in accordance to ASTM D 422(1). For each sieving exercise the shaker was run for 10 minutes. The results of the sieve analysis of some the specimens are shown in Figure 13.

The grain-size distributions of the sheared specimens indicate a departure from a uniformly distributed condition to a well-graded condition as the normal stresses increase. The percentage finer for particles of size 1.18 mm. is only 20% at 15.0 kPa. At 58.2 kPa it jumps to 44%, and at 100.7 kPa it is 56%. However from the point where the normal stress is 450 kPa and continues further to 1177.8 kPa the increase in percentage of particles finer than 1.18 mm. is not very significant. There is on the other hand a gradual increase of percentage finer for the very fine fragments of 0.075 mm. with respect to the increase of the normal stresses. In relation to the

grain size, the peak friction angle for specimens containing larger percentage of coarse grains as observed in Table 2 gives higher values of ϕ from 37.6° to 31°, than the ones with larger amount of fine particles with ϕ around 28°.

Images in Figure 14 show the fragment composition of 4 of the tested samples. It is noted that presentation of cumulative plots take away the bimodal characteristics of the density function plot and that they are somewhat similar to the PSD.

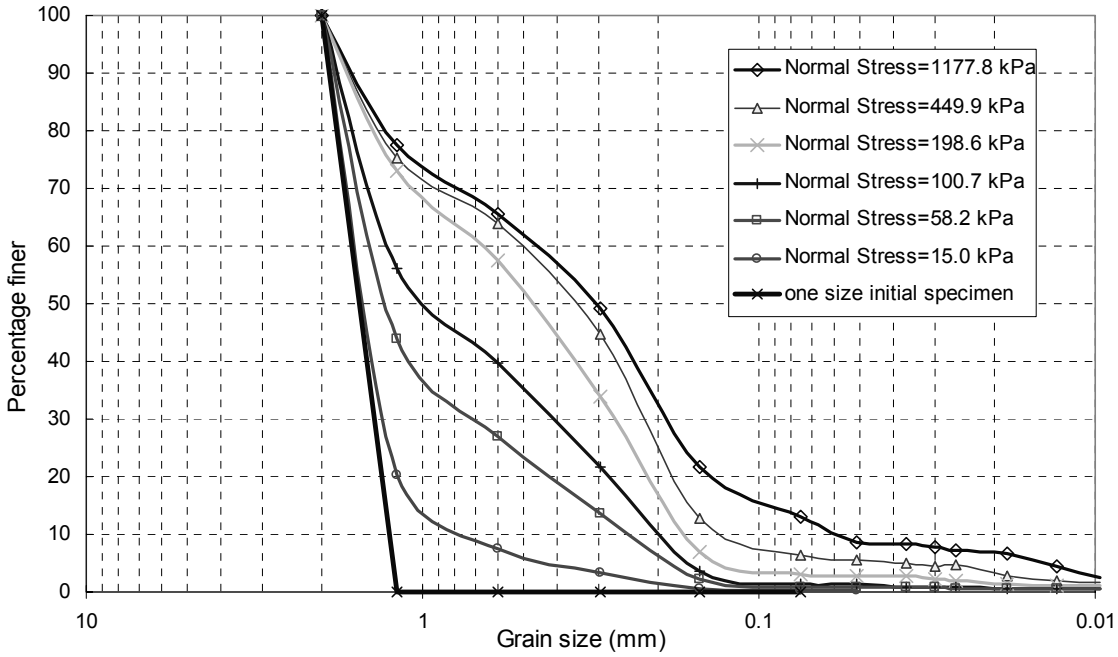

Figure 13 Cumulative Grain Size Distributions (PSD) for Crushed Coarse Sand

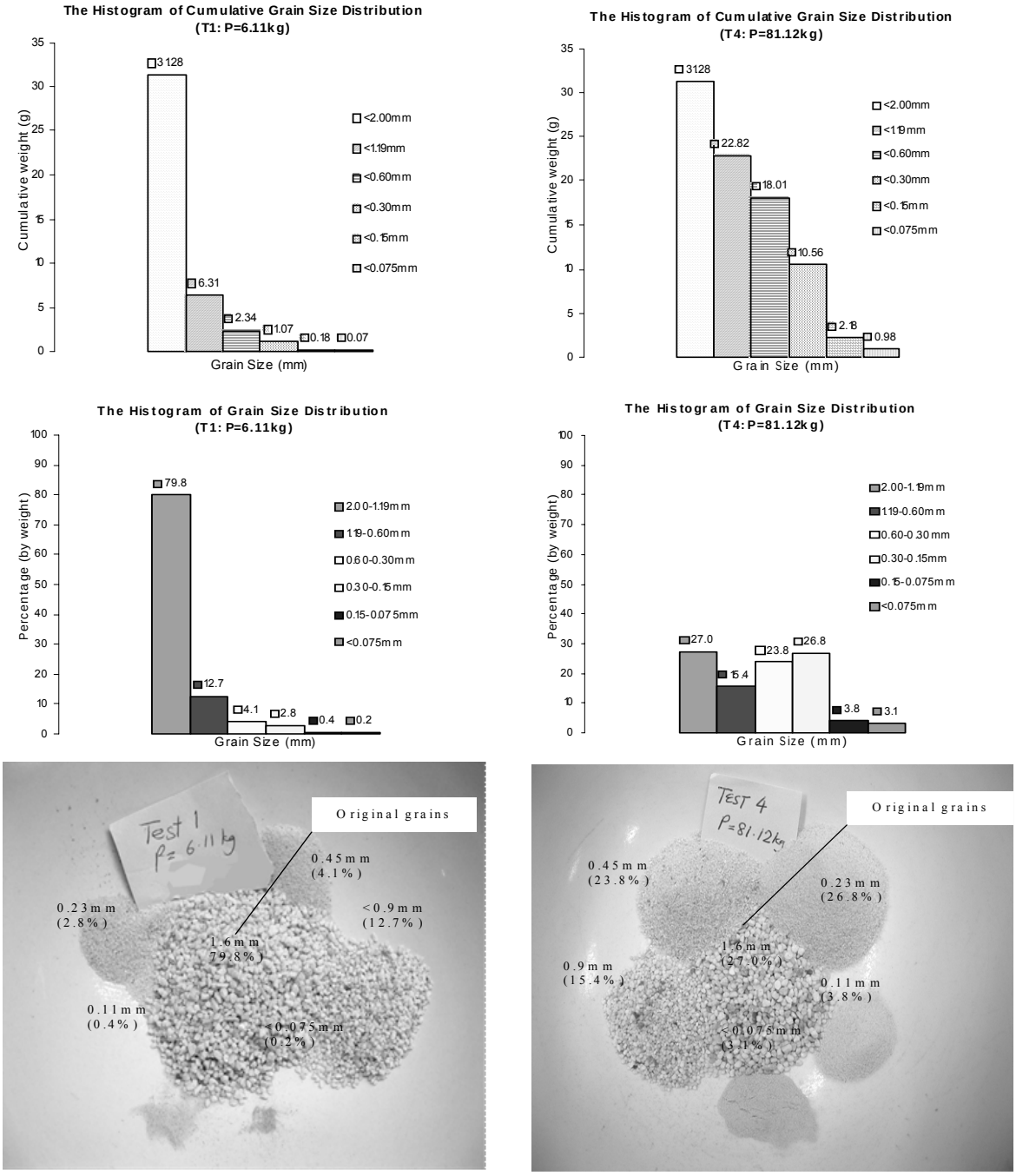

(a) (b)

Figure 14 Crush Composition for the Respective Load Intensities

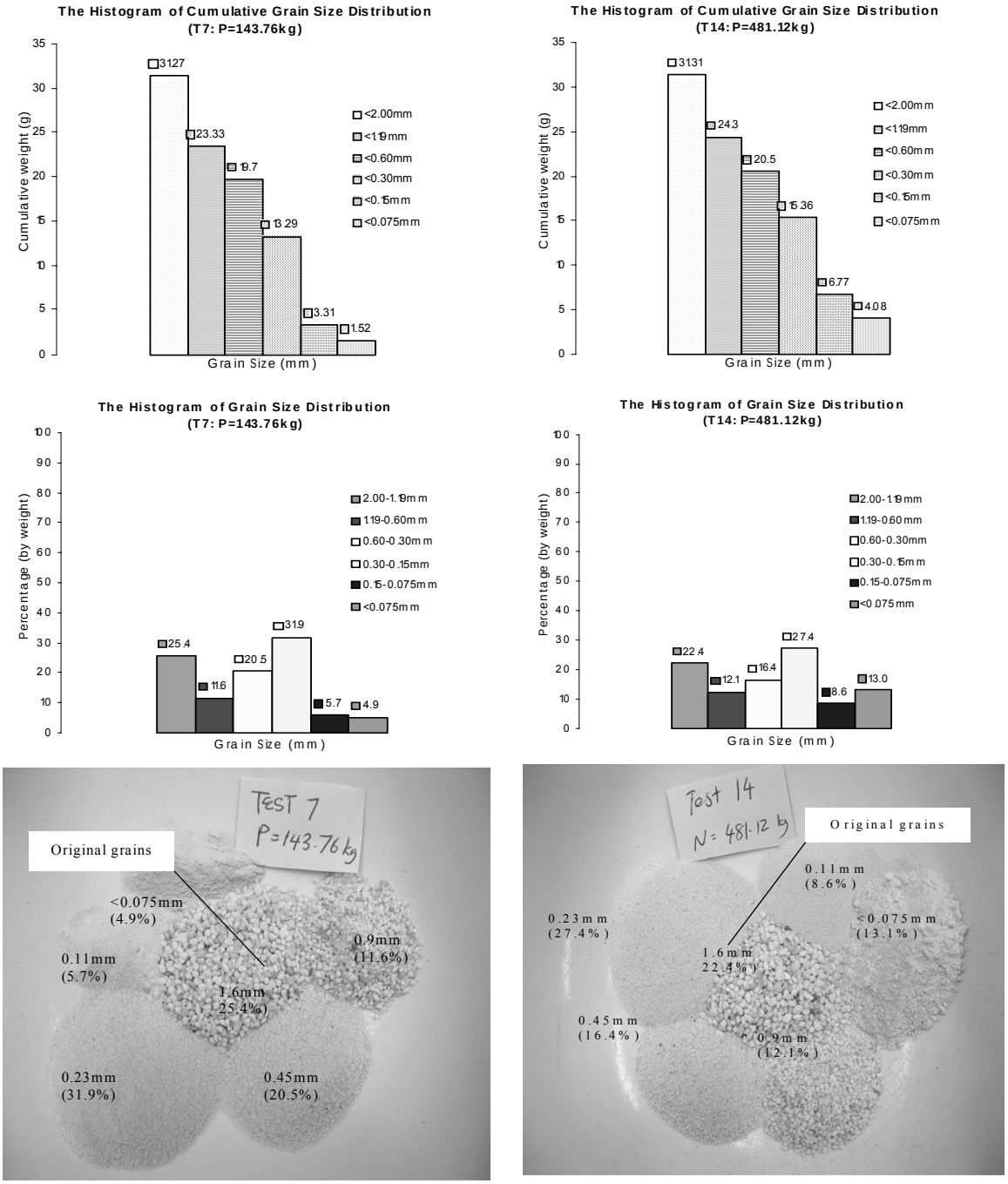

(c) (d)

Figure 14 (continued)

4.2.3 An Empirical Evaluation of Hydraulic Conductivity

As we have indicated earlier in Table 1, the values of hydraulic conductivity can be deduced empirically if the grain size distribution is plotted and the particle size at 10% finer or 15% finer is obtained. The following is the relation of the hydraulic conductivity *k* values using the Hazen equation,

$$k = C(d_{10})^2 \tag{4.7}$$

Using the equation (4.7) the values of hydraulic conductivity can be calculated as the effective diameter of the sand specimens at 10% finer is obtained from the grain-size distribution curves. In the condition where an increase in the normal pressure resulted in a corresponding increase in the shearing stress, it is found that greater amount of fragments are produced. The consequence of this is that the hydraulic conductivity capability of the soil is reduced to a very large degree as indicated in Table 4.

Table 4 Values of The Hydraulic Conductivity *k* in Relation to Changes in Grain Size Distribution

Test	Normal Stress σ (kPa)	d_{10} (mm)	*k* (cm/sec)
1	15.0	0.740	54.76
2	58.2	0.240	5.76
3	100.7	0.200	4.00
4	198.7	0.165	2.72
5	254.1	0.155	2.40
6	296.7	0.152	2.31
7	352.1	0.150	2.25
8	394.6	0.135	1.82
9	450.1	0.125	1.56
10	492.6	0.115	1.32
11	548.0	0.100	1.00
12	786.5	0.077	0.59
13	982.4	0.082	0.67
14	1178.4	0.060	0.36
15	1374.3	0.062	0.38

4.3 FRACTAL DIMENSION OF FRAGMENTED COARSE SAND

Fifteen specimens containing similar diameter of coarse sand particles subjected to increasing values of normal loads and shearing in the Bromhead Torsional Ring Shear apparatus produced fragmented coarse sands of varying sizes. They were mechanically sieved in the laboratory and the results of some of the tests were plotted in the form of grain size distribution curves as illustrated in Figure 13.

Transforming the same data the following Figure 15 demonstrates the exercise involved in obtaining the fractal fragmentation values in relation to the fragmentation process that took place when normal stress was at 15 kPa (Normal load P=6.1 kg.), 100.7 kPa (P=41.1 kg.), 449.9 kPa (P=183.8 kg.) and 1177.8 kPa (P=481.1 kg.) respectively.

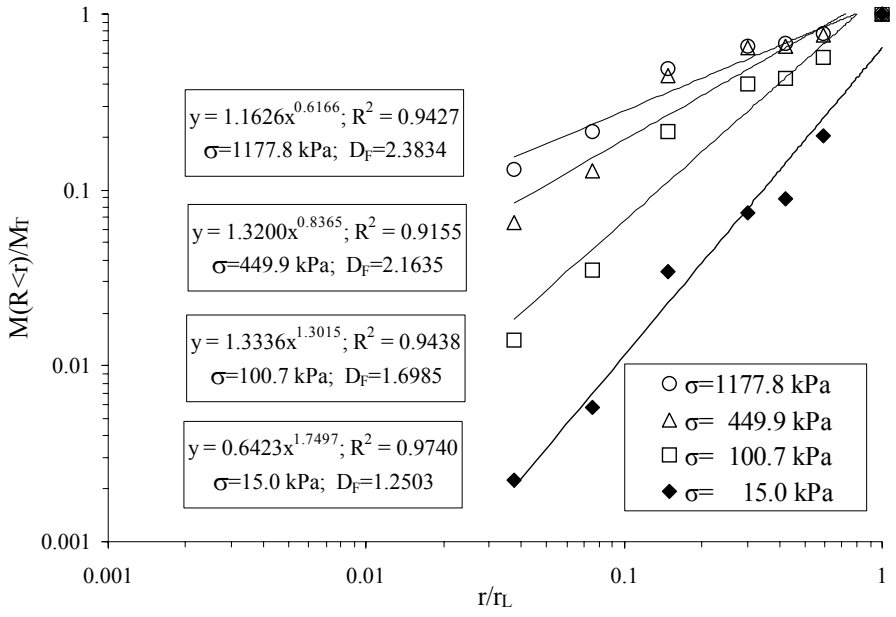

Figure 15 Fractal Fragmentation Dimension D_F for Crushed Coarse 1.6 mm. Quartz Sand in Ring Shear Test

A sample of data of the sieve test is presented in the Appendix A and the exercises involving the manipulation to obtain M ($R<r$)/M_T and r/r_L is also demonstrated. As the result of quantification, fragmentation in all the tests can now be presented in numerical values as illustrated in the following Figure 16.

The observed fractal of the four tested samples in the above figures show an increase in fragmentation with the increase of the applied normal stress in the Ring Shear. In addition, the relationship as observed indicates that the rate of increase in fragmentation of the granular soil is highest in earlier stage and somewhat reduced to a minimal approaching $D_F = 2.3$ as a high shear stress of about 0.5MPa is achieved.

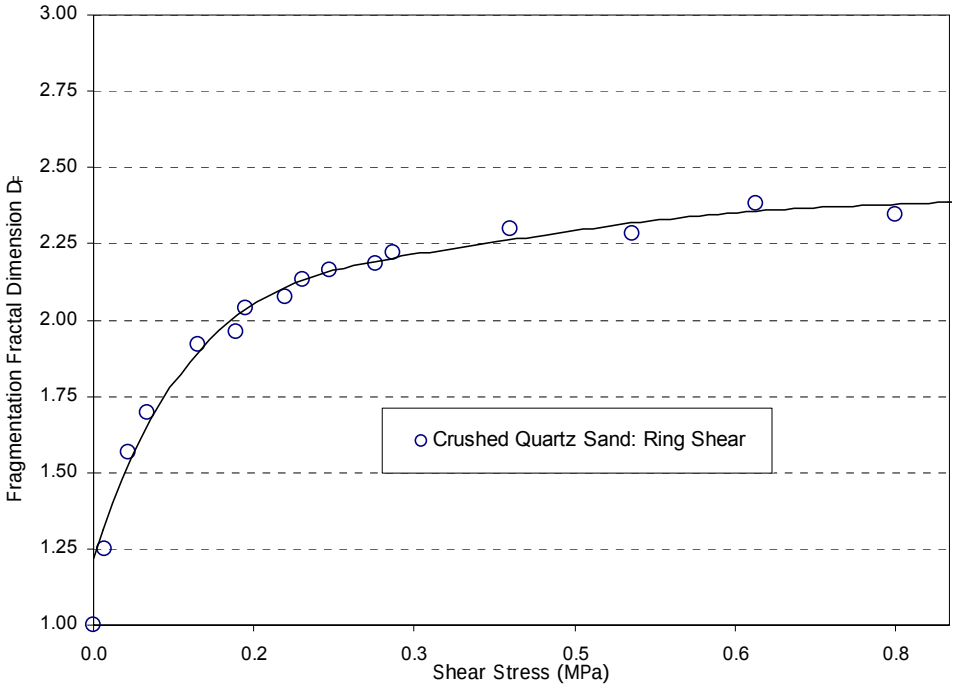

Figure 16 Changes in Fractal Dimension of Sand Subjected to Ring Shear Tests

At lower normal stresses, as granular particles slide and rolls, crushing at point of contact of small included-angles take place to a point until the critical stress is less than the strength of the material. The amount of fragmentation is minimal. As the applied stresses increase, the particle is further broken because at each time the additional stress again exceeds the critical stress of the material. Consequently, the number rough pointed surface is becoming less and with the increase in smaller fragments there is an increase in the integral area of contact. And thus reducing the stresses at point to point contact as now the some of the larger sand grains are 'floating' and surrounded by finer rock fragments. It is also observed that as a particle is broken into smaller and smaller elements it becomes harder to continue breaking the particle until it reaches a point that it ceases to break any further. The process of fragmentation of the sand particles can be related to the diagrams illustrated in Figure 17 indicating the stages of the action of the smaller fragments filling the voids.

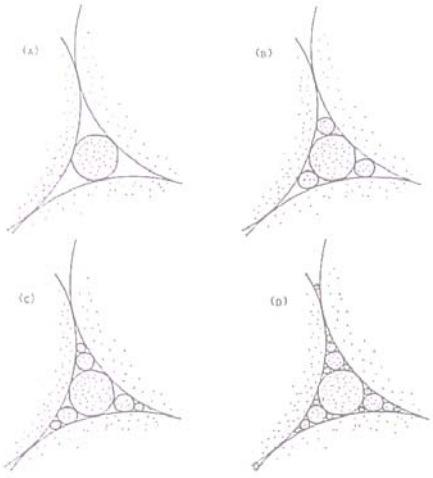

Figure 17 A Pore Filled by Fractal Soil[54]

4.4 AN ANALYSIS ON THE FRACTAL DIMENSION

The plots on Figures 15, 16 and 17 reveal a number of important aspects of fragmentation of granular material concerning fractals. Accuracy on the assumption of fractal self-similarity of fragmentation with respect to the formation of the smaller fragmented particles within the tested samples can be seen as the data shows a close-fit to the power-law giving very good correlations (with R^2 greater than 90 percent). Secondly, the changes experienced by the sand under a combination of normal and shear stresses as illustrated in the diagrams explain the reason why the hydraulic conductivity of the material is reduced as the pores within the sample are gradually being filled by smaller and smaller grains.

As explained earlier, it can be seen that the area of contacts increases exponentially and hence the exerted stresses is more uniformly distributed, thus reducing the effective stress to overcome the material strength rendering lesser and lesser amount of material being crushed.

With the tests data on normal and shear stresses subjected to the soil, Mohr failure envelopes can be obtained and hence the internal friction angle of the material. As discussed earlier, the internal friction angle of the granular material is a very important component of the strength characteristics of the material. If the friction angle is found to be high than it is indicative of the strength of the material. Figure 18 shows interesting relationships of the fractal fragmentation dimension of the sand with respect to the hydraulic conductivity (Hazen) and the strength of the material.

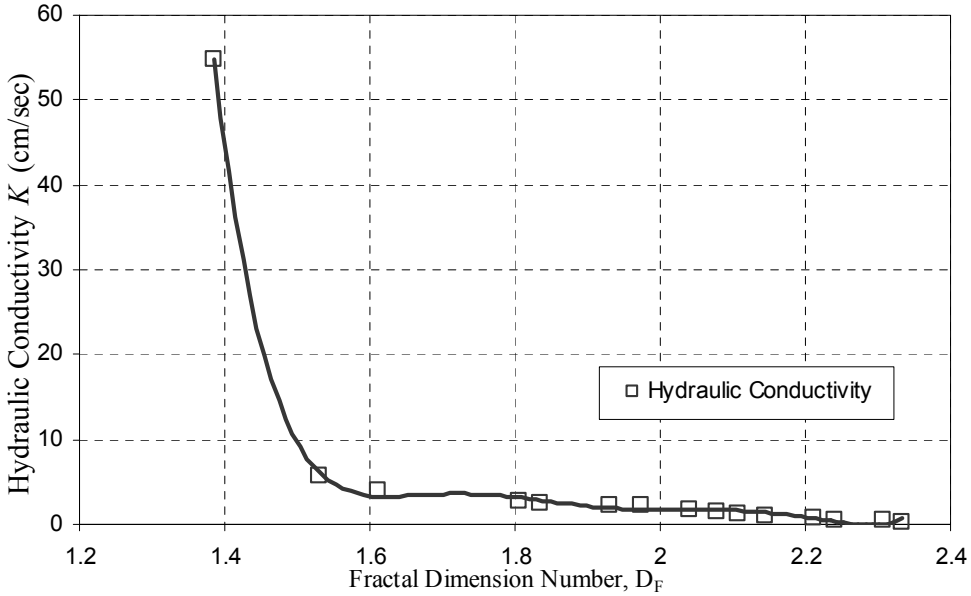

(a)

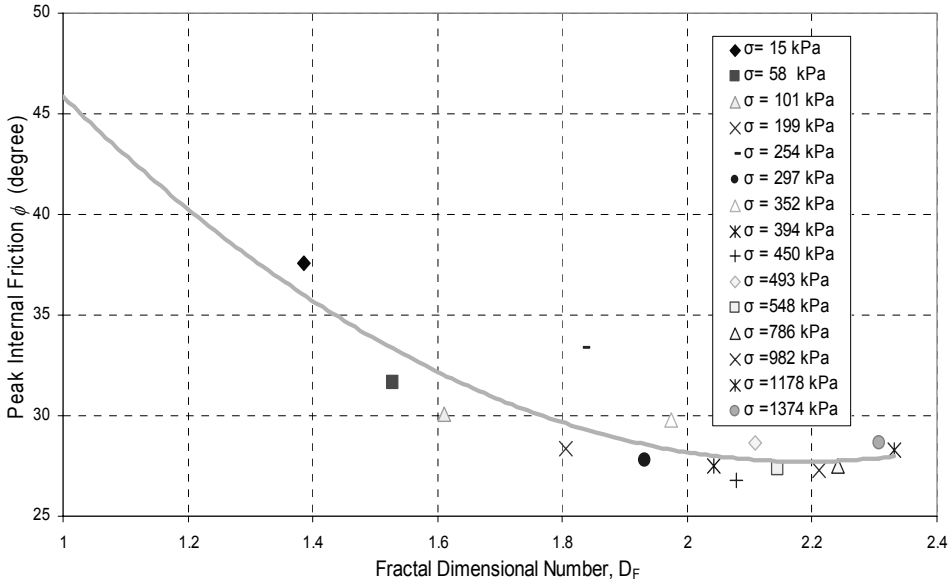

(b)

Figure 18 Changes in (a) The Hydraulic Conductivity and (b) The Angle of Internal Friction of Sand in Relation to Fractal Dimension in Ring Shear Tests

The previous observation reveals that when subjected to smaller stresses at smaller fractal dimensions it was the larger particles (size) that dominate the grain size distribution and vice versa. When these larger particles are in contact to each other it is much harder for these particles to roll over one another, as they need larger displacement to overcome the resistance. Also at this particular juncture due to the dominating scenario of the point-to-point contacts involving the larger particles, the interlocking effect on the friction angle is substantial.

However, as more crushing takes place, finer fragments begin to displace the coarser particles. To overcome resistance the fine fragments can slide or roll over one another without requiring too much effort, as the vertical ride is smaller. As a result, the effect of interlocking phenomena is reduced.

4.5 FRAGMENTATION IN DIFFERENT TYPE OF SANDS

Beside the Quartz sand, crushing of the Calcareous and the Ottawa Sand were also carried out using the Ring Shear Apparatus. Similar preparations for shearing these materials were conducted. It is interesting to note that under magnification the structural form of the materials differs substantially. The photograph of the materials in the following Figure 19 as captured under a microscopic camera, reveals some differences in the structural formations of the (a) Ottawa, (b) Quartz and (c) Calcareous sand with average diameter 0.7 mm.

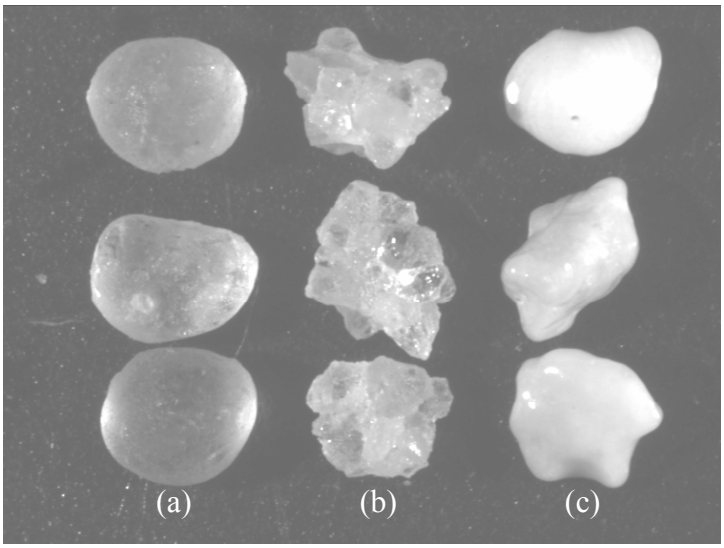

Figure 19 Structural Features of (a) Ottawa,(b) Quartz and (c) Calcareous Sand

The characteristic of fragmentation of the three materials is analyzed from the result of the Ring Shear test as they are subjected to 200, 300 and 400 kg normal load. Torsion shear force is recorded at various intervals and the corresponding shear stresses are obtained. The failed samples are then analyzed by mechanical sieve tests, data of which is used for the PSD plots. Fractal dimensions are then calculated as the data was transformed on the log-log scale. Photographs of the evolution of fragmentation of the sands in the Ring Shear tests with sizes related to the sieve openings are shown on Figure 20. The log-log scale plots of the transformed sieve tests data as presented on Figure 21 provide important information to be used in a discussion on the characteristics of the materials due to the crushing phenomenon.

(a)

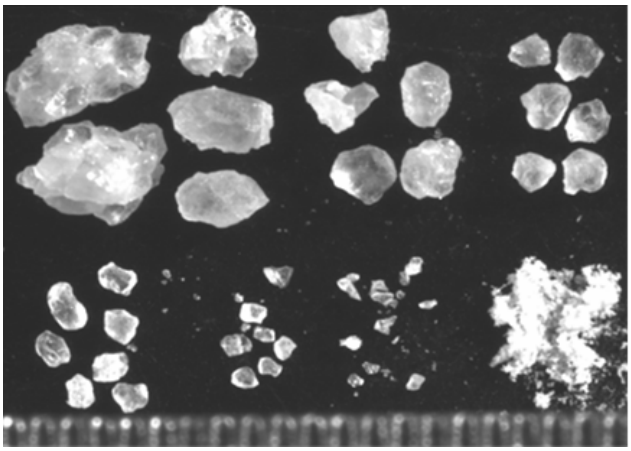

(b)

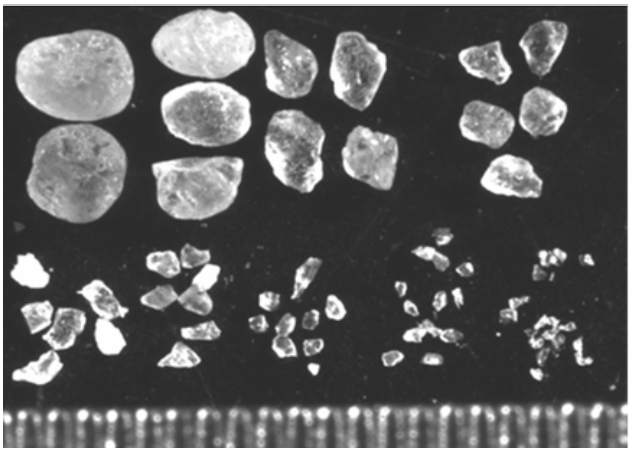

(c)

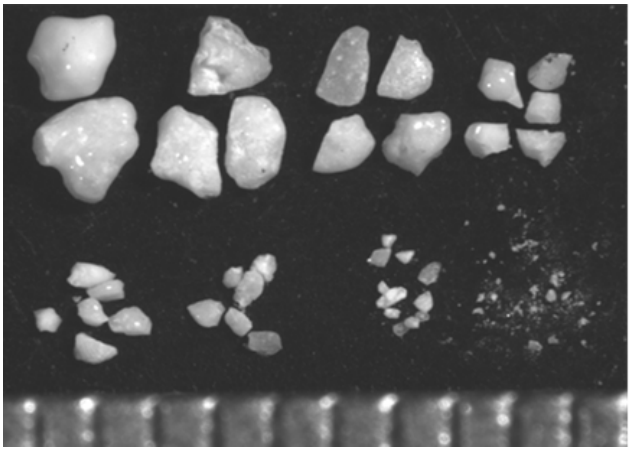

Figure 20 Fragmentation of (a) Quartz, (b) Ottawa and (c) Calcareous sands after Ring Shear Test

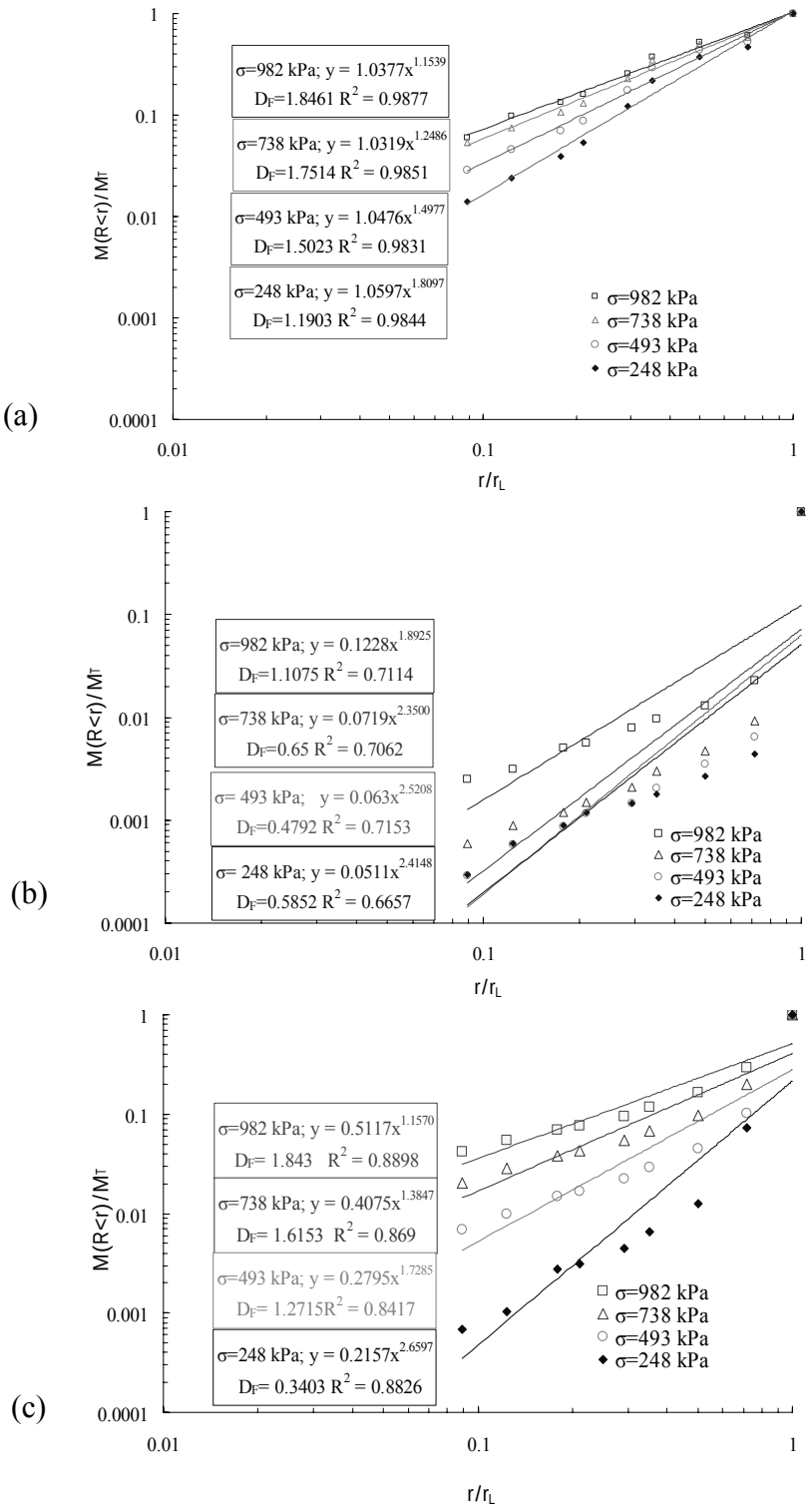

Figure 21 Evaluation of Fractal Fragmentation D_F for (a) Quartz, (b) Ottawa and (c) Calcareous Sand

4.5.1 Observation

The Ring shear tests provide interesting information regarding the shear stresses (τ) of the materials and the fractal fragmentation dimension of the crushed sands and these are summarized in Table 5 and plotted in Figures 22 and 23 as follows.

Table 5 Summary of Test Results

	Calcareous sand		Quartz sand		Ottawa sand	
	τ(kPa)	D_F	τ(kPa)	D_F	τ(kPa)	D_F
P=100kg (σ = 248 kPa)	69.3	0.3403 (R^2=0.883)	121.7	1.1903 (R^2=0.984)	97.4	0.5852 (R^2=0.666)
P=200kg (σ = 493 kPa)	142.0	1.2715 (R^2=0.842)	219.53	1.5023 (R^2=0.983)	209.4	0.4792 (R^2=0.715)
P=300kg (σ = 738 kPa)	178.8	1.6153 (R^2=0.869)	333.3	1.7514 (R^2=0.985)	331.9	0.6500 (R^2=0.706)
P=400kg (σ = 982 kPa)	263.2	1.8430 (R^2=0.890)	464.4	1.8461 (R^2=0.988)	400.6	1.1075 (R^2=0.711)

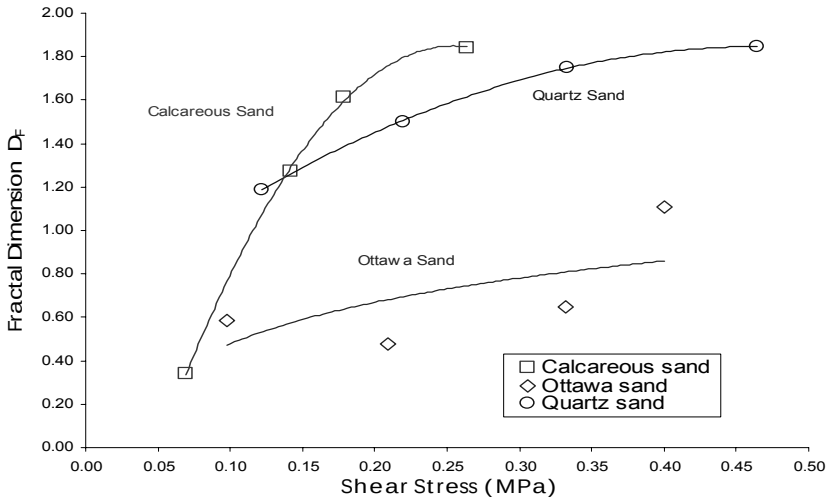

Figure 22 Fractal Fragmentation Dimension in Relation to The Shear Stresses of Different Sands

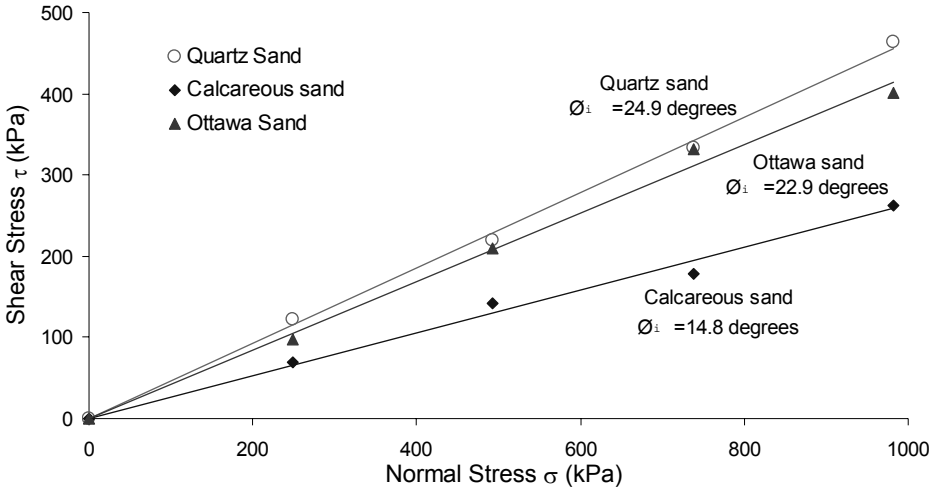

Figure 23 Shear Strength of Quartz, Ottawa and Calcareous Sand (average diameter 0.72 mm) from Ring Shear Test

It was observed that the crushing characteristics of the sands differ in terms of the fragments produced. The angular structure of the Quartz sand produces a great deal of fines at every stage of the crushing. The amount of fragments produced in the sub-angular Calcareous sand was less and minimal amount was obtained from the round-shaped Ottawa samples. The plots on Figure 21(a) show very good-fit of the data and the power-law with high degree of correlations ($R^2 > 0.98$). At the same loading conditions the Calcareous and the Ottawa indicated less and least agreement to the power-law respectively. The conclusion from the observation is that while fragmentation of Quartz was fractal similar features were absent from Calcareous and Ottawa sands.

The fact that the Ottawa sand is a very hard material to crush is demonstrated throughout the experiments. Extremely small amount of fines were produced in all the tests except at the highest normal stress of about 1 MPa. The Mohr-coulomb plots in Figure 23 verify this fact as the angle of friction is 22.9º as compared to Quartz at 24.9º. Although Quartz sand is not as hard as the Ottawa and crushes more easily, the sand demonstrates high resistance in shearing due to its angular physical structure. From the data observed, there seemed to be a trade-off between the physical structure and the material toughness between the two materials.

4.6 CONCLUSION

When the dry granular material is subjected under normal and shear stresses fragmentation takes place. The main reason for this phenomenon is that the point-to-point contacts involving the larger particles are subjected to a much higher stress than the critical strength of the material and hence, the material yields.

Fragmentation continues to a stage when the point-to-point contacts involving a particle reach an optimal condition when crushing appears to cease.

It was observed that as the finer fragments increases when subjected to high normal and shear stresses the value of the incremental fractal fragmentation dimension decreases and eventually arrives at almost a constant.

In the laboratory tests on coarse Quartz of 1.6 mm diameters, the shear stress to overcome the material strength of the dry sand increases almost in direct proportion to the normal stress at higher value of normal stresses. However at lower value the shear force required is greater with respect to the 'average normal stresses'. This implies that when subjected to low stresses when the larger particles dominate, the strength of the material appears to be higher exhibiting higher internal friction angle. The strength of the material gradually reduces as more and more fine fragments enter the system. It also appears that the internal friction angle of the material stabilized at an optimum point when a further increase in stresses will no further affect the fractal fragmentation of the material.

Experiments on 0.72 mm. diameter of Quartz and Ottawa sand reveals higher strength in the former with angle of friction equal to 24.9º while the Ottawa exhibits lower friction angle of 22.9º. The tests indicate the greater effect of the physical structure of the sands in relation to their strength.

5.0 AN INVESTIGATION ON THE ANGLE OF REPOSE OF A BINARY GRANULAR MIXTURE

The angle of repose is the slope at which a heap of soil naturally forms. It is a special characteristic feature of a granular material and has useful applications in the civil and structural as well as other branches of engineering. To understand the effects of finer fragments within a system, it is expected that a laboratory testing procedure such as the one incorporated in this study will encourage innovation and flexibility when faced with the need to scrutinize arrangement of a specified particulate system such that the objectives of the investigation can be realized.

As explained in the earlier chapter, the idea that the value of the angle of repose of a granular material has been generally regarded as an approximation to the angle of friction of the material has found its way to be generally accepted by many earlier researchers. There have been very few investigations with much lesser emphasis has been done in relation to crushing phenomena of the granular soil that may affect its angle of repose. In light of the present investigation on the effect of crushing and fragmentation on the engineering properties of the granular material, it is only fitting to revisit the subject of angle of repose of the material and to reevaluate the findings of the past with the current understanding of the characteristics involving fragmentation in the granular system.

The investigation begins by introducing a particulate system in a statically equilibrium condition and using assumptions in the empirical Rankine equation in order to set up a theoretical analysis on the observations acquired from the laboratory findings.

5.1 DEVELOPMENT OF THE ANGLE OF REPOSE EQUATION

When considering angle of repose it is not exactly the same as relating a material to its angle of internal friction. This is simply because unlike the angle of internal friction, whenever an angle of repose is measured the soil heap that is formed is in direct contact with a basal material. Assuming that the base is frictionless then it is hard to imagine observing a similar formation of heap of earth could be constructed to give the expected value of the angle of repose. Due to this consideration, the angle of repose is to be investigated using two different basal materials with distinct frictional properties.

5.1.1 Assumptions and Limitations to the Problem

In developing the theoretical equation for the angle of repose, the basal friction is considered an integral part of the three important components contributing towards the stability of the constructed soil cone and hence directly affecting the measured value of soil angle of repose. The other two components are related to the internal friction of the material and the slope of the soil that we term as the angle of repose. Several assumptions have first to be made so that a simplified statically determinate problem can be constructed and easily solved.

Assuming that as a heap of granular soil is constructed forming a perfect cone, at an instant of time, part of the slope that includes the toe is acting like a rigid triangular wedge

holding back the rest of the granular material like that of a straight back retaining wall in a simplified slope stability problem. In making this given condition, we are making the assumption that the failure of the system is due to sliding of the retaining wedge that is caused by the active lateral earth pressure exerted on the vertical wall of the wedge.

5.1.2 Slope Stability Problem of the Granular Cone

For a rigid wedge acting like a retaining wall with sloping granular material back fill, much in the same way of that dams a fluid reservoir or that holds the backfill as illustrated in Figure 24, the resistance to failure against sliding depends on a balance of forces between the lateral earth pressure and the basal friction resisting the sliding. The magnitude of the resistance of the basal friction is derived from the net normal forces in accordance to the Coulomb's theory of friction. The analysis however, assumes the only consideration is in the translation rigid wedge movement and ignores the rotational moment about the centroid of the mass.

When a Funnel Test for angle of repose is carried out for granular materials, a slope with an angle β is made with the base. And if the internal friction angle of the material is ϕ and the interface friction angle between the granular material and the base is δ a theoretical solution may be obtained to predict the values of β having known the values of ϕ and δ. The pressure on the vertical wall of the wedge with a sloping backfill is acting in a direction parallel to the slope as described by The Rankine Active Earth Pressure theory asssuming frictionless wall. The following diagram illustrates the various forces acting in the system as discussed above.

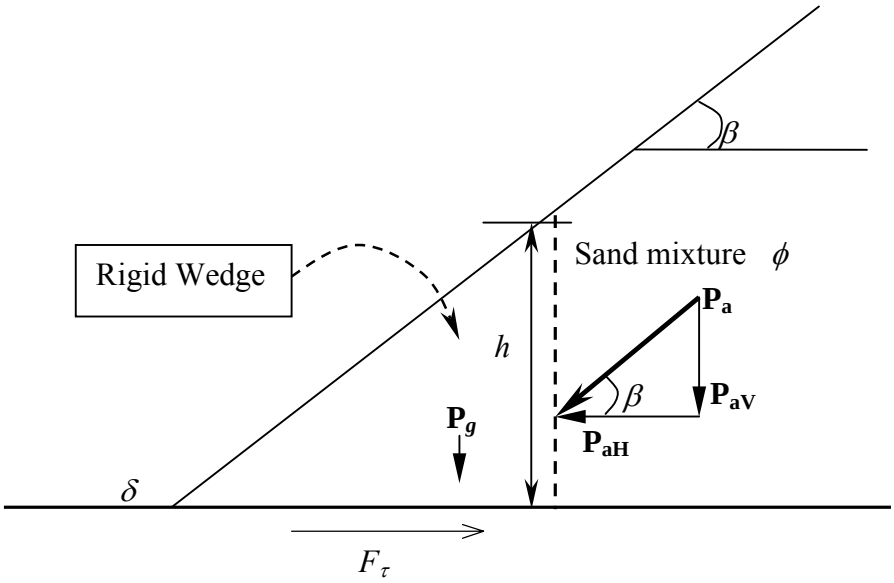

Figure 24 Forces Acting on A Wedge in the Angle of Repose Funnel Test

Rankine Active Earth Pressure is P_a,

$$P_a = \frac{1}{2}\rho g H K_a \tag{5.1}$$

where, K_a is the co-efficient of active earth pressure is given by,

$$K_a = \cos\beta \frac{\cos\beta - \sqrt{\cos^2\beta - \cos^2\phi}}{\cos\beta + \sqrt{\cos^2\beta - \cos^2\phi}} \tag{5.2}$$

When the system is in the equilibrium, the basal friction is equal to the horizontal component of the Rankine active pressure as such,

$$F_\tau = P_{aH} \tag{5.3}$$

According to Coulomb,

$$F_\tau = \sum N.(\tan \delta) \tag{5.4}$$

And the summation of forces acting normally $\sum N$, is the weight of the rigid wedge and the vertical component of the Rankine Active Earth Pressure giving equation (5.3) as,

$$F_\tau = [P_g + P_{aV}] \tan \delta \tag{5.5}$$

Therefore, $$[P_g + P_{aV}] \tan \delta = P_{aH} \tag{5.6}$$

And after substituting all the terms, giving,

$$\tan \delta = \frac{\tan \beta \cos^2 \phi}{2 + 2\sqrt{1 - \left(\frac{\cos \phi}{\cos \beta}\right)^2} - \cos^2 \phi} \tag{5.7}$$

5.2 COMPUTATION OF THE GENERAL EQUATION

The computation of the general equation for the angle of repose β assumes that the basal plane is inclining with an angle θ with the horizontal as shown in Figure 25.

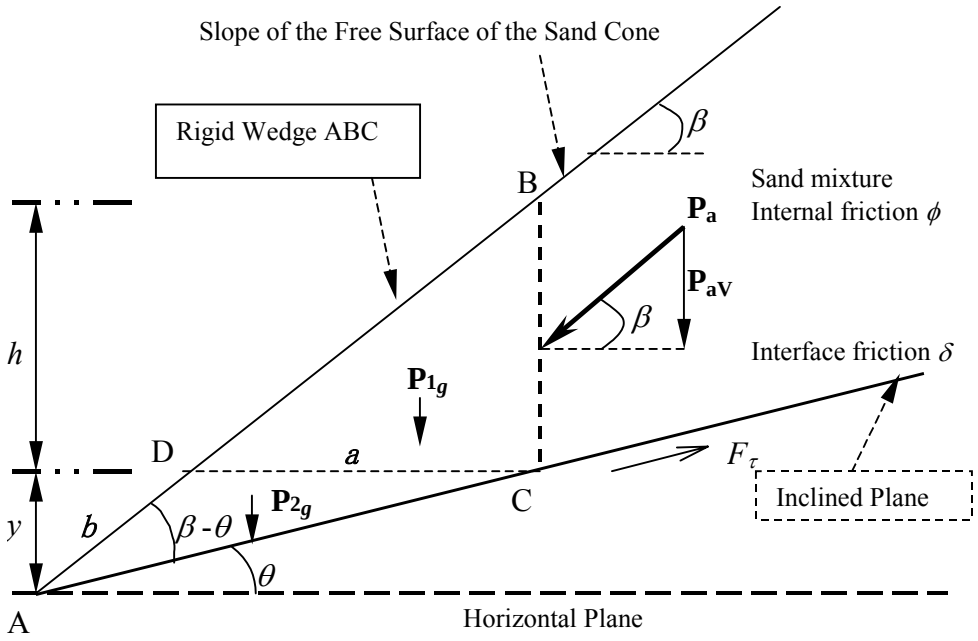

Figure 25 A Diagram Showing Angle of the Sand Cone on An Inclined Plane

Weight of rigid wedge ABC; $W_g = P_{1g} + P_{2g}$

Weight of BCD; $P_{1g} = \frac{\gamma}{2}(h \times a) = \frac{\gamma h^2}{2 \tan \beta}$

since $a = \frac{h}{\tan \beta}$

Weight of ACD; $P_{2g} = \frac{\gamma}{2}(y \times a) = \frac{\gamma h^2}{2 \tan^2 \beta} \cdot \frac{\sin \beta \sin \theta}{\sin(\beta - \theta)}$

since,

$y = b \sin \beta$ and $b = \frac{a \sin \theta}{\sin(\beta - \theta)}$

Therefore, total weight of rigid wedge ABC; $W_g = \frac{\gamma h^2}{2\tan^2\beta}\left[\tan\beta + \frac{\sin\beta\sin\theta}{\sin(\beta-\theta)}\right]$

Components of active pressure, $P_a = \frac{\gamma h^2}{2} K_a$

where,

The coefficient of active earth pressure, $K_a = \cos\beta \frac{\cos\beta - \sqrt{\cos^2\beta - \cos^2\phi}}{\cos\beta + \sqrt{\cos^2\beta - \cos^2\phi}}$

Parallel to inclined plane: $F_{PaT} = \frac{\gamma h^2}{2} K_a \cos(\beta-\theta)$……(5.8)

Normal to inclined plane: $F_{PaN} = \frac{\gamma h^2}{2} K_a \sin(\beta-\theta)$……(5.9)

Components of the weight of the wedge ABC W_g

Parallel to inclined plane: $W_{gT} = \frac{\gamma h^2}{2\tan^2\beta}\left[\tan\beta + \frac{\sin\beta\sin\theta}{\sin(\beta-\theta)}\right]\sin\theta$ ....……..(5.10)

Normal to inclined plane: $W_{gN} = \frac{\gamma h^2}{2\tan^2\beta}\left[\tan\beta + \frac{\sin\beta\sin\theta}{\sin(\beta-\theta)}\right]\cos\theta$ ……....(5.11)

The forces causing sliding of the wedge ABC: F_s = (5.8)+(5.10) = $F_{PaT} + W_{gT}$ …....(5.12)

The interface friction force resisting sliding $F_{f\tau}$

$F_{f\tau}$ = [summation of normal forces to the inclined plane=(5.9) + (5.11)] × tan δ

$F_{f\tau} = (F_{PaN} + W_{gN}) \times \tan\delta$ ……..……..……(5.13)

For the forces to be in the equilibrium condition:

Friction force resisting sliding $F_{f\tau}$ = Forces causing sliding of the wedge F_s

Dividing throughout by $\frac{\gamma h^2}{2}$ we have,

$$K_a \cos(\beta-\theta)+\left(\frac{1}{\tan\beta}+\frac{\sin\beta\sin\theta}{\sin(\beta-\theta)\tan^2\beta}\right)\sin\theta$$

$$=\left[K_a \sin(\beta-\theta)+\left(\frac{1}{\tan\beta}+\frac{\sin\beta\sin\theta}{\sin(\beta-\theta)\tan^2\beta}\right)\cos\theta\right]\tan\delta$$

Substitute for K_a

$$\cos\beta\frac{\cos\beta-\sqrt{\cos^2\beta-\cos^2\phi}}{\cos\beta+\sqrt{\cos^2\beta-\cos^2\phi}}\cos(\beta-\theta)+\left(\frac{\cos\beta}{\sin\beta}+\frac{\cos^2\beta\sin\theta}{\sin(\beta-\theta)\sin\beta}\right)\sin\theta$$

$$=\left[\cos\beta\frac{\cos\beta-\sqrt{\cos^2\beta-\cos^2\phi}}{\cos\beta+\sqrt{\cos^2\beta-\cos^2\phi}}\sin(\beta-\theta)+\left(\frac{\cos\beta}{\sin\beta}+\frac{\cos^2\beta\sin\theta}{\sin(\beta-\theta)\sin\beta}\right)\cos\theta\right]\tan\delta$$

to simplify the equation,

Let, $\cos\beta = A$; $\sin\beta = B$; $\cos\theta = p$; $\sin\theta = q$; $\sqrt{\cos^2\beta-\cos^2\phi}=\sqrt{D}$

Then,

$$\tan\delta=\frac{\frac{A-\sqrt{D}}{A+\sqrt{D}}(Ap-Bq)+\left[\frac{1}{B}+\frac{Aq}{B(Bp-Aq)}\right]q}{\frac{A-\sqrt{D}}{A+\sqrt{D}}(Bp-Aq)+\left[\frac{1}{B}+\frac{Aq}{B(Bp-Aq)}\right]p}$$

Since,

$$\cos(\beta-\theta)=\cos\beta\cos\theta-\sin\beta\sin\theta$$

$$\sin(\beta-\theta)=\sin\beta\cos\theta-\cos\beta\sin\theta$$

$$\tan\delta=\frac{\frac{A-\sqrt{D}}{A+\sqrt{D}}(Ap-Bq)+\left[\frac{(Bp-Aq)+Aq}{B(Bp-Aq)}\right]q}{\frac{A-\sqrt{D}}{A+\sqrt{D}}(Bp-Aq)+\left[\frac{(Bp-Aq)+Aq}{B(Bp-Aq)}\right]p}=\frac{\frac{A-\sqrt{D}}{A+\sqrt{D}}(Ap-Bq)+\frac{pq}{Bp-Aq}}{\frac{A-\sqrt{D}}{A+\sqrt{D}}(Bp-Aq)+\frac{p^2}{Bp-Aq}}$$

multiplying numerator and denominator throughout by, $\left(A+\sqrt{D}\right)^2(Bp-Aq)$

$$\tan\delta=\frac{\left(A-\sqrt{D}\right)\left(A+\sqrt{D}\right)(Bp-Aq)(Ap-Bq)+pq\left(A+\sqrt{D}\right)^2}{\left(A-\sqrt{D}\right)\left(A+\sqrt{D}\right)(Bp-Aq)^2+p^2\left(A+\sqrt{D}\right)}$$

but, $\left(A-\sqrt{D}\right)\left(A+\sqrt{D}\right)=\cos^2\phi$ and substituting the terms in trigonometry back into the above general equation, we have;

$$\tan\delta=\frac{\cos^2\phi\cos(\beta-\theta)\sin(\beta-\theta)+\sin\theta\cos\theta\left(\cos\beta+\sqrt{\cos^2\beta-\cos^2\phi}\right)^2}{\cos^2\phi\sin^2(\beta-\theta)+\cos^2\theta\left(\cos\beta+\sqrt{\cos^2\beta-\cos^2\phi}\right)^2}$$

Hence, the equation for the interface/basal friction on an inclined plane is equal to (Eq.I),

$$\tan\delta=\frac{\cos^2\phi\sin 2(\beta-\theta)+\sin 2\theta\left(\cos\beta+\sqrt{\cos^2\beta-\cos^2\phi}\right)^2}{2\left[\cos^2\phi\sin^2(\beta-\theta)+\cos^2\theta\left(\cos\beta+\sqrt{\cos^2\beta-\cos^2\phi}\right)^2\right]}\quad\text{.....(Eq.I)}$$

5.2.1 The Equation for the Special Condition

The earlier equation (5.7) can be verified by assuming the horizontal base as such; let the inclination of the base plane is zero, that is, $\theta = 0$. And we have,

$$\tan \delta = \frac{\cos^2 \phi \cos \beta \sin \beta + 0}{\cos^2 \phi \sin^2 \beta + \left(\cos \beta + \sqrt{\cos^2 \beta - \cos^2 \phi}\right)^2}$$

$$\tan \delta = \frac{\cos^2 \phi \cos \beta \sin \beta}{\cos^2 \phi \sin^2 \beta + \cos^2 \beta + \cos^2 \beta - \cos^2 \phi + 2 \cos \beta \sqrt{\cos^2 \beta - \cos^2 \phi}}$$

$$\tan \delta = \frac{\cos^2 \phi \cos \beta \sin \beta}{\cos^2 \phi\left(\sin^2 \beta - 1\right) + 2 \cos^2 \beta + 2 \cos \beta \sqrt{\cos^2 \beta - \cos^2 \phi}}$$

$$\tan \delta = \frac{\cos \beta \sin \beta \cos^2 \phi}{2 \cos^2 \beta + 2 \cos^2 \beta \sqrt{1 - \frac{\cos^2 \phi}{\cos^2 \beta}} - \cos^2 \beta \cos^2 \phi}$$

Dividing the numerator and the denominator throughout by $\cos^2 \beta$, we have,

$$\tan \delta = \frac{\tan \beta \cos^2 \phi}{2 + 2\sqrt{1 - \left(\frac{\cos \phi}{\cos \beta}\right)^2} - \cos^2 \phi} \quad \text{.....(Eq.H)}$$

which is in fact the special case equation where the basal plane is perfectly horizontal.

5.3 THE MATHEMATICAL MODEL AND LIMITATIONS

From the final equation (Eq. H) it is shown that the values of the angles, for internal friction, the interface basal friction angle and the slope angle of repose are all inter-related in a very complex manner. One of the reasons is that when using such empirically designed equation (where there are numerous in geotechnical engineering) the solution may have to be presented graphically in order to demonstrate and verify the validity of the results.

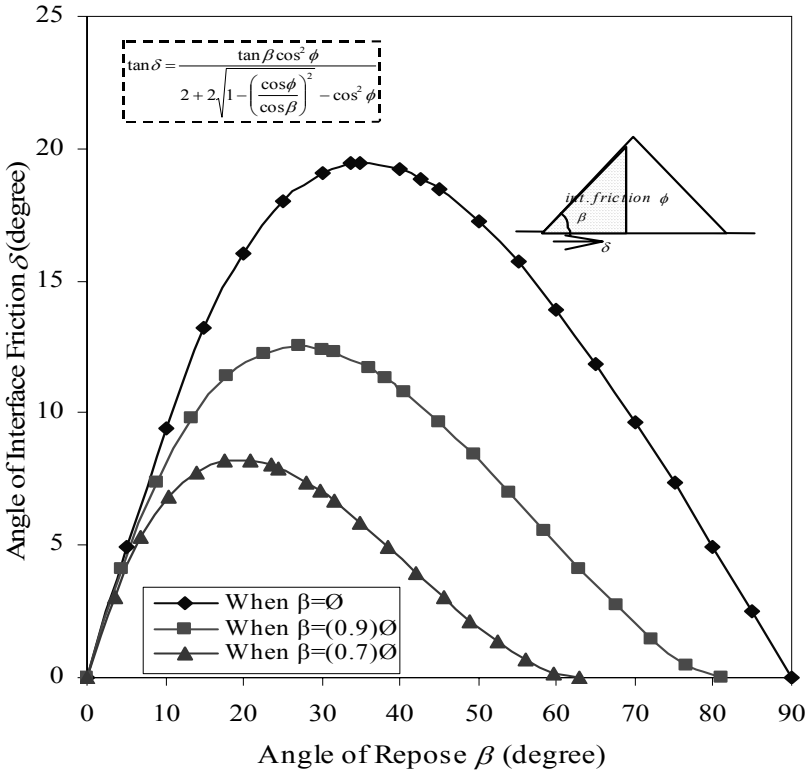

Figure 26 The Values of Interface Friction Angle with Varying Angle of Repose and The Corresponding Inter-granular Friction (Internal Friction) of The Material

The coefficient Rankine active pressure K_a and thus the equation H that was developed later indicated the important rule of thumb followed by the equation where the value of the angle of the slope β, that is also the angle of repose, cannot be greater than the angle of internal friction

ϕ. The three plots in Figure 26 illustrate this property. The plots in general also show that at lower values of angle of repose and angle of internal friction, the interface friction mobilized is small. Depending on the values of angle of repose and the respective angle of internal friction, maximum interface friction is mobilized in order to stabilize the slope when the repose angle is between 20 to 40 degrees. The maximum interface angle from the plot is 19.5° when the angle of repose is the same as the angle of internal friction at around 35°. And if the internal friction of the material is higher than this, only small interface friction is needed to stabilize the system. Thus far the theoretical equation seems to be logical to some degrees and therefore needed data from laboratory tests in order to validate it.

5.4 ANGLE OF REPOSE LABORATORY INVESTIGATION ON FRAGMENTED SOIL

When granular materials subjected to the loads fail in shear, fragmentation of the grains takes place. In this laboratory exercise Quartz sand made up of coarse and fine diameters is used to simulate the fragmented products of the failed material. The choice of introducing the binary mixture of coarse and fines are supported by the earlier findings that the composition of fines has significant contributions to the strength as well as hydraulic conductivity of a particulate. For the tests a large number of specimens are made having composition of fine sand (passing sieve mesh number 150) varying from 0 to 100%. The bases used comprise of a rough plane porous stone base of 8 inches wide and a very smooth plane glass plate 6 inches by 6 inches in dimension representing ground bases of high and low frictional values respectively. The magnified photos of the materials described are shown in Figures 27 and 28 as follows.

Figure 27 Coarse Sand, Fine Sand and Porous Stone Interface (35x magnification)

(a) 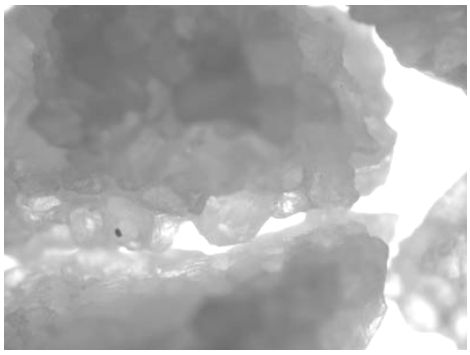

(b) 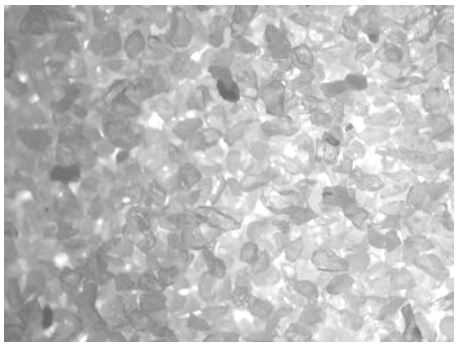

Figure 28 Materials in the Binary Mix (a) Coarse Sand (average 1.6 mm. diameter); (b) Fine Sand Passing (0.10mm.) (35x magnification)

5.5 THE FUNNEL TEST

The laboratory tests of numerous specimens were conducted according to the ASTM Standard Designation: C 1444-00; The Standard Test Method for Measuring the Angle of Repose of Free-Flowing Mold Powders. Due to the fact that the setup of the tests makes use of a funnel through which the sand is dropped as illustrated in Figure 29, the test is also called the funnel test. The spout opening of the funnel used was 0.214 in. located at a vertical height of 1.5 in. from the base. The base of a cone formation was measured using a caliper that measured to the nearest 0.001 in.

Two methods of measurement were conducted to ensure the accuracy of the data. The first is by direct measurement of the slope angle of repose using a protractor. For a specific sample mixture, a set of 5 specimens was tested. And the average of the angles taken on four different sides of the cone was recorded. The second method involved measurements of the base length at four different sections of a specimen with the constant height. The calculation for the angle of repose is obtained as follows,

$$\text{Angle of repose} = \tan^{-1}\left[2H \big/ (D_A - d)\right]$$

where,

H = height of the cone fixed at 1.5 in.

D_A = average of the 4 tests determinations diameter of the base, D_1, D_2, D_3 and D_4.

d = internal diameter of the funnel nozzle, 0.214 in.

Figure 29 Test Setup for the Measurement of Angle of Repose on Porous Stone

(a)  (b) 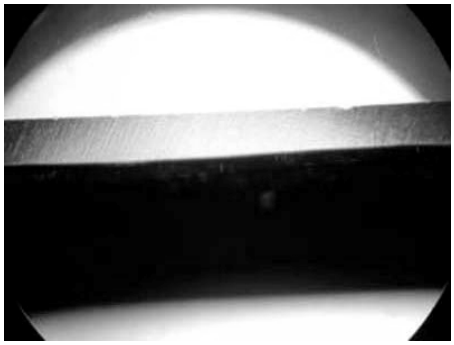

Figure 30 Visual Magnification of Surface Roughness of (a) Porous Stone. (b) Glass PlateBase

5.5.1 Granular Soil on Porous Stone Base

A number of 55 test specimens were conducted consisting 0, 10, 20, 30, 40, 50, 60, 70, 80, 90 and 100 percent of fine soil fragments passing sieve mesh number 150. When the granular mixtures poured down gently on the porous stone base, it was performed in such a way that the mix was laid down as homogeneous as possible to avoid marked segregation and 'pop-corn' effects, whereby all the finer materials lumped together at the bottom of the pile. The observation indicated that rolling as well as activities involving re-arranging the particles beneath the lower layers of the incoming materials governs the behavior in terms of the formation of the slope. As the percentage of fines increases the make up of the slope seems to be govern by the movement of thin layers of fine grains flowing on top of an earlier terrain.

5.5.2 Granular Soil on Glass Base

A number of 55 tests were also conducted consisting specimens with 0, 10, 20, 30, 40, 50, 60, 70, 80, 90 and 100 percent of fine soil fragments passing sieve no. 150. In contrast to the tests carried out with porous stone base, the rolling behavior was not significant. Instead, as the incoming layers exerted increasing loads, the build up continued until the frictional resistance at the base was overcome by the forces causing the slide and consequently lateral spreading originating from the lower layers directly under the overburden materials took place. The actions of building up the loads, the spreading and again the building up were repeated over and over until the build up achieve the desired vertical height according to the setup of the test.

5.6 THE ANGLE OF REPOSE TEST RESULT

The following Table 6 includes the values of angle of repose of a dry granular sand with varying composition of very fine size particles when the particles are dropped on a horizontal base made up of rough porous stone and smooth glass plate. The results are plotted as shown in Figure 31. The data reveals that the methods prescribed resulted in high accuracy in the measurement of the slopes. Sample of the data collection is provided in the Appendix B.

Table 6 Measurements and Calculated Results of Angle of Repose of Sand Mixtures

Base	Porous Stone (Angle of Repose in degrees)			Glass Plate (Angle of Repose in degrees)		
% Fine Component	Visual	Calculated	Average	Visual	Calculated	Average
0	42.18	42.17	42.17	33.56	32.53	33.05
10	40.92	40.63	40.77	33.40	33.54	33.47
20	40.62	40.93	40.77	35.10	35.05	35.07
30	38.92	39.01	38.96	34.90	34.85	34.88
40	38.57	38.22	38.39	36.67	36.91	36.79
50	38.51	38.44	38.48	36.93	36.57	36.75
60	38.49	38.75	38.62	37.93	37.69	37.81
70	37.65	37.80	37.72	38.39	38.01	38.20
80	37.71	37.80	37.75	37.66	37.67	37.66
90	37.27	37.17	37.22	37.12	36.99	37.05
100	37.23	37.19	37.21	36.60	36.82	36.71

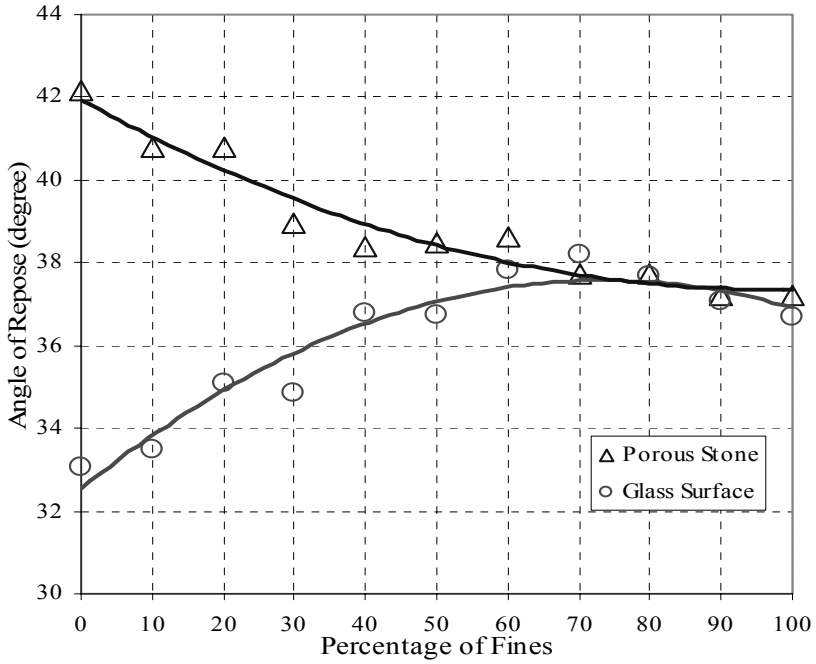

Figure 31 Angle of Repose for A Binary Mixture of Coarse-Fine Sand on Rough (Porous Stone) and Smooth (Glass) Plates

5.6.1 Porous Stone Base

The achieved results have provided some indication that there is a relationship between different compositions of granular soil with the angle of repose. When there is an absence of fines in the mix, the rugged surface of the coarse sand particles that come in contact with the rough surface base interlocks within the valleys of the porous stone as shown as in the Figures 27. The degree of the interlocking characteristics depends on the structural compatibility between the two surfaces. If the 'hills' and 'valleys' on the two sides of the materials match, more work is needed for the particles to move over the 'hills'. Moreover particle-to-particle contacts provide the same opportunity for interlocking to take place between the coarse grains themselves. As a result of high basal resistance and particle-to-particle interlocking effects, the slope angle is the highest at 42 degrees.

As fine particles are introduced, this compatibility that existed earlier between the morphology of the particles and the porous stone surface is reduced because the fines find their way to fill up the valleys making it easier for displacements to take place. Similarly, as the fines get in the way, the interlocking effect between the coarse particles is reduced because of lesser inter-particle contacts. And as a result, the angle of the slope(ie. the angle of repose) is reduced.

5.6.2 Glass Plate Base

The glass plate provides a very smooth surface that is not compatible to the 'hills' and 'valleys' on the surface of the coarse-grain particles. The minimum integral point area of contacts at the base plate interface between the coarse sand particles and the smooth glass surface resulted in an overall minimal resistance to the lateral displacement in terms of the sliding friction. The angle of repose is the least at this juncture.

By introducing fine particles into the system, the integral area of contacts at the interface increases, causing additional friction. As a result of increasing basal friction and similar effect of reduced particle-to-particle contacts (of the larger size grains), the angle of repose increases.

5.6.3 Uniform Basal Friction Factor

The angle of repose in both plots converges and seems to exhibit a uniform value at higher concentration of fines beginning from the point when the component of fines is increased from 60%. Introduction of much more fines in the system with glass base as mentioned earlier

increases the basal contact area to the maximum. At this point all the valleys in the porous stone is filed up with fine particles making effectively similar basal area of contact to the one involving the glass base.

Apparently at this juncture when finer particles are dominant, the presence of coarser particles seems to reinforce the system more within the cone than when no more coarse particles are left at 100% fines. Thus the angle of repose at 100% fines is somewhat slightly lower than the angle of repose at 60% fines.

5.7 LABORATORY EXPERIMENTS ON ANGLE OF INTERNAL FRICTION

The simplest method of determining the internal (inter-granular) friction angle is the direct shear test method using a Casagrande shear box apparatus. In accordance to the testing sample ASTM D3080 recommendations, the maximum grain size tested is one fortieth of the width of the box. Hence, maximum grain sizes passing sieve mesh no. 10 and retained at mesh no. 16 were used with varying contents of fines passing sieve mesh no. 150 mm. Rate of strain in the shearing was maintained at 1.33 mm per minute and measurements of the shear stress and dilatancy were taken at regular intervals. Table 7 gives the result of the average internal friction angle obtained from 21 tests of samples of varying mix at a low normal stress of 20 kPa. Samples of data form the test experiments are available in the Appendix C.

Table 7 The Result of Direct Shear Tests on Mixtures of Coarse and Fine Sand

Mix % of Fine component:	0	23.5	31.6	46.8	63.5	82.6	100
Average Internal Friction Angle (°)	40.7	41.8	41.7	39.6	35.4	35.4	34.7

The result of the tests reflects the dominant nature of either the coarse 1.6 mm.) or the fine (0.1 mm.) particles throughout the shearing of the mix. Samples having no fines exhibit higher friction angle at about 41 degrees as compared to samples of totally composed of fines at angle of internal friction of 35 degrees. It seems therefore the internal friction angle is affected by the size of the particle that dominates the test sample.

5.8 BASAL INTERFACE FRICTION ANGLE TEST USING A TILT TABLE

The other component after completing tests on angle of repose and angle of internal friction is to obtain the interface friction angle. It was decided that the interface angle could be obtained using a Tilt Table (Adjustable Inclined Table). The base plates used in carrying out Funnel Tests is again introduced. Figure 32 demonstrates the use of porous stone base on the inclined bench.

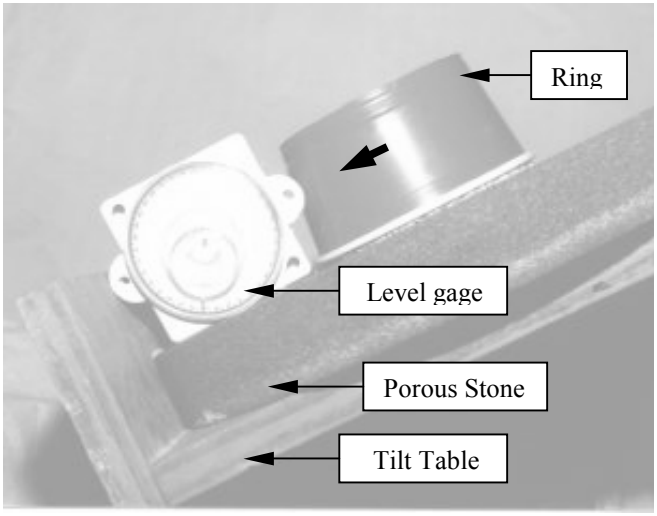

Figure 32 A Test Setup for The Interface Friction Angle Using An Adjustable Inclined Bench

Sand oven dried at 105°C for 24 hours was cooled down and poured very slowly to fill a very light weight plastic ring placed on either the porous or the glass base plates. The ring was then gently lifted up just to create a no-contact gap between the ring and the base plate thus leaving only the grains-base plate contact. The inclination of the bench is gradually increased via a mechanism that allows one end of the bench to be manually raised by turning a wheel located at the end of the bench in a clockwise direction. And thus, the angle at which sliding initiates is taken as the interface angle between the sand sample and the base plate.

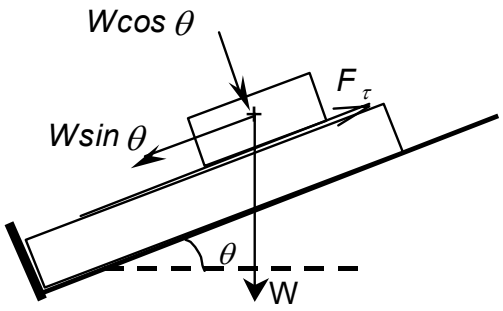

Figure 33 The Schematic Diagram of Forces Acting on the Inclined Bench

Assuming the interface friction is F_τ and the interface friction angle is δ referring to Figure 33**,** Coulomb equation 5.4 gives,

$$F_\tau = \sum N.(\tan \delta) \qquad \text{and} \qquad N = \mathrm{W}\cos\theta$$

The force causing the sliding is,

$$F_s = \mathrm{W}\sin\theta$$

For static equilibrium condition; Basal friction force = Force causing sliding

$$F_\tau = F_s$$

giving, $\tan \delta = \tan \theta$

Therefore, interface friction angle δ is simply the inclination angle θ read off from the gage.

5.8.1 Experimental Observation on Basal Friction

Samples of sand thoroughly mixed for mixtures varying from 0 to 100% fines content were used to fill up the ring throughout the experiments. By closely observing the movement of the ring,

the angle at which sliding failure took place was recorded. In order to obtain a reliable data, altogether more than 80 trials were carried out. The results of the tests are indicated in Table 8 as follows,

Table 8 The Result of Interface Friction Angle Tests Using Glass And Porous Stone Base for Varying Combination Binary-Mixtures of Sand

GLASS PLATE BASE		POROUS STONE BASE	
Percentage of Fines	InterfaceAngle δ (degrees)	Percentage of Fines	InterfaceAngle δ (degrees)
0	7.9	0	29.6
10	10.1	15	29.5
20	11.6	25	29.0
30	12.2	35	27.7
40	12.4	50	25.4
50	15.7	65	24.3
60	17.2	75	22.0
70	15.1	85	21.8
80	18.3	100	21.7
90	19.2		
100	20.3		

5.8.2 Action of Granular Soil on Porous Stone

There is quite a distinction result seen between the extreme ends of the tests in relation to the composition of the mixtures. The interface fiction angle is close to 30° for mixtures made of 0 to 30 percent of fine (0.1mm. diameter) materials and as the contents of the fines increases to 70 to 100 percent the interface angle is reduced to approximately 22°. The observation of dominance of the coarse particles for the former and the fine particles for the later case is an important contributing factor resulting in the different basal friction resistance. When the coarse particles dominate the rough points and edges of the surfaces of the particle were compatible to the

contours of the porous stone surface. Because of this condition they interlocks each other and resist the immediate movement of the sliding. Each particle in contact with the base has to overcome a certain distance and particle-to-particle contact to initiate sliding. The weight component however assists in the sliding.

On the other hand when the fines dominate the fine particles position themselves in a way to fill the voids and reduce particle-to-particle contacts between the large grains. As a result, much less interlocking phenomena occur and resistance to sliding is reduced giving a rather low basal friction of 22°.

5.8.3 Action of Granular Soil on Glass Plate Base

The glass plate with a very smooth surface represents an ideal condition of minimal basal resistance to horizontal movement. It is due to this particular reason it is used in the tests to study the effects of particle contacts. In contrast to the tests carried out using the porous stone base. The increase in the basal friction is gradual from about 8° when only coarse particles were present, to approximately 20° when it comprises entirely of fine grains. The gradual increase seems to coincide perfectly to the increase in the amount of fines component in the mixtures.

The result reveals a very important factor in terms of frictional resistance, which is the contact area. Since the surface of the glass is very smooth interlocking does not take place at the interface between the grains and the base. In order to slide the particles do not have to overcome any displacement or rotation. The resistance is therefore purely dependent on the area of contact of the grain particles and the base.

The aggregate of the contact area is minimal when there were only coarse particles because of the marked points and edges of the surfaces of these grains. And as fine grains were introduced they began to fill the voids and eventually displaced the coarse particles to represent the maximum contacts between the grains and the base. It is also interesting to note that in both tests using porous stone and glass plate, the interface friction angles seem to converge to about 20°- 22° when the fine grains are dominant. The relationships between the angle of repose, angle of internal friction and the angle of interface friction can be observed from the plots in Figure 34 for the tests using the porous stone base and in Figure 35 for the tests using the glass plate base.

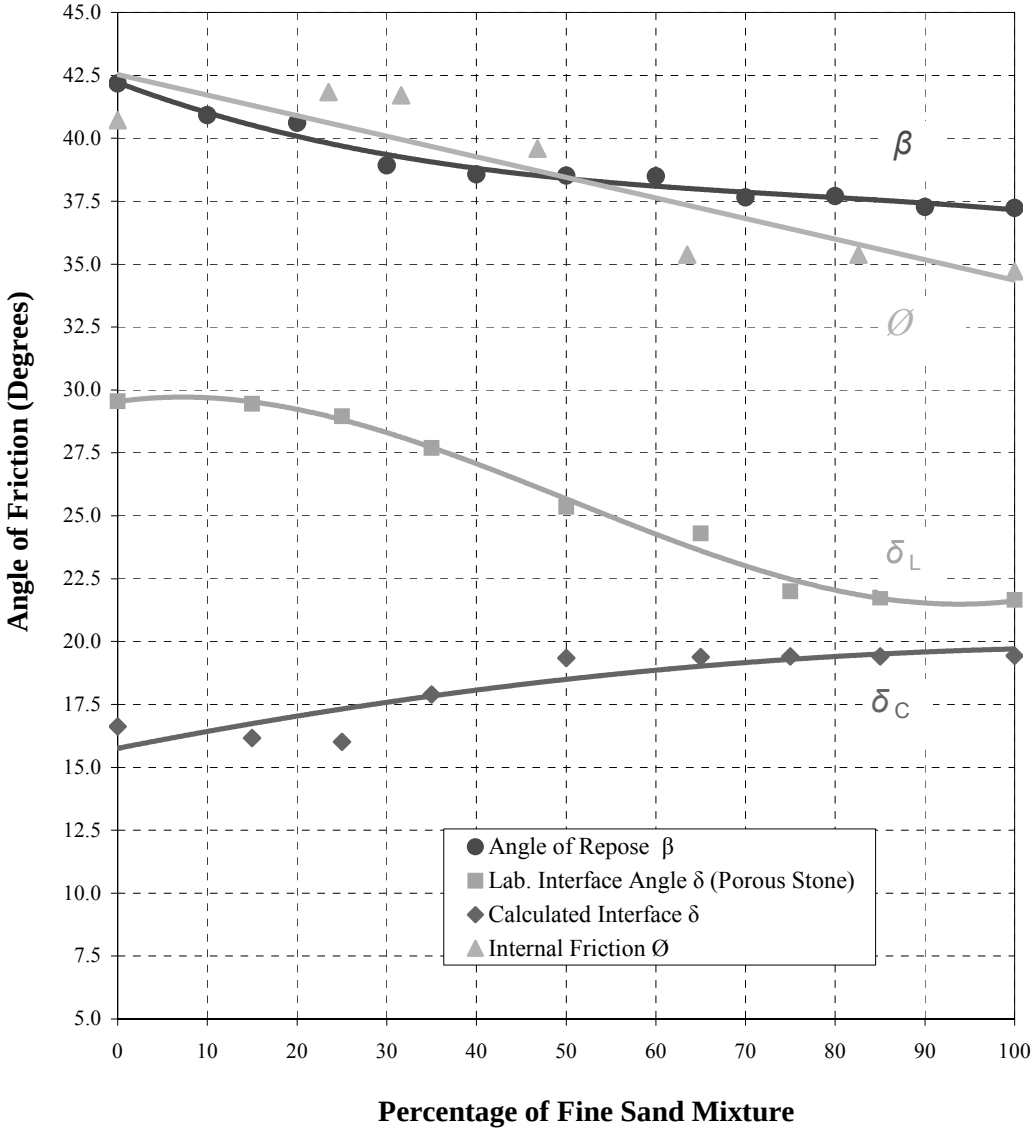

Figure 34 Test Results on the Angle of Repose and Interface Angle Using Porous Stone Base for Various Coarse-Fine Sand Mixtures with the Friction Angle of the Specimen

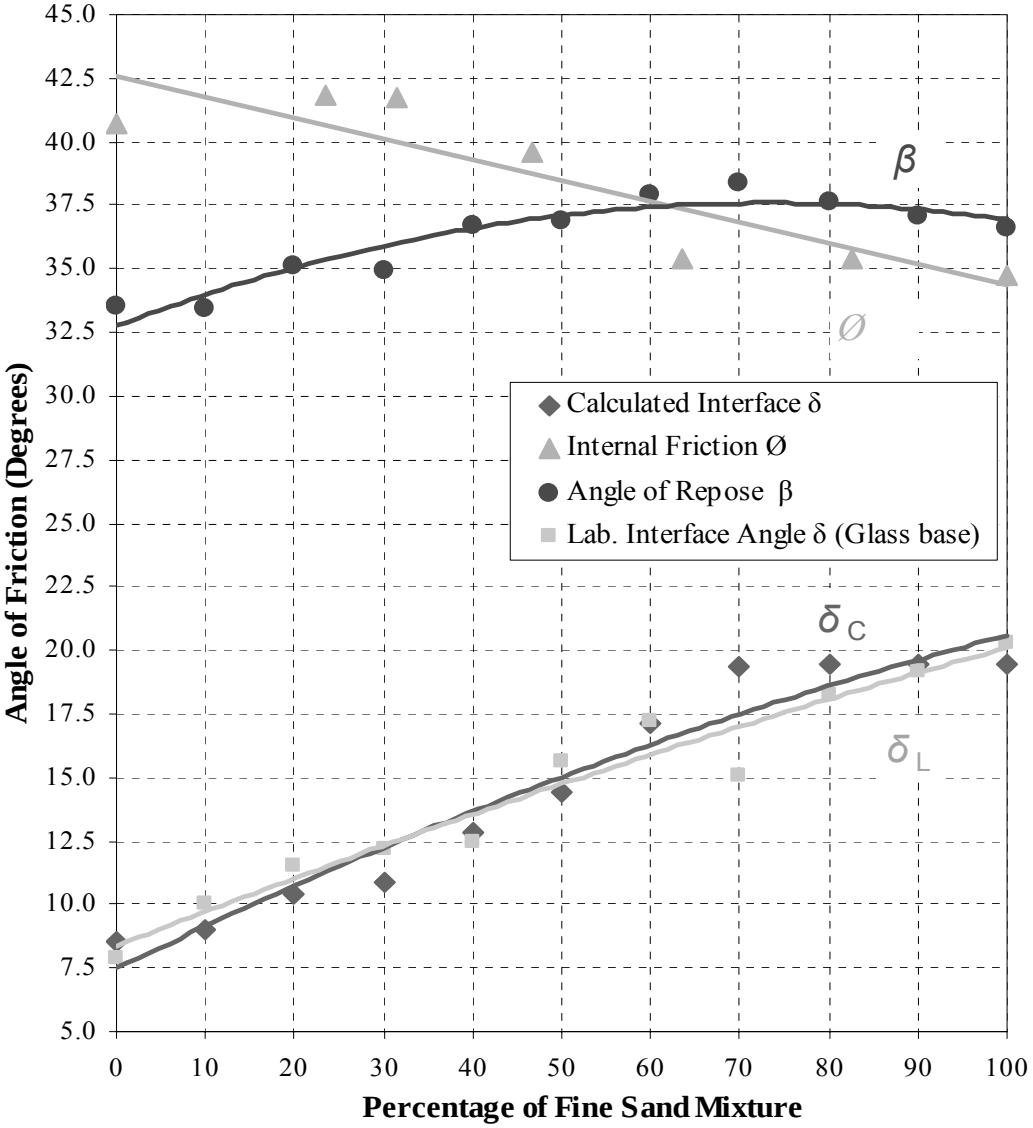

Figure 35 Test Results on the Angle of Repose and Interface Angle Using Glass Plate Base for Various Coarse-Fine Sand Mixtures with the Friction Angle of the Specimen

5.9 ANALYSIS AND OBSERVATION

The values for the angle of internal friction $\emptyset$, the angle of repose β and the interface friction δ obtained from the laboratory tests are plotted in Figures 34 and 35. And the data collected for both cases using porous stone and glass plate base as illustrated earlier could also be verified by using the equation (H),

$$\tan \delta = \frac{\tan \beta \cos^2 \phi}{2 + 2\sqrt{1 - \left(\frac{\cos \phi}{\cos \beta}\right)^2} - \cos^2 \phi}$$

In this exercise, theoretical values of interface friction angle can be verified by introducing the β and $\emptyset$ into the equation provided the values of $\emptyset$ is always larger than or equal to β. The data obtained indicates that this fact is true for almost all cases with the exception of a few where the difference between the angles was less than 1.5°. The results of the calculated theoretical values is tabulated as shown in the appendix and also plotted in the figures 34(a) and 34(b). As observed from the plots, the equation seems to satisfy the laboratory results using glass plates perfectly, however the laboratory results using the porous stone base differs slightly from the theoretical especially when there is limited amount of fine aggregate components in the binary mixtures. The almost perfect fit of the laboratory results and the calculated values of the interface friction on the glass plate is due to the fact that only sliding friction based on contact area takes place on the glass base. This condition accurately satisfies the basis by which the theoretical equation was formed.

5.10 ANGLE OF REPOSE IN SLOPE EVOLUTION BY SHALLOW PLANAR SLIDING

Many natural slopes and rockfill structures are made of a mixture of rock fragments and sand-size particles[55]. Natural as well as man-made cut slopes undergo weathering and that denudation takes place evenly at an equal rate everywhere on the slope and as a result slope recession models were developed. A variety of mathematical models of slope development applying the parallel rectilinear slope recession theory are presently available. The Lehman model of slope stability evolution mathematical model is one of them.

The mathematical model assumes that the debris from the weathered slope will accumulate at the bottom of the slope and form a pile of scree (talus) with an angle α (scree angle) that leans against the original slope. The model allows information regarding the slope such as the slope height, the original inclination of the slope and the scree angle be used to predict the amount of retreat at the top of the slope and the amount of advance of the toe of the new slope.

The slow and gradual nature of the slope failure modeled by Lehman with each individual amount weathering off the slope ended up at the bottom of the slope the formation of which is identical to the angle of repose investigated in this study, the scree angle is therefore modeled as the angle of repose for a granular slope.

5.10.1 Lehman Model: Slope Stability Evolution

The mathematical model developed by Lehman in 1933 is described from the diagram in Figure 36 and the related equations as follows.

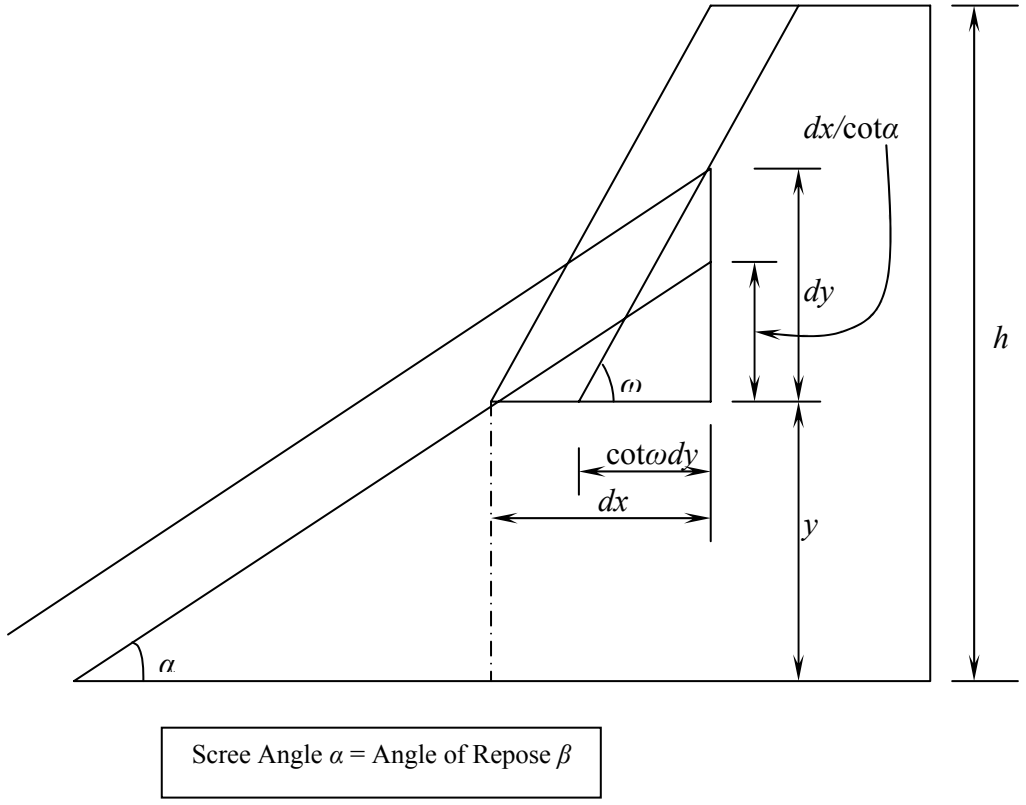

Figure 36 Infinitesimal Increase of the Heap of Debris at the Bottom of A Slope (Lehman 1933)

The ratio of the volume removed to the volume deposited at the toe is; $\frac{V_R}{V_D} = 1 - c$

where, c = coefficient of volume expansion of the soil.

Volume removed = Volume deposited

That is, $(dx - dy \cot \omega)(h - y) = (1 - c)(dy - \frac{dx}{\cot \alpha}) y \cot \alpha$

thus, $\frac{dx}{dy} = \frac{h \cot \omega + (\cot \alpha - c \cot \alpha - \cot \omega) y}{h - cy}$

The retreat $x = K(l + m)\ln\left[\frac{m}{m - y}\right] - Ky$

where, $K = \frac{(1 - c)\cot\alpha - \cot\omega}{c}$

$$l = \frac{h\cot\omega}{\cot\alpha - \cot\omega - c\cot\alpha} \text{ and } m = \frac{h}{c}$$

By knowing the original slope angle ω, the height of the slope h, the angle of repose β (that is α in the above Lehman equations) and the coefficient of volume expansion of the soil c, the retreat of the slope and the advancement of the new slope toe could be obtained.

5.11 EXPERIMANTAL MODELING OF BASAL SLOPE

Volume of soil removed from the slope due to shallow planar sliding failure may also land on a sloping basal plane. To simulate this condition through a laboratory testing the funnel test is carried out at different inclination angle of the base using the adjustable tilt table. The oven dried coarse granular sand (1.6 mm. diameter) was slowly laid and gradually formed a heap of sand cone on a predetermined inclination of the base.

The photographs in Figures 37(a) and 37(b) illustrate the set up of the test and reveal the characteristic features of the cone formation on both the porous stone base and the glass plate base. While the face of the progressive slope on the porous stone appears planar and linear the sloping face of the cone on the glass plate appears concaved in shape making it slightly more complicated to measure the angle of repose.

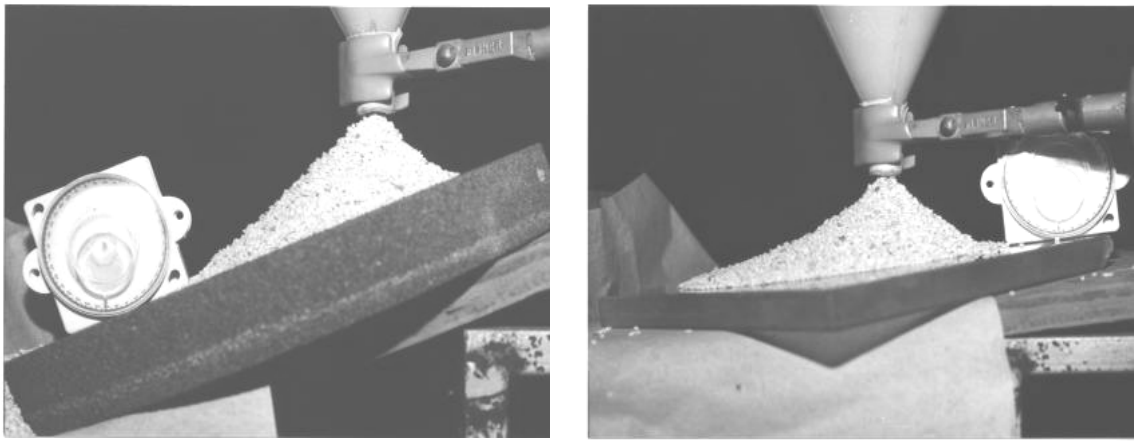

(a) (b)

Figure 37 Formation of Angle of Repose of Granular Sand on An Inclined Plane Using (a) Porous Stone Base and (b) Glass Plate Base

5.11.1 Theoretical and Laboratory Results

The diagram from Figure 25 indicates that the angle β is constant with respect to θ and the theoretical evaluation of the interface friction δ is obtained using the following equation (I).

$$\tan\delta = \frac{\cos^2\phi \sin 2(\beta-\theta) + \sin 2\theta\left(\cos\beta + \sqrt{\cos^2\beta - \cos^2\phi}\right)^2}{2\left[\cos^2\phi \sin^2(\beta-\theta) + \cos^2\theta\left(\cos\beta + \sqrt{\cos^2\beta - \cos^2\phi}\right)^2\right]}$$

Taking from the previous tests result; angle β = 42.2˚ and ϕ = 42.5˚ for porous stone base, angles δ can be plotted against the adjusted inclination θ to give the theoretical calculated values. When the progressive slope of the cones were measured experimental values of angle β were obtained and consequently the laboratory results for the δ .

Similarly, taking angle of repose for the coarse sand on the glass plate as β = 33.6˚ and ϕ = 42.5˚ the theoretical interface friction can be compared to the outcome due to the angle β measured on the inclined bench. The result of the tests using the porous stone and the glass plate is tabulated in Table 9 and comparison between the plots of theoretical and laboratory values of δ are presented in Figure 38.

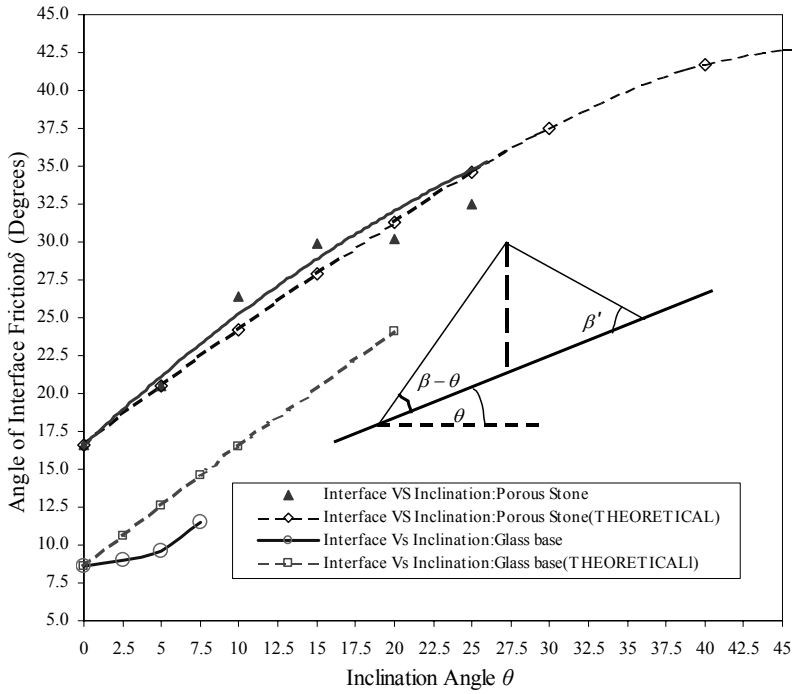

Figure 38 Interface Friction δ of Granular Sand (-2.0+1.18 mm.) on An Inclined Plane Using (a) Porous Stone Base and (b) Glass Plate Base

The laboratory data and the calculated theoretical values for the interface friction angle indicate a high degree of consistency for the sand specimens tested on porous stone base as compared to the glass base. On the glass base the sand particles slide easily. Inaccuracy in glass

base is partly due to difficulty in acquiring accurate measurement of the concave shaped piles formation of the sand on the glass. However, the increase in the interface friction as the inclination is increased was found to be consistent.

Table 9 Angle of Repose β for Coarse Sand on Inclined Plane

Porous Stone	Inclination θ°	0	5	10	15	20	25
	β°-θ°	42.2	37.2	32.5	27.5	21.7	16.0
Glass Plate	Inclination θ°	0	2.5	5	7.5		
	β°-θ°	33.6	27.0	20.3	17.5		

5.12 CONCLUSION

The angle of repose is an important material property for a granular material and it is found to be relevant in the study of fragmentation. Its usefulness is not only realized in the geotechnical engineering field but also in other field of studies such as in powder technology. The following are some of the conclusions made from the investigations carried out related to the angle of repose.

- A general equation relating the angle of repose, angle of internal friction and interface friction angle is developed taking an assumption that at an instant the failure of the slope of the sand cone is influenced by the basal friction as well as the slope angle and the internal friction angle. And that the angle of repose on a horizontal level is a special case of the equation.

- The influence by the interfacial friction developed between the material and the base in contact on the angle of repose is significant.

- In the binary mixtures, it is observed that the effect of basal friction increases when the resistance is purely related to the area in contact in the absence of interlocking characteristics between the material and the base. Thus displaying higher angle of repose.

  The interlocking phenomenon developed that is may be due to compatibility of the surface roughness between the base and the grains produce the reverse effect when fine fragmented particles are introduced. The particle-to-particle contacts are reduced and hence lower angle of repose.

- When constructed on a given rough surface, the angle of repose can be regarded a close approximation of the angle of internal friction and may be used in a quick estimation work. One such relevant application of the angle of repose is in prediction of slope retreat and toe advancement in slope evolution model developed by Lehman. The effect of fragmentation in the denudation process, the type and the slope of the base at the toe of the slope will have substantial influence on the outcome of the prediction.

6.0 ABRASION IN GRANULAR MATERIALS

6.1 INTRODUCTION

Problems involving fines has long been recognized by highway engineers. Large quantities of fines produced during crushing, handling and placement (that is compaction) may render the material unsuitable for road construction. Flexible pavement distresses such as fatigue cracking and rutting and rigid pavement distresses including pumping/ faulting and cracking have been attributed to high fines content of the base material[56]. The amount of fines produced in either one of the activities involving granular materials in the construction of roads has been the focus of many earlier researchers[57, 58]. However, the problem remains an open challenge for a clear understanding of the production source of fines and the method of prediction of the quantity.

In the following tests samples of round and angular small size gravels were used to recognize the source and the process of abrasion in relation to the shape and structure of the aggregates. In simulation of the handling activity, a rotating Jar mill apparatus was engaged. Fractal analysis was also carried out to establish the fractal dimensions of the gravels before and after abrasion in an exercise to investigate the fractal geometry of the processed materials and also to quantify the grain size distribution of the product of the abrasion tests.

6.2 JAR MILLING TEST

The porcelain jar used in the mill has a dimension of 6 inches in diameter and 6inches in length. Test specimens are placed in the jar together with 65 small cylindrical porcelain charges before the lid is put on to close the jar. It is important that the jar is well sealed and tightened prior to the milling. The photograph in Figure 39 shows the equipment involved in the jar milling process described in the section.

Figure 39 Jar Milling Apparatus Including the Jar and the Lid, the Charges and the Roller Milling Machine

6.2.1 The Test Procedure

The jar and the charges were initially washed and oven-dried before weighted. A sample of 100 grams of small size (average diameter of 5 mm.) angular gravels was also washed, oven-dried and weighted, and then placed in the jar together with the charges. With the lid tightened, the jar was then mounted on the two cylindrical rollers for 20 minutes milling at 50 revolutions per

minute in one stage for a total of three stages of 1-hour duration. At every stage, the sample was unloaded and individual gravels were closely inspected using a microscopic camera that is connected to a computer. Unlike impact actions that comes together with abrasion in other degradation tests such as the L.A degradation/abrasion test. Impact action hardly affects the small sample during the test resulting in very minimal broken gravels.

The images of the 'worn down' particles were processed and then they were analyzed using the ImageJ 1.29X program developed by The National Institute of Health, USA. Progressive changes in the material were recorded continuously until the completion of the milling stages. The products of the milling were also put through 12 minutes of mechanical sieving for the grain size distribution analysis. Similar exercises were also carried out for the round gravels prepared in a similar manner in order to establish the basis for comparison between the two types of gravels.

6.3 THE ABRASION TEST RESULTS

6.3.1 The Physical Abrasive Effect

The degradation of the gravels that occur during the test takes place mainly as a result of abrasion. In this exercise the wearing down of the particle physical shape and roughness is captured using a computerized electronic camera Nikon SMZ1500 utilizing Omnimet software program enterprise version 4.5 B021. The images of both the angular and the round gravels before and after the abrasion in the jar mill test as presented in the Figures 40 and 41 respectively, show signs of surface attrition for the after abrasion effects.

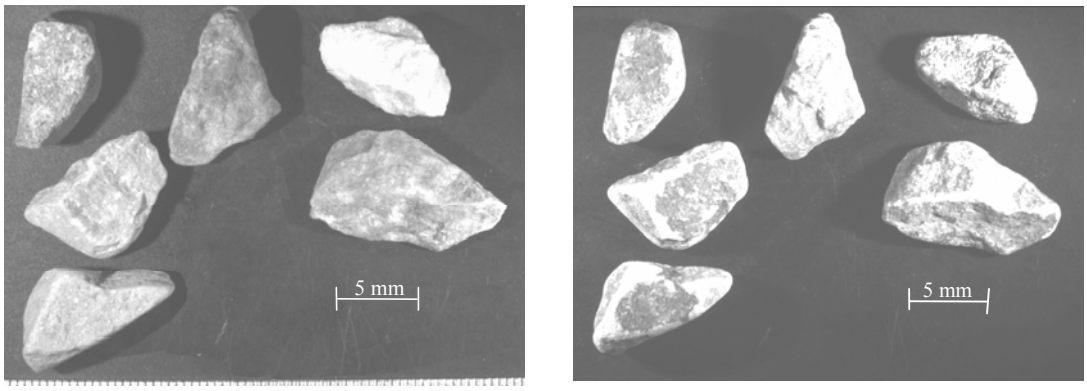

(a) (b)

Figure 40 (a) Angular gravels before abrasion and (b) Angular gravels after abrasion

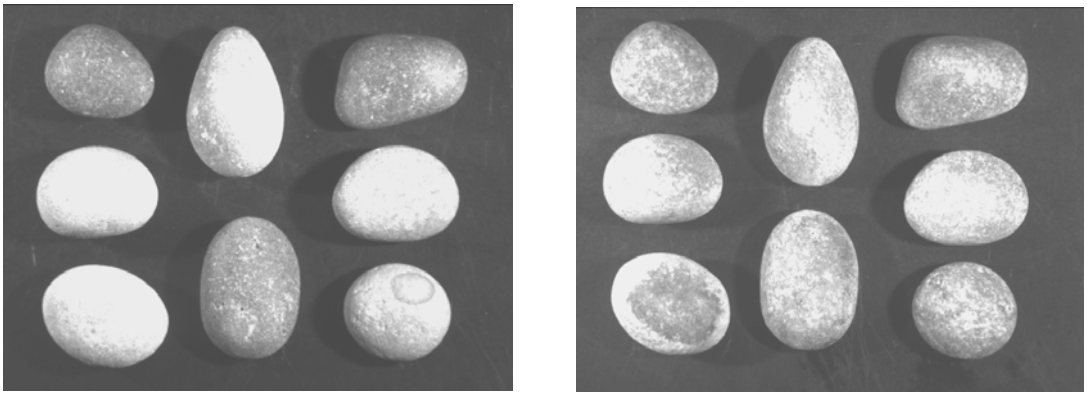

(a) (b)

Figure 41 (a) Round gravels before abrasion and (b) Round gravels after abrasion

For the images to be captured by the electronic camera a close scrutiny on the intensity and direction of the lighting is required and not to over emphasized the importance of placing the objects exactly back in the original position for the after abrasion photographs. Applying adequate light intensity and direction from any available source is much more crucial in producing a binary image of the particles to be utilized when performing the area-perimeter analysis by means of the ImageJ program.

6.3.2 Area-Perimeter Fractal Analysis

In the usage of the ImageJ program, a high contrast 756x570 pixels 8-bit greyscale image production is the key. The image is processed alternately applying the freehand selection and wand tools in preparing the two-dimensional image of the objects and finally to produce a binary presentation for the area-perimeter analysis. Table 10 and Table 11, each shows the area and the related perimeter of the angular and round gravels before and after abrasion respectively. Introducing the area against perimeter data into Excel, log-log plot for the power-law fractal analysis is obtained as shown in following figures 42 and 43 for the angular gravels and figures 44 and 45 for the round gravels presenting before and after abrasion effects.

Table 10 Area and Perimeter of Angular Gravels before and after Abrasion

Before abrasion test		After abrasion test	
Area (sq. mm)	Perimeter (mm)	Area (sq. mm)	Perimeter (mm)
40.60	26.14	37.76	25.08
49.97	30.49	45.05	28.59
43.65	26.96	39.90	25.24
52.01	29.76	49.95	28.4
77.00	36.38	70.54	33.93
46.37	29.61	42.69	27.86

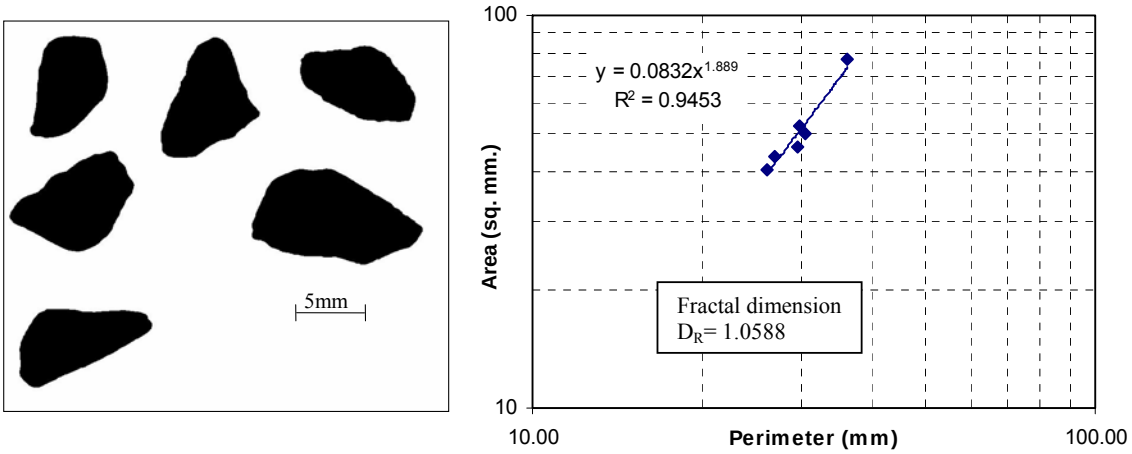

(a) (b)

Figure 42 (a) Binary Image of Angular Gravels before Abrasion (b) Fractal Dimension before Abrasion is 1.0588

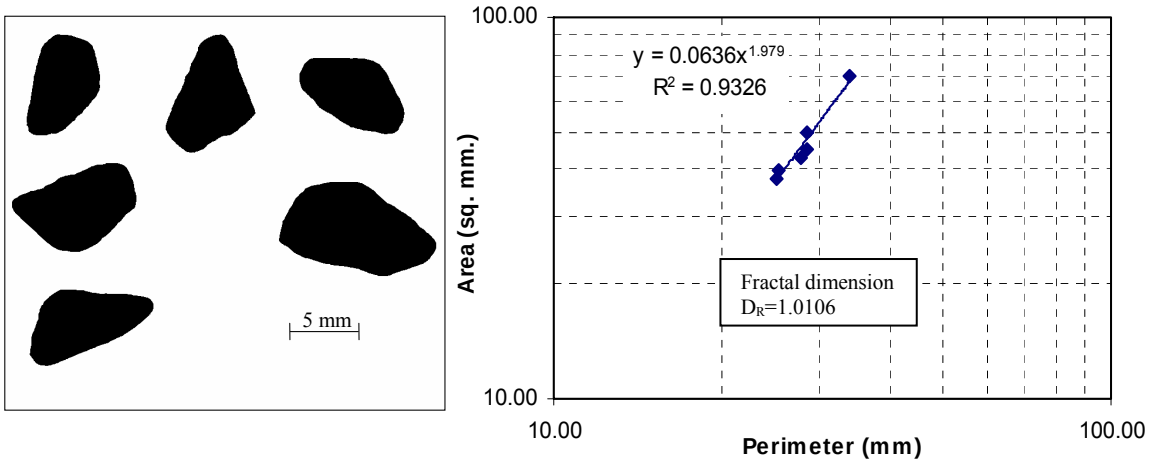

(a) (b)

Figure 43 (a) Binary Image of Angular Gravels after Abrasion (b) Fractal Dimension after Abrasion is 1.0106

Table 11 Area and Perimeter of Round Gravels before and after Abrasion

Before abrasion test		After abrasion test	
Area (sq. mm)	Perimeter (mm)	Area (sq. mm)	Perimeter (mm)
38.23	23.30	36.08	22.61
54.09	28.79	51.96	28.21
48.44	27.20	47.63	26.91
46.53	25.92	45.19	25.42
43.96	25.11	41.59	24.44
55.30	28.31	54.14	27.95
39.22	23.45	38.07	23.03
48.51	26.38	45.57	25.41

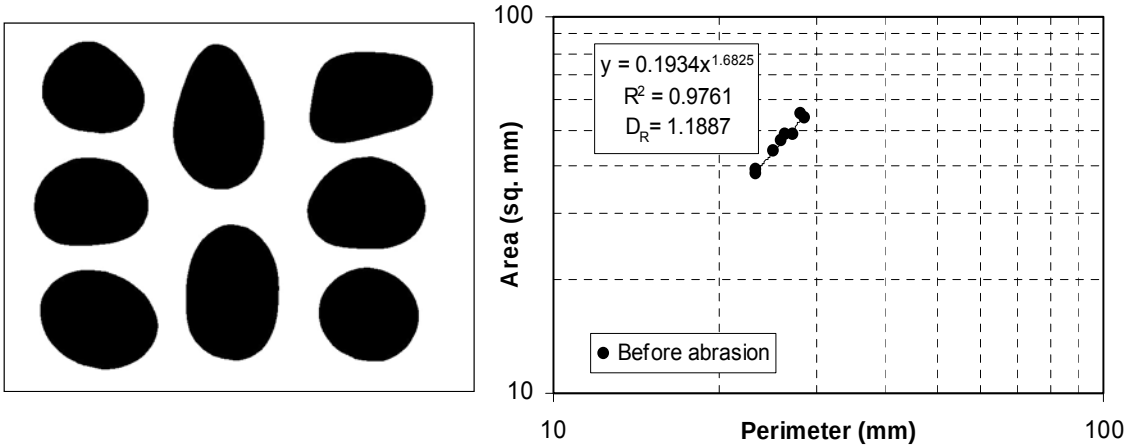

(a) (b)

Figure 44 (a) Image of Round Gravels before Abrasion. (b) Fractal Dimension before Abrasion is 1.1887

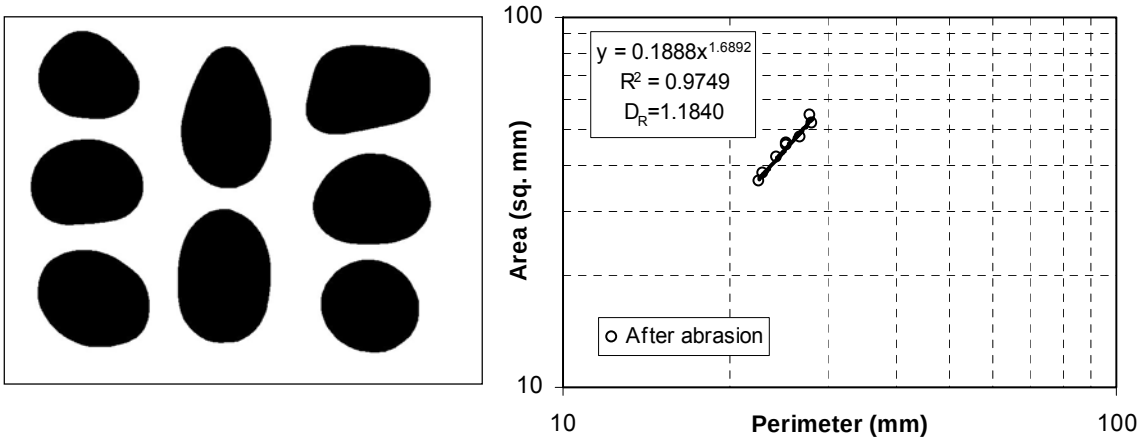

(a) (b)

Figure 45 (a) Image of Round Gravels after Abrasion. (b) Fractal Dimension after Abrasion is 1.1840

The fractal dimension D_R of the particles is evaluated using the area-perimeter method introduced by Mandelbrot and later Hyslip and Vallejo[33]. It was shown that the ratio of linear extent for a group of similar shaped particles (such as circles, squares et. al.) is constant (that is, $P/A^{1/2}$ =constant; where P is the perimeter and A is the area). By evaluating the ratio of linear extent within a group of geometrically similar fractal shapes, a fractal dimension can be developed. This fractal dimension yields a quantitative measure of the roughness of the common shape. According to Mandelbrot[59] the ratio of linear extents of fractal patterns are in themselves fractal and thus;

$$c = \frac{(perimeter)^{1/D_R}}{(area)^{1/2}} \tag{6.1}$$

Where, c is a constant value for similar fractal shapes and D_R is the roughness fractal dimension of the particle group/population.

From equation (6.1) area against perimeter for the group of particles can be plotted on a log-log scale and the slope m of the best-fit straight line is obtained as illustrated in Figures 41 (b) to 44 (b). And hence the fractal dimension is obtained since D_R is the ratio between 2 and m (that is $D_R = 2/m$). From the plot in Figure 44 (b) m= 1.6892. The fractal dimension for the group is 2 divided by 1.6892 giving D_R = 1.1840.

6.4 THE GRAIN SIZE DISTRIBUTION

The initial material placed in the jar mill comprises of gravels passing ¼ inch (6.30 mm.) and retained on no. 4 (4.75 mm. opening) sieves. As mentioned earlier, at every end of the three stages the test products were taken out from the jar and put through the mechanical sieving apparatus. Tables 12(a) and (b) present the results of the sieve tests for the angular and the round gravels respectively.

Out of 291 numbers of angular gravels 20% were found to be broken after 1 hour of testing in the jar mill and the amount of fines increased from 3.29 grams after 20 minutes to 6.37 grams after 40 minutes and finally 8.56 grams after an hour. On the other hand, from 238 numbers of round gravels less than 3% were broken after 1 hour of the test and the amount of fines increases from 0.61 grams to 1.50 grams and finally constitute only 2.32 grams after an hour of milling.

Table 12 Mechanical Sieve Analysis of (a) Angular and (b) Round Gravels Throughout Abrasion

(a)

ANGULAR	After 20 min.		After 40 min.		After 60 min.	
Sieve no.	Retained wt. (g)	% retained	Retained wt. (g)	% retained	Retained wt. (g)	% retained
4	90.69	91.27	83.21	83.93	79.18	80.39
10	5.03	5.06	8.77	8.85	10.02	10.17
20	0.19	0.19	0.57	0.57	0.48	0.49
40	0.07	0.07	0.09	0.09	0.09	0.09
60	0.02	0.02	0.02	0.02	0.04	0.04
100	0.06	0.06	0.04	0.04	0.03	0.03
140	0.00	0.00	0.01	0.01	0.03	0.03
200	0.01	0.01	0.06	0.06	0.06	0.06
pan	3.29	3.31	6.37	6.43	8.56	8.69
	99.36	100.00	99.14	100.00	98.49	100.00

Table 12 (continue)

(b)

ROUND	After 20 min.		After 40 min.		After 60 min.	
Sieve no.	Retained wt. (g)	% retained	Retained wt. (g)	% retained	Retained wt. (g)	% retained
4	98.65	98.72	97.58	97.74	96.52	96.88
10	0.53	0.53	0.48	0.48	0.59	0.59
20	0.09	0.09	0.18	0.18	0.13	0.13
40	0.01	0.01	0.05	0.05	0.03	0.03
60	0.01	0.01	0.01	0.01	0.02	0.02
100	0.01	0.01	0.02	0.02	0.01	0.01
140	0.01	0.01	0.01	0.01	0.01	0.01
200	0.01	0.01	0.01	0.01	0.01	0.01
pan	0.61	0.61	1.50	1.50	2.31	2.32
	99.93	100.00	99.84	100.00	99.63	100.00

From the data a statistical analysis of the fragmentation can be performed by plotting the cumulative particle size distribution (PSD) as well as the power-law fractal distribution as illustrated in Figures 46 and 47.

6.5 OBSERVATION

As the jar revolves during the test, the segregated gravels are squeezed by the cylindrical charges that are also present within the container. This particular condition makes the individual grain particles packed closer together as they rolled over in the jar making right the condition in simulation of handling. The large amount of fines as the product of abrasion coming from the angular gravels is a proof to the point made earlier regarding the tendency of crushing at the edges and pointed corners of a particle.

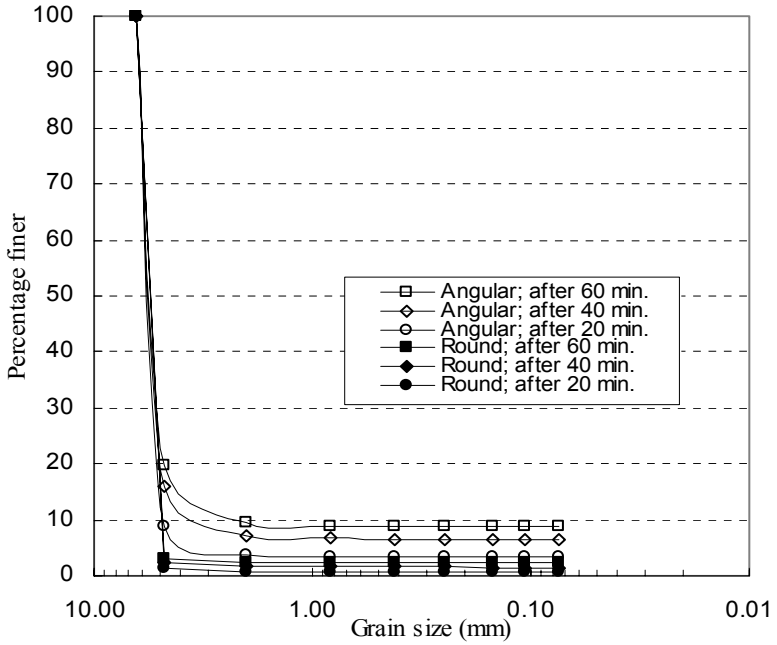

Figure 46 The Cumulative Grain Size Distributions (PSD) for the Products of Abrasion

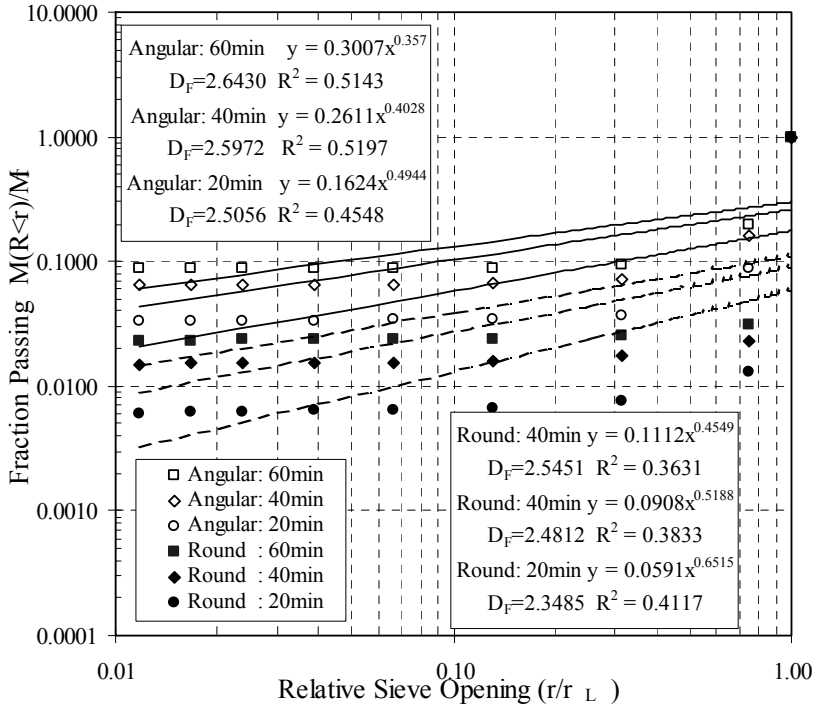

Figure 47 The Power-law Fractal Plots for Fragmentation due to Abrasion in Angular and Round Gravels

The peripheral fragmentation is depicted by the area-perimeter reduction of the grain visually and quantitatively. Studying the Tables 10 and 11 indicates that reduction in area and perimeter of the particles images is more in angular than in round gravels. Fractal dimension of the initial angular gravels is 1.0588 and after the jar milling the fractal dimension is 1.0106, giving a reduction of 0.0482. In the case of the round gravels the initial fractal dimension of the particles is 1.1887 and the after milling fractal dimension is 1.1840, giving a difference of 0.0047.

As the fractal dimension of the area-perimeter indicates the roughness of the particles, it can be seen that there is a reduction in roughness in both types of particles. Nevertheless, the reduction of roughness is more significant in the angular gravel population as compared to the round materials.

Referring to the sieve analysis conducted, it is observed that after one hour of similar test conditions, the initial amount of the original angular material was reduced by 20 percent while the rounded granular material was not much affected with just a reduction of 3.2 percent. Throughout the tests, the production of fines in angular gravels stands at four to five times larger than that produced in the round gravels. The difference in the cumulative size distributions as well as the fractal dimensions between the angular and round gravels can also be seen as illustrated in Figures 46 and 47.

Abrasion of the gravels in the jar milling test produces two main particles namely the initial large grains and the fines. It is therefore only logical that the correlations for the plots involving other points in between, is somewhat very low and arguably the products may be

interpreted as non-fractal. Even so, if a comparison of fragmentation fractal dimension D_F between the angular and the round material is made, fragmentation of the population[33] (the measure of the size-number relationship of the population) is again proven to be greater in the angular than in the round gravels. The relationship between the fractal dimension of the gravels and the amount of fines produced is shown in Figure 48 and the result of fractal analyses of the grain is tabulated as follows.

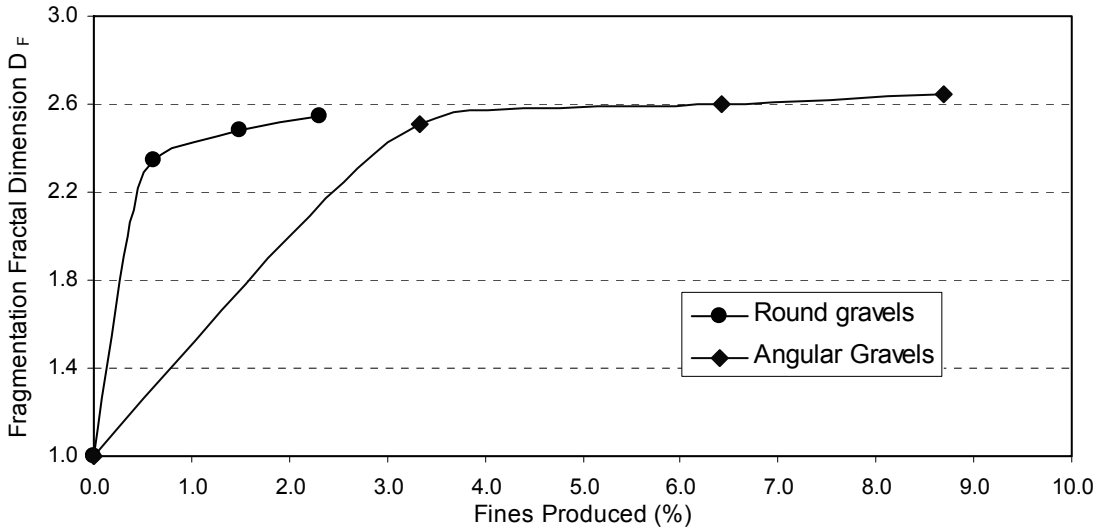

Figure 48 The Relationship between the Amount of Fines Produced (percentage by weight) and the Fragmentation Fractal Dimension D_F

Table 13 (a) Roughness Fractal Dimension D_R . (b) Fragmentation Fractal Dimension D_F due to Abrasion in The Jar Mill before and after Abrasion

	Angular Gravels		Round Gravels	
Evaluation:	Before abrasion	After abrasion	Before abrasion	After abrasion
D_R	1.0588	1.0106	1.1887	1.1840
Reduction: (roughness)	0.0482		0.0047	

(a)

	Angular Gravels		Round Gravels	
Test duration (minutes)	% of fines by weight	D_F	% of fines by weight	D_F
20	3.34	2.5056	0.61	2.3484
40	6.43	2.5972	1.50	2.4812
60	8.69	2.6430	2.31	2.5451

(b)

6.6 CONCLUSION

The power-law fractal plots for the area-perimeter analysis of the selected groups of angular and round gravels in figures 41 to 44 display very strong correlation values of R-squared between 0.93 to 0.98 With a large reduction of original material and the production of a large amount of fines, the fractal dimension of the angular gravels was reduced from 1.058 to 1.0106. Consequently, the (degree) fragmentation increases as identified by the measure of D_F from 2.5056 to 2.6430.

As for the round gravels, the roughness measure D_R reflects what was predicted, and that is the reduction of roughness is only from 1.1887 to 1.1840 with a lower measure fractal fragmentation dimension of 2.5451 after 60 minutes of milling.

Fragmentation due to abrasion is more significant in the more angular particles than rounded particles when subjected to similar testing condition. It can also be concluded that the roughness measure D_R and the measure of fragmentation D_F utilizing fractal techniques have been successfully applied to quantify the measure of abrasion in both materials.

7.0 FRAGMENTATION OF GRANULAR MATERIALS AND THE MODULI OF ELASTICITY

7.1 INTRODUCTION

For the calculation of the elastic deformation experienced by soils when they are subjected to either static or dynamic loads the knowledge of the elastic moduli (Young's modulus of elasticity E, shear modulus G, and Poisson's ratio, ν) of the material is required. Although the response of soils to these kinds of loads may not be strictly represented as linear elastic, solutions based on linear elastic behavior are commonly used for the estimation of stresses or strains in the field. It forms an important component in the theoretical methods of pavement designs not only that of the pavement surface but of the unbound granular base as well[(60)]. These elastic constants are needed to predict stresses and strains in the pavement layers. As a result of fragmentation of the granular base during the life of a pavement structure the values of these elastic moduli could change.

Total crushing episode of larger granular materials begins with this chapter which look at the experiences of the spherical glass beads and small gravels when subjected to a range of static loads. Crushing behavior of these materials was first studied and using an ultrasonic velocity Pundit testing apparatus (Model CT-30, produced by ELE International) on the fragmented materials the effect of crushing induced by these loads on the elastic moduli of the spherical

glass beads, angular and round gravels were investigated. Laboratory tests using the Universal Testing Machine (UTM) to induce a range of static loads on the materials were also carried out as described in the following sections.

7.2 FRAGMENTATION UNDER STATIC LOADING

An initial laboratory experiment was carried out with a Plexi-glass tube of 2.0 inches in diameter is filled with the 5.0mm.diameter glass beads having specific gravity of 2.5 to a depth of twice the tube diameter. For meaningful test results, it is found necessary to maintain a ratio of sample diameter to the maximum particle size of approximately 6:1 or greater. The recommended maximum diameter of a granular material is approximately 0.333 inches (that is 8.5 mm). The tube is set up right with a steel plug at the bottom on which the beads are rested and a 2.0 kg piston head pressing against the grains at the top of the beads. The objective of the exercise is to impose a crushing condition to the grains and to investigate the crushing characteristics of the perfectly spherical beads.

7.2.1 The Static Load Fragmentation Investigation Routine

The UTM is a constant-stress testing machine. Applied load readings were easily read-off from the screen since it was set to exert only very low increments of 10lbs reading (22 kgf) at a time. For example to achieve a maximum compressive load of 10,000 lbs, the sample was loaded for 150 minutes. As the material compresses under the uni-axial loading forces it will exert a radial pressure within the plexi tube thus subjecting it to tension. To avoid breakage of the cylinder at low loads, a number of hose clamps were used as shown in the Figure 49.

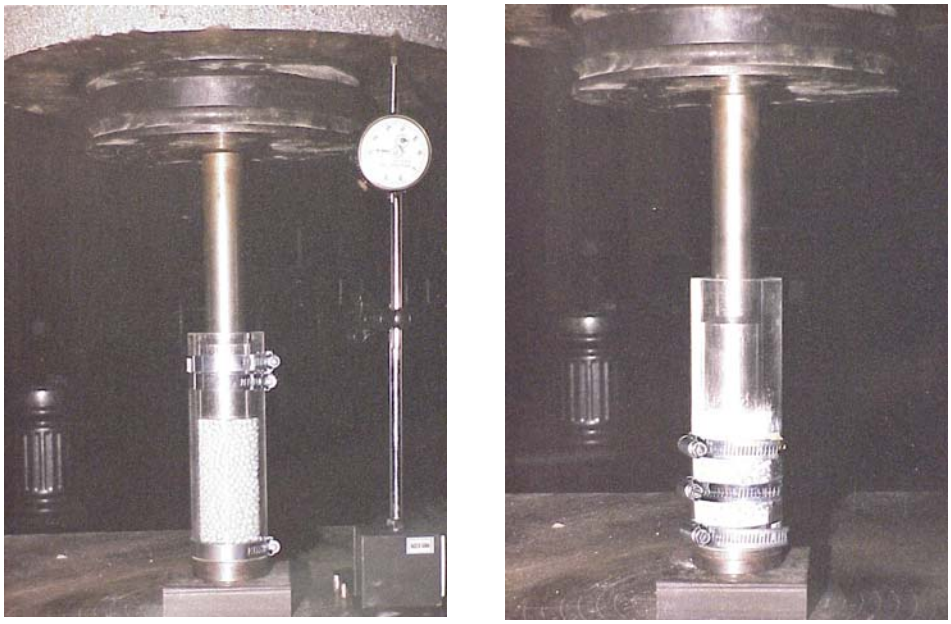

(a) (b)

Figure 49 Fragmentation of 5mm. Glass Beads Induced by Static Compression Using The UTM (a) Before Load Application, and (b) After Crushing Load

The glass beads were loaded to three different crushing loads of 4560 lbs. (10.0 MPa), 5360 lbs.(11.8 MPa) and 10850 lbs (23.8 MPa). Due to the position of the individual grains and the consequent manner by which the particle-to-particle contact points developed, varying stresses were experienced by individual bead in the specimen and hence the formation of chaotic non-uniform force chains in the system as suggested by Cundall and Strack in Figure 3[18].

At these three loading stages a fragmented sample was taken to another compression machine and further subjected to a set of three different compressions under which the ultrasonic waves were passed through for the evaluation of the elastic moduli. Thereafter the samples were sieved to obtain the PSD and consequently the associated fractal fragmentation dimension.

7.3 FRAGMENTATION CHARACTERISTICS OF GLASS AND GRAVELS

7.3.1 Glass Beads

Glass is a material which normally behaves elastically. The crushing of the glass beads serves the purpose of understanding the action of crushing of perfect spheres[61]. After the completion of this exercise, similar samples of angular as well as round gravels used earlier in Chapter 6 were put under the same routine as the glass beads. The crushing within the plexi glass cylinder containing the glass beads and the rocks were found to be different. This can be expected because of the different material strength, structure and texture of the grains.

As the compression load was increased, sporadic explosions of individual glass beads were observed. These small explosions occurred more rapidly all over the particulate system without any particular pattern, the result of which sudden decreases of compression were observed. The total crushing of a sphere creates sudden addition of voids. With reduced points of contacts compression was reduced and as the particles again packed together a new stress chain was developing with a different set of contact points.

Eventually the point-to-point contact between the spheres was reduced as the amount of fragments increased. At the maximum compression load applied, there were only isolated occurrence of explosion and in addition a high degree of material packing was observed at the top of the cylinder and a lesser degree of packing took place at the bottom plug as can be seen from Figure 50.

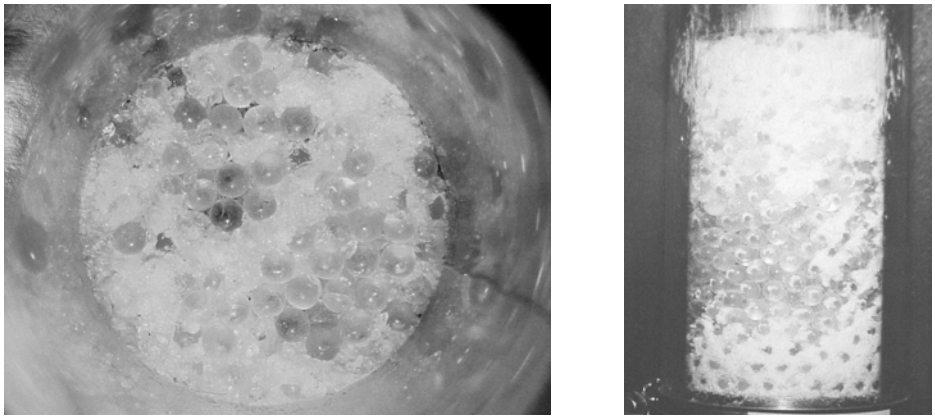

(a) (b)

Figure 50 (a) Highly Packed Glass Beads and Fragments on the Top Column, and (b) Migration of Fines within the Fragmented Particulate System

7.3.2 Gravels

The uniform gravels used in the experiment were initially obtained from a natural soil mixture of various sizes of coarse grain materials and put through a sieving process for selection. These gravels were then thoroughly washed and oven-dried and carefully hand picked to ensure they fall into either category of the angular or the round gravels As natural rock materials, the gravel may have lines of faults and micro cracks and cracks within them. Because of the non-uniform structural shape of the rocks, the initial voids in gravels are higher than glass beads. And similarly with the angular gravels which has a higher void ratio than the round gravels. In addition, the surface texture of the three materials is also different with the roughest surface as being presented in the angular gravels and the round gravels being smoother and the perfectly smooth texture of the glass beads surface area.

All the characteristics mentioned above seem to dictate the way crushing takes place in the gravels. The more irregular the shape of the particles within a particulate system the point-to-point contact between the individual grains becomes less defined. There was also an absence of explosive crushing as observed in the crushing of glass beads, however sounds of cracks are being heard as the compression is applied. In contrast to the glass beads, total crushing was mostly observed to have taken place on the top most layers of the gravels column where they were in contact with the loading piston. The crushed gravels form compact layers at the top while the gravels at the bottom layers were not very much affected. Figure 51 indicates that angular gravels fracture more than the round gravels as shown in Figure 52. There were more migration of the fragments within the angular than the round gravel and this can be observed from the images of the composition of the materials rested at bottom of the cylinder as seen in Figures 51 (b) and 52 (b).

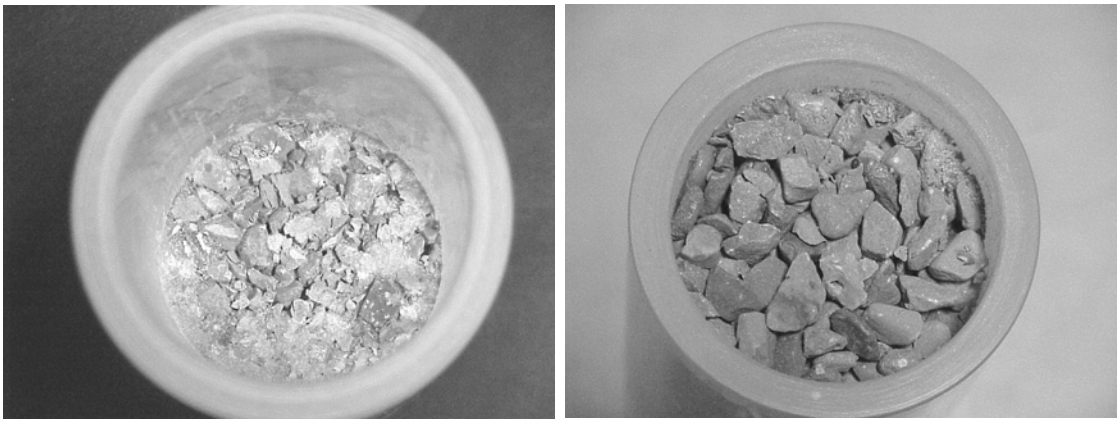

(a) (b)

Figure 51 Crushed Materials after Compaction Viewed from (a) Top Layer (in Contact with Loading Piston) and (b) Bottom Layer in Angular Gravels

(a) (b)

Figure 52 Crushed Materials after Compaction Viewed from (a) Top Layer (in Contact with Loading Piston) and (b) Bottom Layer in Round Gravels

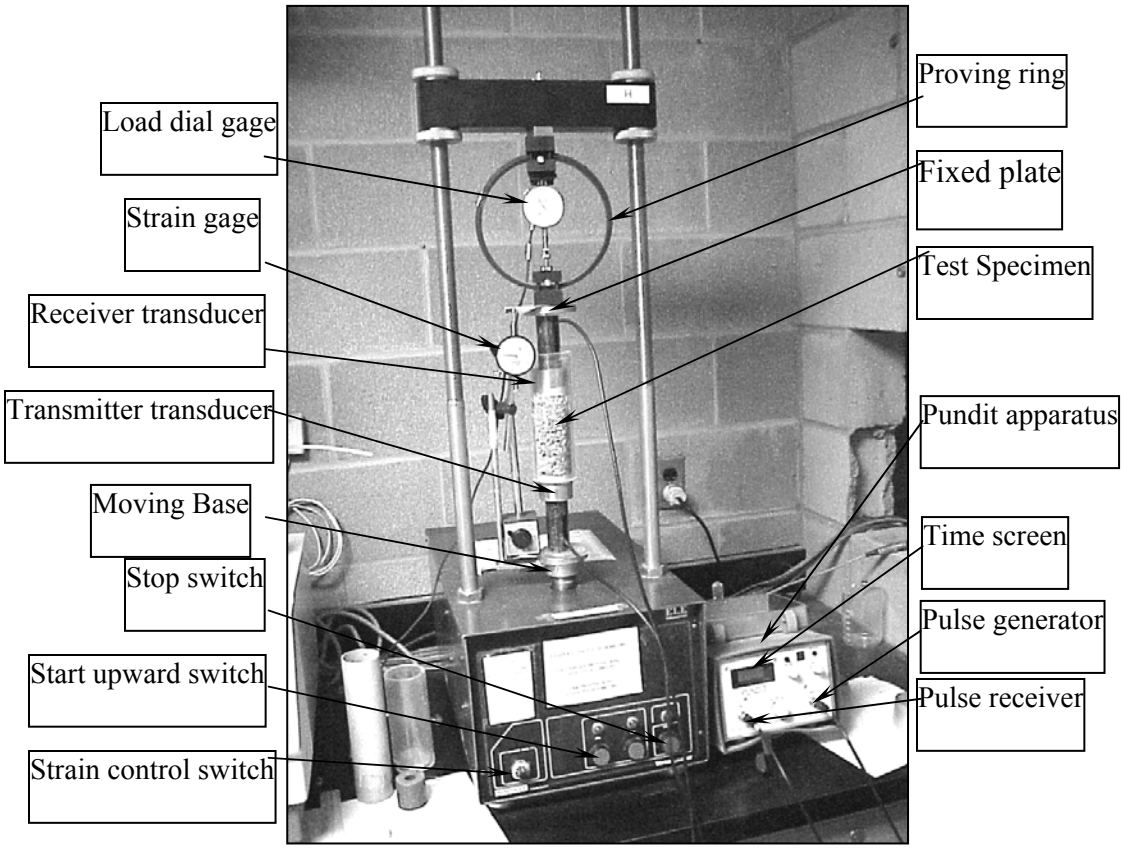

Figure 53 Compressed Specimen in the Versa Loader Compression Machine Subjected to Ultrasonic *P* and *S* waves

7.4 MEASUREMENT OF THE PROGRESSIVE *P* AND THE SHEAR *S* WAVES

In order to evaluate the elastic moduli, the values of the *P* and the *S* waves are required. To obtain the measurement of the waves a supersonic pundit apparatus was used on the crushed specimens in a test set up as shown in Figure 52.

Immediately after the fragmentation and the compression of a sample in the UTM were completed, extra care was taken so that as little disturbance as possible occurred when the sample still remaining in the same plexi-glass tube was transferred to the Versa Loader machine. The installation of the shear waves transducer set and then switching to the compressive waves set were carried out to get the appropriate results. A better result is expected if the tests were performed in such a way that the arrangement of the particles within the sample remains unchanged.

To find the elastic modulus of the sample, the velocities of compressive wave, V_p and the shear wave, V_s are obtained using a pundit apparatus that measures the time travel across the sample between the transmitter and the receiver transducers. The cylindrical shaped transducers that measure 50mm. in diameter have the central frequency of 54kHz. for the *S*-wave (shear wave) and 180kHz. for the *P*-wave (compression wave) respectively. As the transducers used for the *P*-wave and the *S*-wave measurements are different, great care is taken during the process of switching from one set of transducers to the other.

The pundit apparatus with a high degree of accuracy of 0.1E-6 measures the travel time through the sample at compression pressures of 100 kPa, 200 kPa and 500 kPa. The average of two readings for each test specimen is recorded at each compression load. The consistency and accuracy of the apparatus at these readings were demonstrated in tests carried out earlier for the purpose of obtaining Young's modulus of binary soil samples by Loboguerrero[35]. The shear and compressive wave velocities are calculated as shown in an example in Table 14 and the velocities are then used to obtain the moduli of the sample using equations (2.3), (2.4) and (2.5) as follows.

Table 14 *P*-wave and *S*-wave Velocities through a Crushed Glass Beads Sample

Load Dial Reading	Versa Loader Machine	*P* wave Transducers		*S* wave Transducers		*P* wave Velocity		*S* wave Velocity	
	Compressive Pressure σ_c (KPa)	sample length d(m)	time (1xE-6) seconds	sample length d(m)	time (1xE-6) seconds	ρ Density (kg/m³)	V_p m/s	ρ Density (kg/m³)	V_s m/s
60	100	0.1040	63.8	0.1050	111.6	1546.8	1630.1	1532.1	940.9
125	200	0.1035	60.0	0.1040	99.4	1554.3	1725.0	1546.9	1046.3
320	500	0.1030	56.3	0.1035	86.6	1561.9	1829.5	1554.3	1195.2

Young's modulus of elasticity, $$E = \frac{V_s^2\left(3V_p^2 - 4V_s^2\right)\rho}{V_p^2 - V_s^2} \qquad (7.1)$$

Poisson's ratio, $$v = \frac{1}{2}\left(\frac{V_p^2 - 2V_s^2}{V_p^2 - V_s^2}\right) \qquad (7.2)$$

Shear modulus, $G = \rho V_s^2$ (7.3)

7.5 RESULTS OF THE FRAGMENTATION AND ELASTIC MODULI OF GLASS BEADS

7.5.1 Fragmentation of the Glass Beads

Fragmentation in the glass beads due to the applied static loads is presented by the PSD curves and the related the power-law fractal fragmentation dimension plots in Figures 54(a) and 54(b). The correlations for the plots in Figure 54(b) were found to be very good and they improved as the higher degree of crushing was attained. Similar to the earlier crushing trends seen in the fragmentation of sands are also observed in the experiments with the fragmentation of the glass beads. The increase in the amount of the fragments of the glass beads is associated to the increase in the fractal fragmentation number by evaluation of the power-law plots.

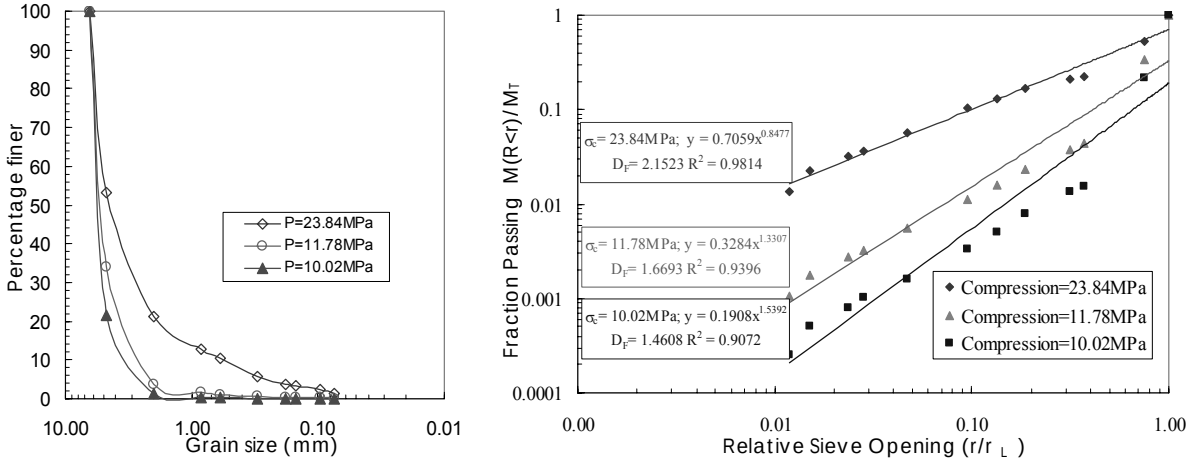

(a) (b)

Figure 54 Fragmentation in Glass Beads

7.5.2 Elastic Moduli of the Glass Beads

With increasing pressures applied in the Versa Loader machine from 100 to 200 and 500 Kpa, vertical deformations take place. Higher values of wave velocities V_p and V_s can be expected as shown in Table 14 as the length of the samples are reduced. These deformations are certainly affected by the quantity of glass bead fragments as a result of crushing in the UTM. The samples experienced a change in the volume and in the density of the material. However, with such a relatively small deformation as the porosity was in the range of 0.36 to 0.31 for the initial condition to the final maximum load applied condition, coupled with the sensitivity of the equipment in measuring loosely packed material, the plots in Figure 55 do not indicate significant effects due to increases in the fractal fragmentation dimension.

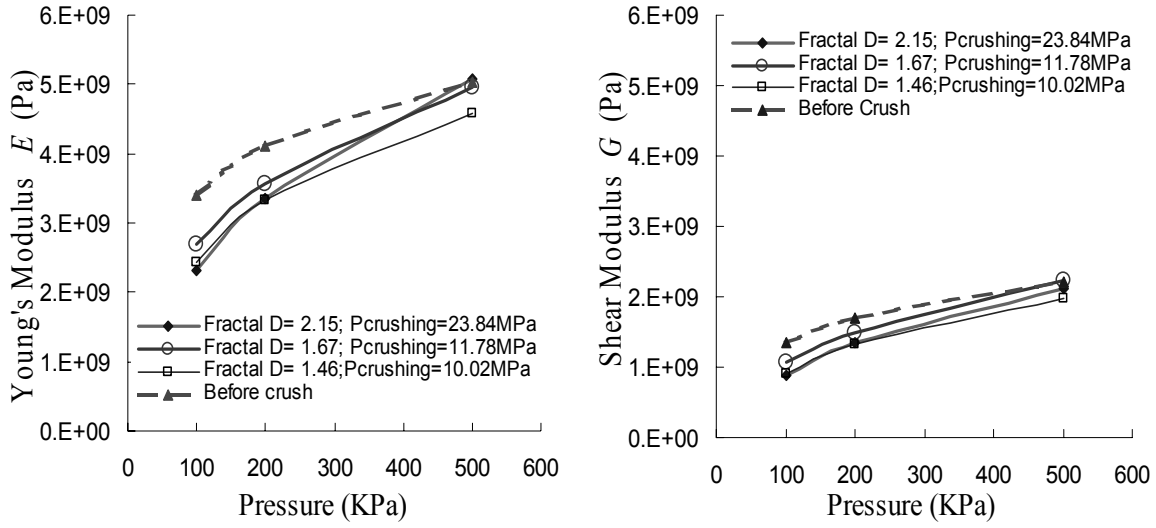

Figure 55 Effect of Compression in Versa Loader Machine on (a) Modulus of Elasticity *E* and (b) Shear Modulus, *G* of Crushed Samples

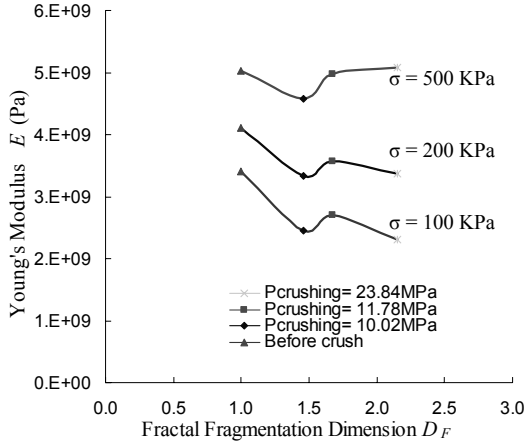

(a)

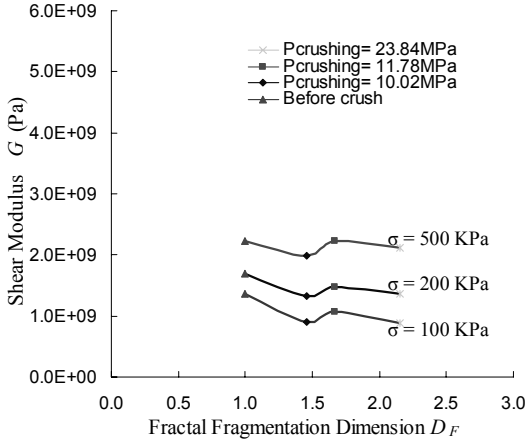

(b)

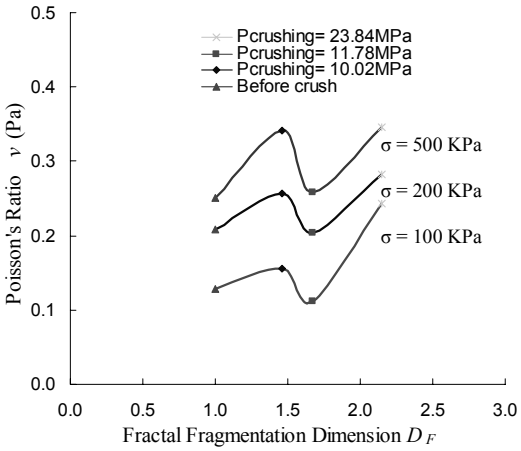

(c)

Figure 56 Effect Fragmentation on (a) Young's Modulus of Elasticity, (b) Shear Modulus and (c) the Poisson's Ratio of Glass Beads

A relationship between the elastic moduli and the fragmentation of the glass beads can be obtained as shown in the Figures 56(a), 56(b) and 56(c). For a compression between100 KPa to 500KPa the measured elastic modulus (Young's modulus) of the glass beads is between 2 to $5x10^9$ Pa and the shear modulus is between 1 and $2x10^9$ Pa. The accuracy of the tests is quite good since elastic modulus obtained is only less by approximately 10^1 to the values mention in some text[61].

When the glass beads begin to crush the values of elastic and shear moduli drop slightly. Originally it may need a larger stress to achieve a particular strain, however with some amount of fragments the strain is increased making the system less stiffer then previously and hence a very slight drop in the moduli.

7.6 TEST RESULTS OF FRAGMENTATION AND ELASTIC MODULI OF GRAVELS

7.6.1 Fragmentation of the Gravels

Gravels that were loaded to crush in the UTM were fragmented in the manner presented in the photos in Figure 51, and 52. The fragmented product of the compressed sample is presented by the PSD and the corresponding power-law plots as shown in Figures 57(a) and 57(b) for round gravels and Figures 58(a) and 58(b) for angular gravels.

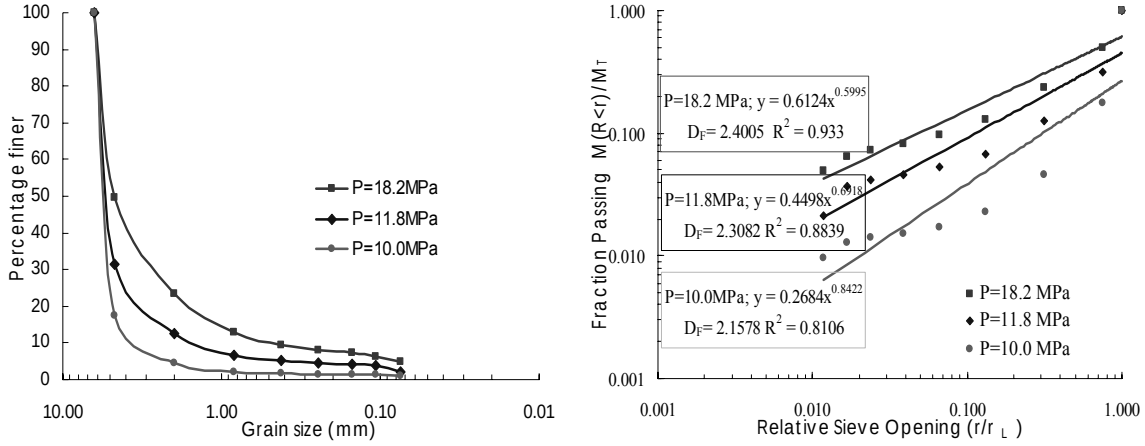

(a) (b)

Figure 57 Fragmentation in Round Gravels

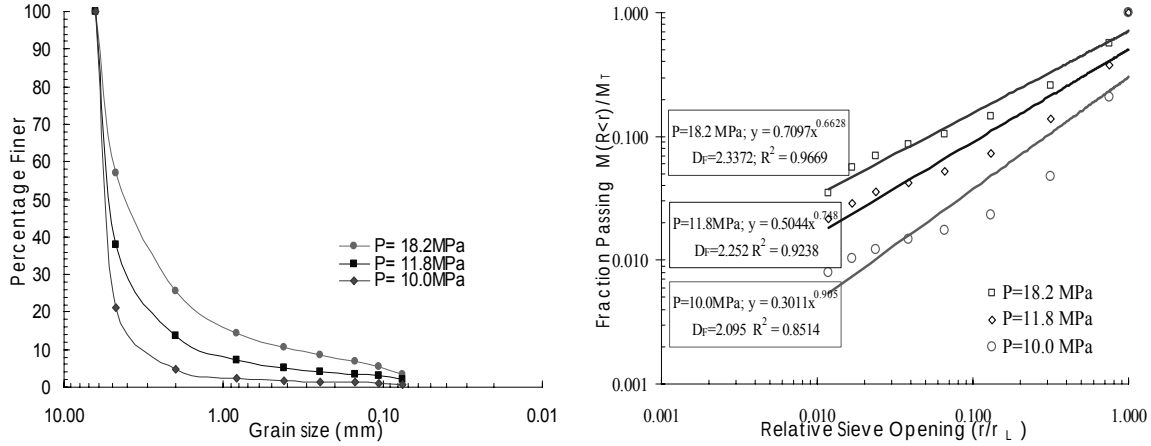

(a) (b)

Figure 58 Fragmentation in Angular Gravels

The results due to static compression loading on mix gravels with different structural shape shows that slightly more fragments were produced in the round gravel for the given crushing compressions of 10 MPa, 11.8MPa and 18.2MPa. The fractal dimensions of the crushed samples were also slightly higher in the round gravels although the power-law plots seemed to indicate that the correlations are better in the fragmented angular specimen. In general however, the experiments on the crushing of the two types of sample due to static loading gave out almost identical results in terms of the production of fragments.

The following plots in Figure 59 illustrate the relationship between the crushing compression and the fractal dimension of the fragmented materials for both the round and the angular shaped gravels used in the elastic moduli tests.

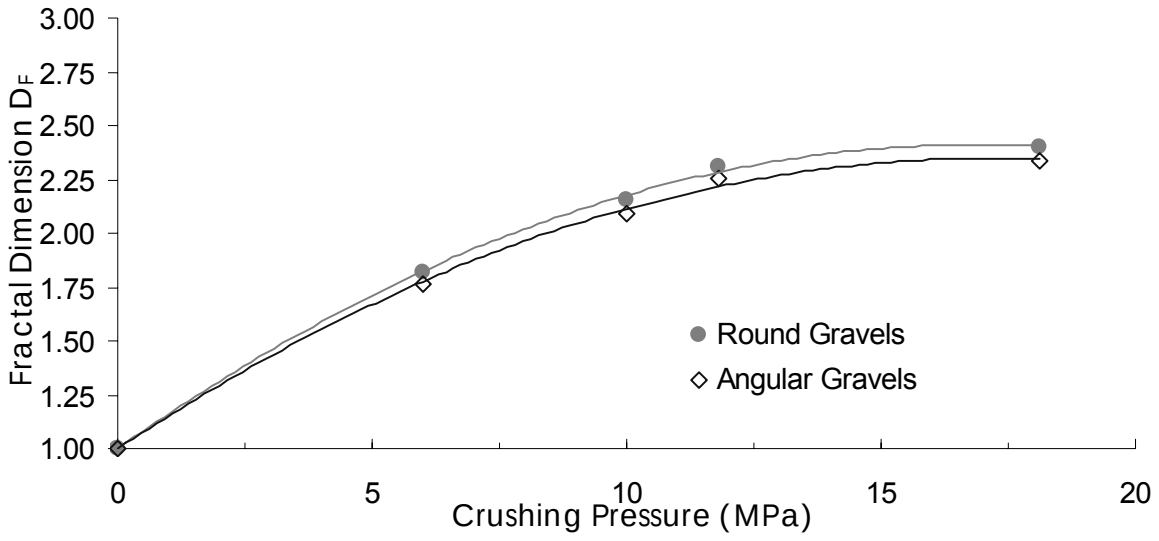

Figure 59 Relationship between the Fragmented Gravels and the Compressive Pressure

7.6.2 The Elastic Moduli of Small Gravels

Tests for the elastic moduli of the gravels were performed on the gravels using similar procedures as the one used for the glass beads in the earlier exercise. A sample of the calculated result of the tests for the elastic moduli on round gravels subjected to a compressive load of 10.0 MPa is presented in Table 15(a) and (b).

As the gravels crushes under compression, the particulate system deforms. At every stage of compaction the density therefore increases while the porosity decreases. The elastic moduli on the other hand as obtained in Table 15 (b) were calculated using the equations presented earlier (EQ 7.1, EQ 7.2 and EQ 7.3). The overall data can be related to fragmentation as shown in the following plots in Figure 60 (a), (b) and (c).

Table 15 Result of (a)*S*-wave and *P*-wave Velocities for Gravels Crushed at 10 MPa and (b) Computation of Poisson's Ratio, Young's Modulus and Shear Modulus

Load Dial Reading	Versa Loader Machine	*P* wave Transducers		*S* wave Transducers		*P* wave Velocity		*S* wave Velocity	
	Compressive Pressure σ_c (KPa)	sample length d(m)	time (1xE-6) seconds	sample length d(m)	time (1xE-6) seconds	ρ Density (kg/m³)	V_p m/s	ρ Density (kg/m³)	V_s m/s
60	100	0.1167	84.0	0.1170	125.0	1635.6	1388.9	1631.2	935.95
125	200	0.1166	74.5	0.1168	112.0	1636.7	1565.1	1633.3	1043.2
320	500	0.1165	66.0	0.1166	97.0	1638.5	1764.7	1636.8	1201.9

(a)

Versa Loader Machine Compressive Pressure σ_c (KPa)	Poisson's Ratio v	Young's Modulus (Pa)	Shear Modulus (Pa)
100	0.0841	3.10E+09	1.43E+09
200	0.1002	3.92E+09	1.78E+09
500	0.0673	5.05E+09	2.36E+09

(b)

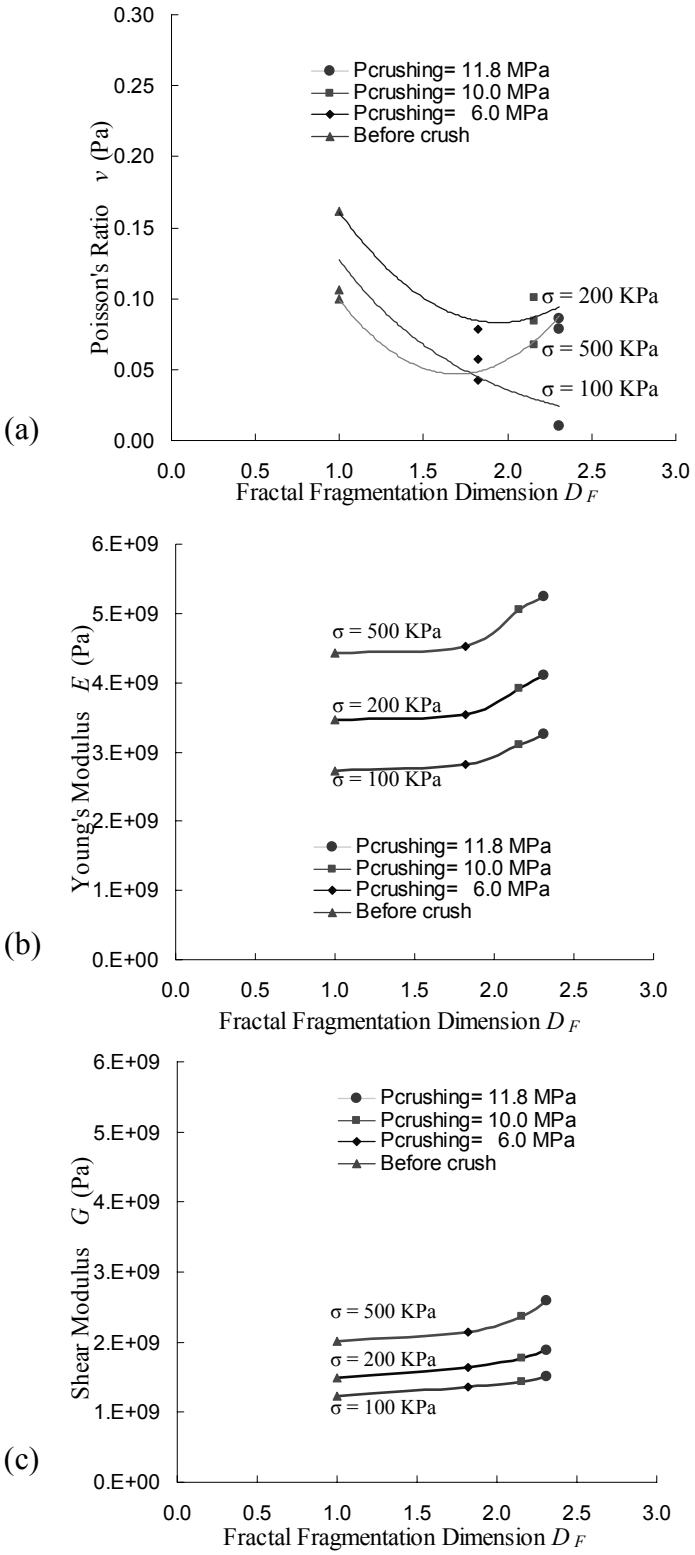

Figure 60 Effect of Fragmentation on (a) the Poisson's Ratio, (b) Young's Modulus and (c) Shear Modulus of Elasticity of Gravels

Poisson's ratio for the granular soil varies over a narrow range[62] The values obtained based on the calculated ultrasonic compressive and shear waves velocities show an overall smaller Poisson's ratio. As observed from Figures 60(b) and 60(c) the response to a larger compression load in the Versa Loader is a higher value of elastic moduli. By increasing the crushing of the gravels as indicated by the fractal dimension numbers, the Young's elastic modulus and the shear modulus for the gravels follows a pattern of gradual increase in values of the moduli. For example, when subjected to a compression of 500 KPa in the Versa Loader machine, the initial unbroken gravels gives the E=4,430 MPa. When crushed at 10.0 MPa, the E=5,050 MPa. and finally the Young's modulus for the gravels crushed at 11.8 MPa., is 5,247 MPa.

7.7 CONCLUSION

Laboratory tests using the ultrasonic pundit apparatus on granular samples of glass beads and small gravels with average size of 5.5 mm is a complex exercise mainly because the free movement of these mostly loose materials during the tests. The results of the progressive and the shear wave velocities of the consequent state of fragmentation will record erroneous reading if the particles arrangement were altered. As the transducers are highly sensitive, a slight error in recording will most of the time provide a misleading result.

The elastic moduli obtained when using the glass beads does not indicate an increase in value with respect to increase in fractal dimension except for the ones when the compression in the Versa Loader was at the compression pressure of 500 KPa. The main reason for this is that the glass beads are always very fluid and moves with the slightest agitation.

Crushing tests carried out on specimens of round and angular gravels using the UTM shows almost identical results in terms of fractal dimension evaluation. The elastic moduli tests performed on round gravels crushed within 11.8 MPa indicate that The elastic moduli increase with the increase in rock fragments denoted by the fractal fragmentation number. The analysis carried out in the tests shows a good promise in the application of fractal fragmentation to the response of elastic constants of granular material systems.

8.0 FRAGMENTATION OF GRANULAR MATERIALS AND ITS EFFECT ON THE HYDRAULIC CONDUCTIVITY

8.1 INTRODUCTION

Investigation on the effects of presence of water in a soil is a very important aspect of study in geotechnical engineering. A build up of pressure in the soil may create all kinds of structural problem in the field. Somewhat this is analogous to the blood pressure in a human body. If pressure is high the body may get sick. It was mentioned earlier that a build up of water pressure damages the road pavements and this leads to the ultimate failure to the pavement structure. To avoid the unwarranted condition, water that enters the granular domain of the system should be able to flow out with ease. This however may not be the case if crushed granular material is in place instead of the initially selected rocks with a uniform size is used.

The investigative work on the hydraulic conductivity of the granular soil related in the chapter involves a number laborious assignment in the laboratory. To understand the flow characteristics in the granular phase, the material used were selected into the two types referred as the angular shaped and the round shaped gravels. Each individual stone was carefully inspected and selected to prepare a total specimen weight of 6 kilograms of gravels that fall into the two groups.

To induce crushing the UTM is used to simulate static load and the soil mechanics Standard Compaction Proctor is used to simulate dynamic load. The compacted and fragmented sample in the steel cylinder was then transferred to a constant head permeameter set up as shown in Figure 64. The specimen was oven dried after the tests on the hydraulic conductivity of the sample was performed and again further crushing was induced and the next cycle of tests was repeated.

8.2 FRAGMENTATION BY DYNAMIC LOAD

The induced fragmentation by static load in the UTM has been carried out and the results were presented in the previous chapter. For the dynamic loading simulation using the standard proctor test (based on ASTM Designation 698-91), the resultant crushing of the gravels is due to pounding action of the drop hammer. Crushed gravels subjected to 100 blows, 200 blows and 500 blows were tested for the hydraulic conductivity. The following Figures 61 (b) and 62 (b) show almost identical PSD plots. However, the fractal dimensions obtained from the data indicate a slight difference between the two results as can be seen from Figures 61 (a), 62 (a) and 63.

Just as in the static loading situation, in relation to the energy imported to the gravels, the value of fractal dimensions of the products were found to be almost identical. It is also observed that fractal dimensions of the specimens were much higher in the dynamic loading than the static loading indicating higher degree of fragmentation.

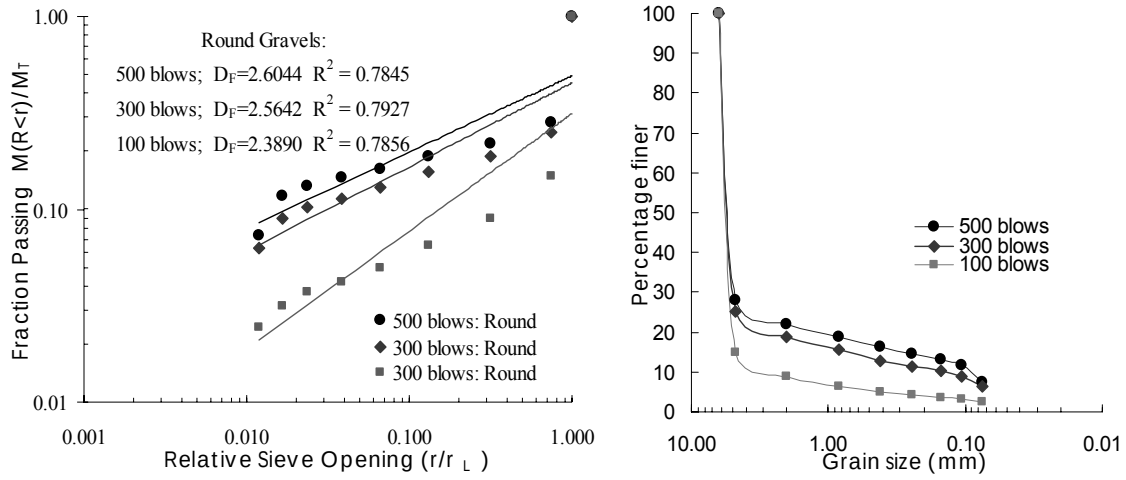

Figure 61 (a) Fragmentation Fractal Dimension D_F and (b) The Particle Size Distribution of the Round-Shaped Gravels

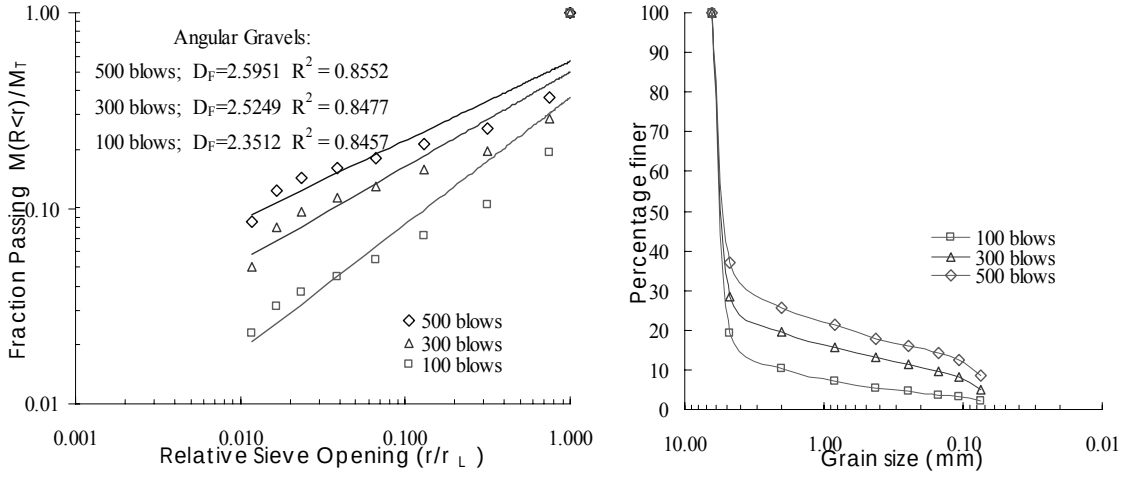

Figure 62 (a) Fragmentation Fractal Dimension D_F and (b) The Particle Size Distribution of the Angular-Shaped Gravels

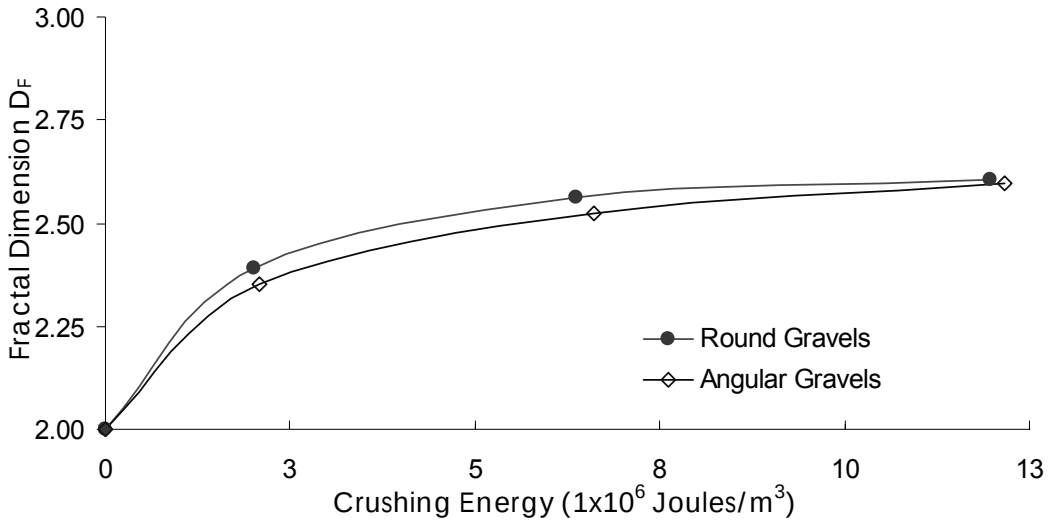

Figure 63 Measured Fragmentation Fractal Dimension D_F of the Crushed Round and Angular Gravels Subjected to Standard Proctor Compaction

8.3 HYDRAULIC CONDUCTIVITY OF POROUS MEDIA

Darcy in 1856 proved by experimental results that the discharge (seepage) velocity v is proportional to the imposed hydraulic gradient i (head difference i across a sample length, L) in a simple relationship as follows.

$$v = ki \tag{8.1}$$

and, $$q = ki.\mathrm{A} \tag{8.2}$$

where k is the hydraulic conductivity[37] in cm/s

q is flow discharge in cu. cm/s , and

A is the x-section area perpendicular to the flow lines in sq.cm.

The coefficient k , also known as coefficient of permeability[36, 63] represents the seepage velocity for $i = 1$ and has a velocity dimension $[LT^{-1}]$. The hydraulic conductivity is a measured quantity which characterizes a porous medium and the fluid which flows through the medium. The size of the soil grains affects the flow in the soil because the pore size, which is the primary variable, is related to particle size. It was stated by Lambe[64] that the permeability of a cohesionless soil is approximately proportional to the square of an effective diameter. Other important factors are the void ratio of the soil and the shapes and arrangement of the pores. The only important variable of water is viscosity, which is sensitive to temperature. The hydraulic conductivity of a soil is therefore a soil property which indicates the ease with which water will flow through the soil.

8.4 CONSTANT HEAD PERMEABILITY TESTS

The constant head method of testing that has been found to be suitable for granular materials is adopted in the exercise. The testing procedure follows the recommendations of the ASTM D 2434 as presented in The Soil Testing Manual, Department of Civil and Environmental Engineering, University of Pittsburgh[65]. The apparatus set up shown in Figure 64 is using the K-605 combination permeameter with the in-flow at the bottom.

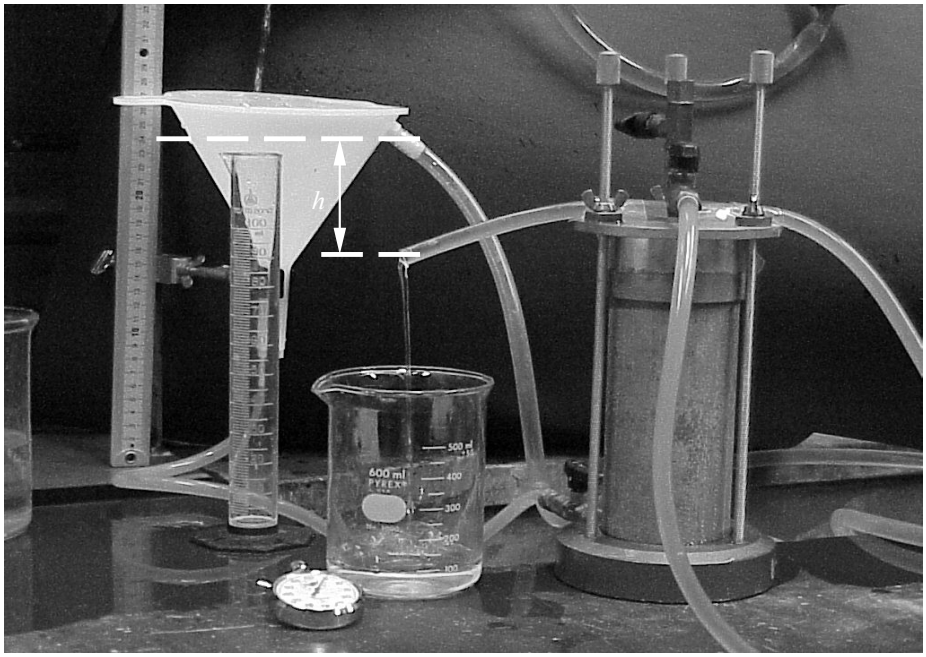

Figure 64 The Hydraulic Conductivity Test Set-up

8.4.1 Additional Procedures

As effects due to the different level of crushing needed to be recorded it was necessary for additional apparatus and measures were included in order to obtain a higher accuracy data. Every single material especially the fines produced as a result of the crushed gravel need to be kept within the chamber and not lost during all the tests until completion. In the permeameter, porous stone filter-units were installed at the bottom as well as at the top of the specimen. To avoid clogging of these porous stones by the fines transported outwards by water, a layer of thin durable paper filter is also installed. The filters are wrapped around the porous stone units each with a rubber band in such a way that during the tests flow is forced through the units rather than around them.

The thickness of the base plug at the bottom of the chamber during which the specimen was crushed was designed to perfectly fit the total thickness required to place the filter unit as the chamber was set up in the permeameter. The perfect fit was the key to the leak-proof tests. Adequate tests were then carried out to evaluate the hydraulic conductivity of the filter-units. Using an equation (EQ. 8.3) for equivalent hydraulic conductivity the determination of vertical flow in stratified layers the *k* values for the tested samples were obtained.

$$k_{V(equivalent)} = \frac{h}{\left(\frac{h_1}{k_{V_1}}\right)+\left(\frac{h_2}{k_{V_2}}\right)+\left(\frac{h_3}{k_{V_3}}\right)} \qquad (8.3)$$

Water entering chamber from the a constant water level reservoir through the bottom passes the bottom filter unit into the gravel specimen and moves through the top filter and exits via a tube attached to the top lateral valve as shown in the schematic drawing in Figure 65. At a specific head difference at least 3 flow discharges need to be measured in order to obtain a steady data that can be used. Measurement of time was by using a stop clock to indicate the duration to collect 500 ml. of water. Interference due to trapped air bubbles constantly occur and the temperature of the water also need constant monitoring because it can vary significantly at certain time.

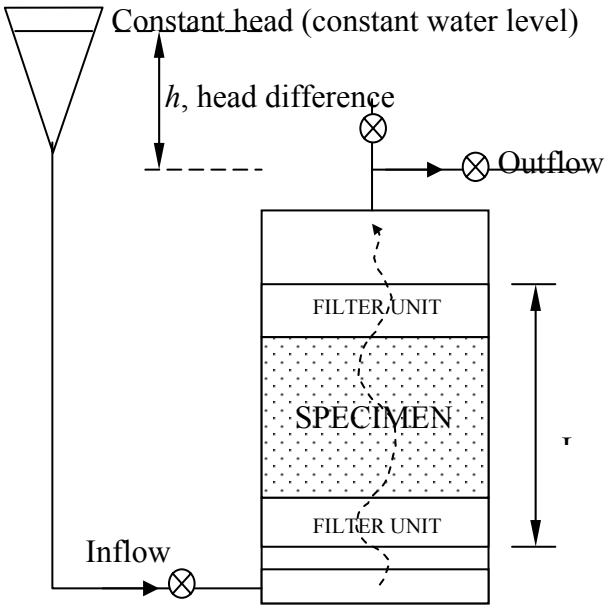

Figure 65 The Schematic Drawing of the Constant Head Test with In-Flow at Bottom

If h, is increased a higher value of discharge q is obtained since they are directly proportional to each other. For each specimen, testing time of 6 to 8 hours was required to conduct an average of 5 different values of h. A straight line plot can now be constructed to obtain the equivalent hydraulic conductivity ($k_{V\,(equivalent)}$) and thus the value for the hydraulic conductivity of the specimen is calculated from the equation (8.3).

After completion of a test, the filter units were carefully extracted from the chamber while leaving the soaked specimen perfectly intact. The base plug is again fitted at the bottom of the chamber and the gravels are oven dried at 300˚C for a duration of 24 hours. After a cooling off period, the specimen is subjected to a higher degree of crushing and after which the process

of saturation and then the exercise of measuring of the discharges at various heads is repeated. From the beginning, measurements of the specimen height (L) and weight were constantly recorded to closely monitor the integrity of the composition as well as the changes in the void ratio of the gravels.

8.4.2 A Sample of Test Data

The following Table 16 shows a sample of the test data after a specimen of angular gravels was crushed at 18.24 MPa. and the data is used to obtain the equivalent hydraulic conductivity from a straight line plot as in Figure 65. The description of the related angular gravel specimen is presented as follows in Table 17;

Table 16 Test Specimen Description

Type of specimen	: Angular-shaped gravels (average diameter: 5.5 mm.)
Crushing Load Pressure	: 18.24 MPa
Specific gravity G	: 2.67
Dry weight W_s	: 571.87 g.
Height of gravel	: 10.55 cm.
Length of medium, L	: 13.05 cm. (porous stone filters: 2.5 cm.)
A,(chamber x-section)	: 31.44 sq. cm.
Sample dry density γ_d	: 1.724 g/c.c.
Void ratio, e	: 0.551 (Porosity, n : 0.355)
Filter (porous stones) k_p	: 0.0145cm/s
Measured $k_{V\ equivalent}$	: 0.0367cm/s
Measured k_{gravel}	: 0.0576cm/s

Table 17 Hydraulic Conductivity Laboratory Test Data for Angular Gravels Subjected to Static Compression Pressure of 18.24 MPa

Time t (sec)	h (cm)	(X) Hydraulic gradient $i = h / L$	Flowrate v =(Q/A)/t (cm/sec)	Hydraulic conductivity $k_T = v / i$ (cm/sec)	Water temperature (˚C)	At 20˚C $k_{T=20} = v / i$ (cm/sec)	(Y) Adjusted Flowrate v = (Q/A)/t (cm/sec)
1320	2.7	0.2069	0.0120	0.0582	25.0	0.0517	0.0107
880	5.9	0.4521	0.0181	0.0400	25.0	0.0355	0.0160
495	7.3	0.5594	0.0321	0.0574	26.0	0.0498	0.0279
466	9.5	0.7280	0.0341	0.0469	25.0	0.0416	0.0303
400	14.5	1.1111	0.0398	0.0358	26.0	0.0310	0.0345

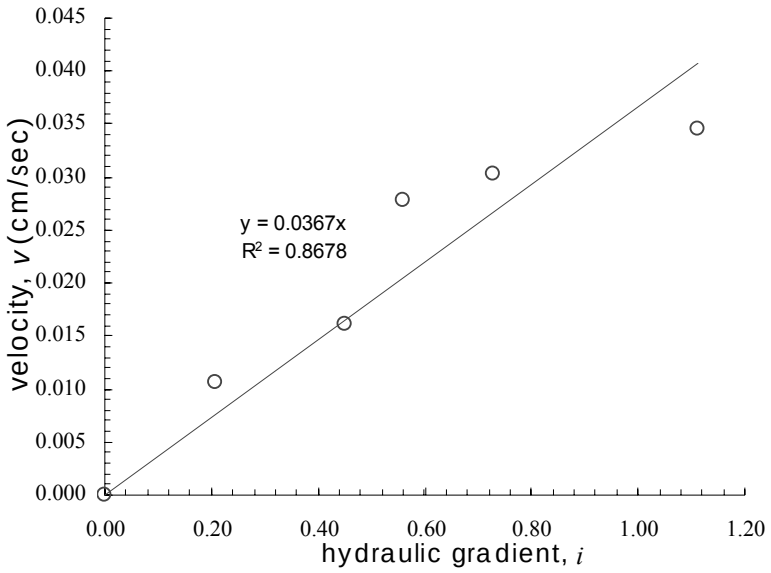

Figure 66 Hydraulic Conductivity ($k_{V\ equivalent}$ = 0.0367 cm/s) for Angular Gravels Subjected to 18.24 MPa

8.5 HYDRAULIC CONDUCTIVITY OF FRAGMENTED GRAVELS DUE TO STATIC AND DYNAMIC LOAD

Hydraulic conductivity tests were conducted on four samples from round gravels and four from angular gravels. The first sample from each of the group represents the condition before crushing takes place. The next three represent progressive fragmentation as a result of increased crushing loads either in static or dynamic modes. As the materials break, the volume decreases and the finer fragments migrate into the voids. As a result of reduced void ratio and porosity, the ease at which the water can flow through the specimen is affected.

The following plots show the result of the hydraulic conductivity tests for the round gravels in Figure 67 (a) and for the angular gravels in Figure 67 (b). due to static axial compressive load. The laboratory results in the case of dynamic loading by conducting repeated blows of the standard proctor are presented for the evaluation of k by plots in Figure 68 (a) for the round gravels and in Figure 68 (b) for the angular gravels. Tables 18 (a) and (b) summarize results of the tests and the affect of the increased fragmentation signified by the fractal dimensions. From the data, a relationship between the hydraulic conductivity of the gravels and the fractal dimensions can be established, and this demonstrated by the plots in Figure 69.

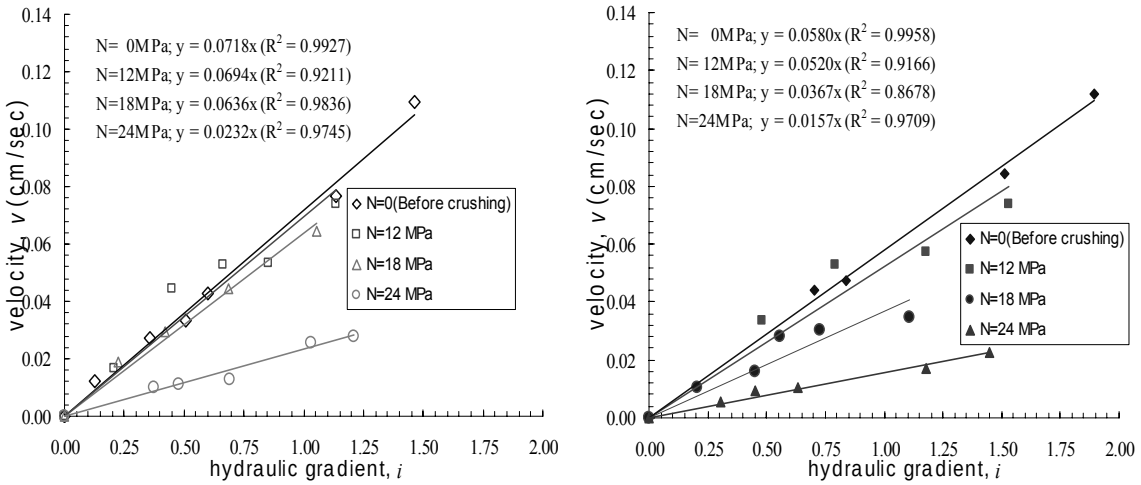

(a) (b)

Figure 67 Laboratory Evaluation of Hydraulic Conductivity *k* for Fragmented (a) Round Gravels and (b) Angular Gravels Subjected to Static Load

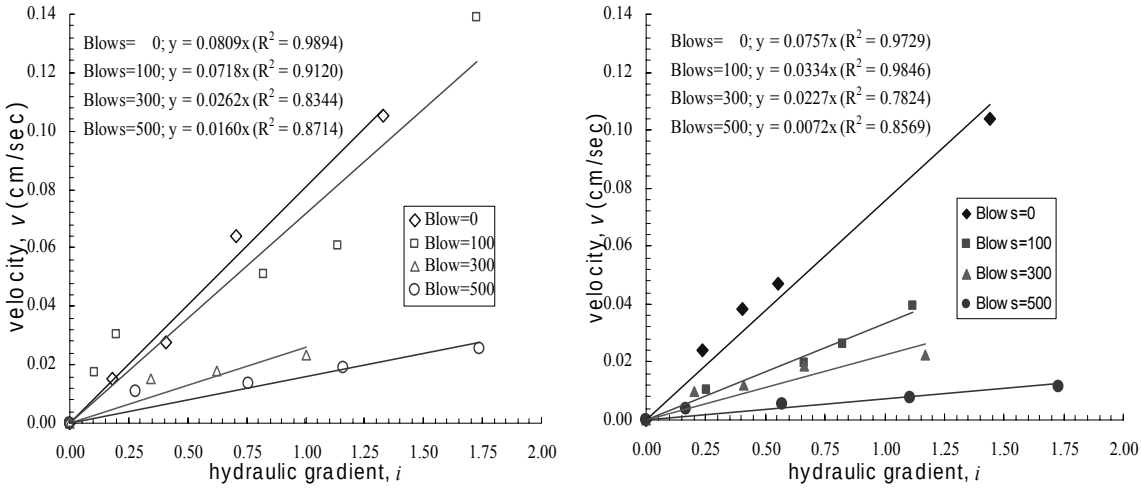

(a) (b)

Figure 68 Laboratory Evaluation of Hydraulic Conductivity *k* for Fragmented (a) Round Gravels and (b) Angular Gravels Subjected to Dynamic Load

Table 18 Summary of the Test Result due to (a) Static Compression and (b) Dynamic Loading

Static Compression Pressure, N (MPa)	Round Gravel			Angular Gravel		
	Fractal D_F	Void ratio e	k (cm/s)	Fractal D_F	Void ratio e	k (cm/s)
0	1.0000	0.681	0.343	1.0000	0.836	0.150
12	2.3082	0.616	0.329	2.2520	0.711	0.117
18	2.4005	0.530	0.250	2.3372	0.551	0.058
24	2.4200	0.462	0.027	2.3500	0.422	0.016

(a)

Dynamic Loading E(# blows)	Round Gravel			Angular Gravel		
	Fractal D_F	Void ratio e	k (cm/s)	Fractal D_F	Void ratio e	k (cm/s)
0	1.0000	0.667	1.024	1.0000	0.829	0.520
2 MJ/m^3(100blows)	2.3890	0.599	0.451	2.3512	0.681	0.047
6 MJ/m^3(300blows)	2.5642	0.517	0.032	2.5249	0.601	0.026
12 MJ/m^3(500blows)	2.6044	0.496	0.016	2.5951	0.461	0.006

(b)

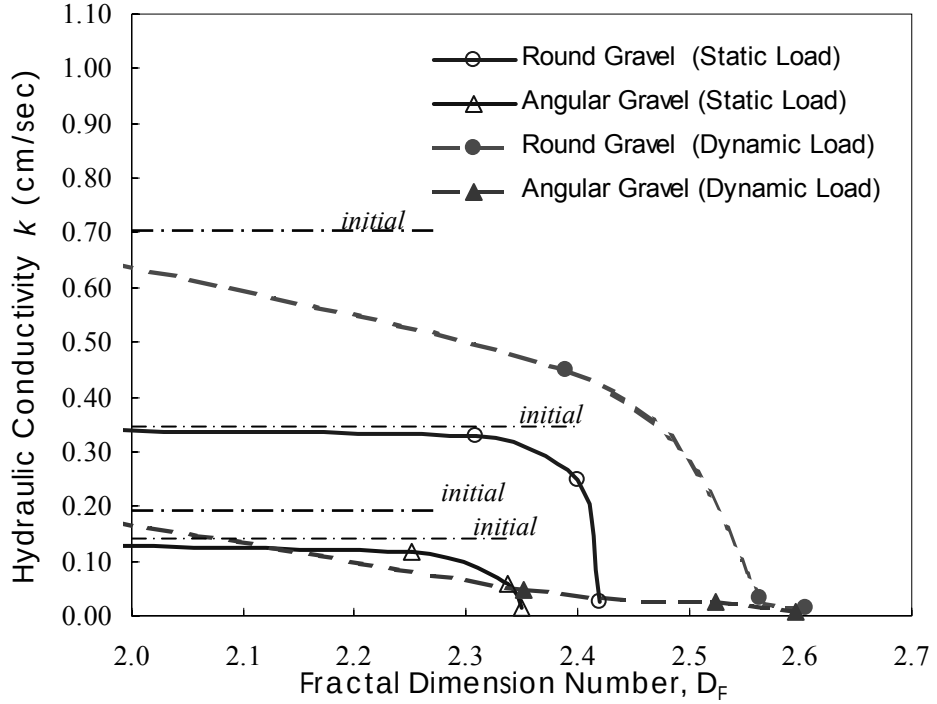

Figure 69 Hydraulic Conductivity of Round and Angular-Shaped Gravels in Relation to the Fragmentation Fractal Dimension due to Static and Dynamic Loads

The laboratory results show that the values of hydraulic conductivity of fragmented round-shaped grains and fragmented angular-shaped grains each falls within a certain band. Flow of water is more efficient on rounded surface with smooth texture than in bodies with sharp corners and jagged surfaces. As a result of fragmentation due to high axial compression, the efficiency of flow in round gravels as well as the angular gravels is affected. The effect of finer fragments in round gravels on the hydraulic conductivity is very significant beyond fractal dimension 2.3 when the permeability is greatly reduced. Besides the fines fragments are in fact angular-shaped grains with various sizes. This explains the less pronounced plot presented in the angular gravels. Flow of water in the angular gravel has been always inefficient and as the rocks transformed into numerous smaller angular particles the hydraulic conductivity is reduced but the reduction is not as much as those encountered in the round gravels.

Basing on the fractal dimensions, laboratory results so far indicate that under similar magnitude of crushing load the round gravels appear to be producing more fragments than the angular gravels. Clearly, the increase of the fragments reduces the hydraulic conductivity. However, the reduction in the ease of flow in the round gravels is counter balanced by the efficiency of the fluid flow around smooth rounded grains giving a slightly higher value of k in fragments with round gravels. The shape of the unbroken gravels remaining in the medium as well as the amount of fragments could have therefore affected the hydraulic conductivity characteristics of the fragmented medium.

8.6 A COMPARISON OF THE LABORATORY AND ANALYTICAL SOLUTIONS

Estimation of hydraulic conductivity of clean granular soil may be carried out by using the following equation which is derived from the Kozeny equation as follows[66];

$$k = \frac{2g}{C_s}\frac{\rho}{\mu}D^2\frac{e^3}{1+e} \tag{8.4}$$

where,

g is the acceleration of the gravity.

μ/ρ is the kinematic velocity of water.

C_s is a particle shape factor, which varies from 360 for spherical particles to about 700 for angular particles.

e is the void ratio

D is a weighted or characteristic particle diameter and is obtained from grain-size analysis using the equation: $D = \frac{\sum M_i}{\sum (M_i / D_i)}$

where, M_i is the mass retained between two adjacent sieves and D_i is the mean diameter of the adjacent sieves openings.

The k values from the Hazen's formula, $k = 100D_{10}^2$ are also presented in the following Table 19, where the results of the two methods and the laboratory data are tabulated.

Table 19 Hydraulic Conductivity k (cm/s) from Analytical Solutions and the Laboratory Results

Round Gravels			
Crushing Blows:	100	200	300
Fractal Dimension D_F	2.3890	2.5642	2.6044
Laboratory k (cm/s)	0.451	0.032	0.016
Kozeny (EQ. 8.4)	5.247	0.955	0.468
Hazen's	1600	1.690	0.810
Angular Gravels			
Crushing Blows:	100	200	300
Fractal Dimension D_F	2.3512	2.5249	2.5951
Laboratory k (cm/s)	0.470	0.026	0.006
Kozeny (EQ. 8.4)	2.986	0.535	0.220
Hazen's	361.0	2.560	0.706

Comparing the results between Kozeny's solution and Hazen's solution it is found that solutions using Kozeny equation gives a better fit to the results obtained in the laboratory than Hazen's solutions. It is also interesting to note that the shape factor used for the angular is almost twice the value of the shape factor for the round gravels. Even with these factors the flow is still very much over estimated. Analytical and empirical solutions formulated by earlier researchers have not considered fragmentation as a contributing factor, instead focused on shape and the one size of the grain may it be the effective size as in Hazen or mean diameter as in Kozeny. The laboratory works involving fractal dimension analysis giving a specific value for fragmented particles therefore may be able to be factored in to provide a better prediction. Since the tested specimens consist the shape (round or angular) characteristics as well as fractal characteristics, the Kozeny's may be improved by including both factors instead of only the shape factor C_s as presented in equation (8.4).

8.7 CONCLUSION

The investigation performed in the laboratory using the constant head permeameter have been successful in providing an insight into the problems issued by fragmentation phenomenon in granular soils. The hydraulic conductivity of a soil decreases as the fractal fragmentation dimension of the soil D_F increases. The effect of the shape of the particles, (ie. spherical or angular) has been rightly recognized by earlier researchers by correctly factoring in a higher shape factor value (C_s =700) for the angular grains with respect to spherical grains (C_s =360). As a result, the hydraulic conductivity in soils with round-shaped (spherical) reveals a higher k than angular samples and this is verified in the laboratory tests.

The study on fractal dimension presents a promising tool in improving the prediction of the hydraulic conductivity property of fragmented granular materials. The main advantage of evaluating a whole population of fragmented material with a number can perhaps be utilized to modify existing analytical solutions.

Increased dynamic loading and static loading to crush the gravels seemed to produce almost identical fractal dimension plots for the angular as well as the spherical particles. The repetitive pounding of the standard proctor in the dynamic loading simulation appears to encourage more fragmentation than the static loading. However, the hydraulic conductivity seemed to be on the higher band than those fragmented due to the static loading. When the grains were repeatedly agitated the fragments experienced a more all rounded process of fragmentation unlike those subjected to static loads and this slight difference in the particle orientation may have given the water an easier passage when the tests were conducted.

9.0 SUMMARY AND CONCLUSIONS

The investigation on fragmentation of granular materials performed in this research was focused on various laboratory and theoretical techniques. The laboratory techniques involved tests that caused fragmentation in granular materials as well as tests that measured the changes in engineering properties of the materials as a result of fragmentation. The theoretical analyses evaluated the level of fragmentation in the granular materials. As a result of the wide range of laboratory activities new information regarding fragmentation phenomenon and its effect on the engineering properties of the granular material has been acquired. Two distinct types of fragmentations namely peripheral fragmentation and total fragmentation were initially recognized. Fragmentation levels were analyzed from particle size distributions (PSD) before and after fragmentation of the granular materials and by the use of the fractal dimension concept from fractal theory.

Abrasion as a result of peripheral fragmentation of angular and round gravels of 5.5 mm. diameter as observed and evaluated in tests using the Jar mill apparatus was found to only break the sharp corners of the particles and this changed the profile of the particles. The test results showed that abrasion of the angular grains produce more than four times as much fines than the round gravels accompanied by higher fractal fragmentation number, D_F. An area-perimeter evaluation on the images of the particles performed before and after abrasion was conducted using ImageJ software program. As a result of the particles becoming more rounded the fractal

dimension of their profiles decreases in value with more significant reduction is obtained in angular than in round-shaped gravels.

Crushing tests that involve total fragmentation as well as peripheral fragmentation were observed when fragmentation was induced using the Ring shear apparatus in shearing mode, the Universal testing machine in the static compression mode and the Standard proctor in the repeated impact mode. Fragmentation of the particles that had undergone total destruction of the grain structure produces smaller particles with a wide range of sizes. Evaluation of the fragmentation by the fragmentation fractal dimension D_F as well as the particle size distribution (PSD) curve shows that as a result of changes in the PSD from uniform to well-graded the fractal fragmentation dimension increases in value.

As a result of fragmentation, the engineering properties of the granular materials such as, the elastic moduli, the hydraulic conductivity and the internal angle of friction, were affected. The observations were as follows;

- Using the wave velocities measured by an ultrasonic velocity apparatus (Pundit type), it was determined that fragmentation causes an increase in the elastic moduli of granular materials.
- Using the constant head method with an upward flow permeameter, it was determined that the hydraulic conductivity decreased with an increase in the level of fragmentation.
- Due to the particles becoming more rounded as the level of fragmentation increases and with the inclusion of higher proportion of finer particles surrounding the larger more angular grains, the angle of internal friction decreases with fragmentation.

Fragmentation due to weathering was analyzed in terms of the angle of repose of a binary mixture of soil. The angle of repose is important in the slope stability study involving slope evolution as suggested by the Lehman model that takes into account of this special characteristic property of the granular material. Failed materials consisting of large as well as fine particles that are exposed to weathering fall and form talus with a certain angle of repose at the toe of a slope. The magnitude of the angle of repose defines the progression of the toe of the slope as well as the retreat at the crown. A theoretical relationship between the angle of repose and the inter-granular friction of the grains and the interface base friction was therefore developed.

From the results of the funnel test using smooth surface glass base and rough porous stone base it was evident that the angle of repose a granular material is affected by the interface friction between the granular material and the base material. The different compositions of the binary granular mixture also affected the angle of the sand pile.

The introduction of fractal analysis method and the focus on establishing a relationship that provides a different perspective and physical meaning between rock fragments fractal dimensions and its engineering properties have also resulted in some encouraging and exciting findings. For example, a comparison of the laboratory results to that as predicted theoretically by Kozeny's, it is found that among the other factors considered, hydraulic conductivity can be better estimated with the inclusion of the degree of fragmentation of the porous medium. On this note the knowledge of fractal fragmentation dimension D_F that quantifies the fragmentation provides an encouraging prospect in the prediction for example that of the hydraulic conductivity of a crushed granular material.

APPENDIX A

BROMHEAD RING SHEAR

Table 20 Sample of Ring Shear Test Data for Normal Stress: 15 kPa

Load (kg)	6.11
Verical Stress (kg/cm²)	0.1525
L (cm)	15.72
Area of the Sample (cm²)	40.05
R2 (cm)	5
R1(cm)	3.5

December 3, 2001
Test 11

Machine Rate(grade		1.2

grades	time	Vertical (0.001")	A	A(kg)	B	B(kg)	τ (kg/cm²)
0	9:00:00	0	0	0.10	0	0.13	0.01060
1	9:00:50	-22	29	1.05	32	1.21	0.10344
2	9:01:40	-49	32	1.15	38	1.41	0.11718
3	9:02:30	-73	28	1.02	42	1.55	0.11735
4	9:03:20	-96	29	1.05	32	1.21	0.10344
5	9:04:10	-99	25	0.92	33	1.25	0.09899
6	9:05:00	-100	24	0.89	39	1.45	0.10674
7	9:05:50	-110	21	0.79	41	1.52	0.10533
8	9:06:40	-119	12	0.49	42	1.55	0.09339
9	9:07:30	-124	21	0.79	44	1.62	0.10995
10	9:08:20	-128	21	0.79	40	1.48	0.10379
12	9:10:00	-151	23	0.85	42	1.55	0.10987
14	9:11:40	-152	28	1.02	37	1.38	0.10965
16	9:13:20	-155	24	0.89	30	1.14	0.09287
18	9:15:00	-169	32	1.15	32	1.21	0.10793
20	9:16:40	-168	29	1.05	31	1.18	0.10189
25	9:20:50	-160	32	1.15	26.5	1.03	0.09945
30	9:25:00	-161	29	1.05	19	0.77	0.08338
35	9:29:10	-162	25	0.92	25	0.98	0.08665
40	9:33:20	-169	35	1.25	19	0.77	0.09237
50	9:41:40	-154	35	1.25	27	1.04	0.10471
60	9:50:00	-160	41	1.44	19	0.77	0.10135
80	10:06:40	-139	46	1.61	5.5	0.32	0.08799
100	10:23:20	-132	47	1.64	5	0.30	0.08871
125	10:44:10	-127	48	1.67	4	0.27	0.08866
150	11:05:00	-118.5	40	1.41	6	0.33	0.07978
200	11:46:40	-92	54	1.87	2.5	0.22	0.09532
250	12:28:20	-85	62	2.13	13	0.57	0.12350
300	13:10:00	-46	42	1.48	12	0.54	0.09204
360	14:00:00	-38	39	1.38	22	0.87	0.10298

d_h	τ (kPa)
0.000	0.00
0.074	10.15
0.148	11.50
0.223	11.51
0.297	10.15
0.371	9.71
0.445	10.47
0.519	10.33
0.594	9.16
0.668	10.79
0.742	10.18
0.890	10.78
1.039	10.76
1.187	9.11
1.336	10.59
1.484	10.00
1.855	9.76
2.226	8.18
2.597	8.50
2.968	9.06
3.710	10.27
4.452	9.94
5.937	8.63

Refer to the plot on Figure 11(b) for the shear stress-displacement relationship.

Table 21 Sieve Analysis and Manipulation of Grain Size Distribution for Fractal Dimension

Normal Load is 6.11kg.					
Sieve size	wt. of sieve	wt of sieve + soil	soil wt.	% retain	% pass
16	503.9	528.87	24.97	79.83	20.17
20	487.52	491.04	3.52	11.25	8.92
30	382.75	383.2	0.45	1.44	7.48
50	459.33	460.6	1.27	4.06	3.42
100	356.09	356.98	0.89	2.85	0.58
200	300.88	300.99	0.11	0.35	0.22
pan	370.3	370.37	0.07	0.22	0.00
			31.28	100.0	

Sieve	Sieve size	r/r_L	$M(R<r)/M_T$
#10	2	1	1
#16	1.19	0.595	0.2017263
#20	0.84	0.42	0.0891944
#30	0.6	0.3	0.0748082
#50	0.297	0.1485	0.0342072
#100	0.15	0.075	0.0057545
#200	0.075	0.0375	0.0022379
pan			
D_F=3.0-	1.7497		
=	1.2503		

D_F=1.2503

As plotted on Figure 15: Fractal dimension of the fragmented granular soil.

Table 22 Crushing of Quartz Sand at Increasing Normal Load (N)

N (kg)	kPa	Fractal,D_F	ϕ(degree)
6.11	15	1.3852	37.6
23.76	58.2	1.5291	31.67
40	101	1.6108	30.09
80	199	1.8056	28.36
103.76	254	1.834	33.36
120	297	1.9313	27.82
143.76	352	1.9733	29.81
160	394	2.0417	27.52
183.76	450	2.0789	26.82
200	492	2.1084	28.62
223.76	548	2.1447	27.34
321.12	786	2.2409	27.47
401.12	982	2.2117	27.27
481.12	1178	2.3325	28.3
561.12	1374	2.3083	28.61

Refer to the plot in Figure 18(b).

APPENDIX B

ANGLE OF REPOSE (FUNNEL TEST)

Table 23 Sample of Test Data for 100% Coarse and 100% Fine Sand with Porous Stone Base

	BASE:	Porous stone						
	#16: 100%	Fines: 0%						
No.Test	**i**	**ii**	**iii**	**iv**	**D**	**(D-d)/2**	**2H/(D-d)**	**ϕ**
1	3.565	3.612	3.757	3.65	3.646	1.716	0.874	41.158
	42.75	44.5	42.5	42.25	43.000			
2	3.275	3.3	3.3	3.375	3.313	1.549	0.968	44.075
	42.75	42	42.75	42	42.375			
3	3.524	3.34	3.359	3.59	3.453	1.620	0.926	42.804
	41.75	42.3	41.9	41.5	41.863			
4	3.59	3.59	3.665	3.475	3.580	1.683	0.891	41.710
	42.3	41.5	40.65	42.8	41.813			
5	3.675	3.5	3.655	3.786	3.654	1.720	0.872	41.091
	41.2	41.5	41.5	42.45	41.663			
			Ave:	(visual)	42.181		(calculated)	42.167
	#16: 0%	Fines: 100%						
No.Test	**i**	**ii**	**iii**	**iv**	**D**	**(D-d)/2**	**2(H-h)/(D-d)**	**ϕ**
1	3.96	3.96	3.985	4.04	3.986	1.886	0.758	37.168
	38.5	37	37	37.5	37.500		(h=0.08)	
2	3.969	3.99	3.95	3.996	3.976	1.881	0.755	37.048
	38.15	37.65	38	37.75	37.888		(h=0.08)	
3	3.65	3.65	3.75	3.75	3.700	1.743	0.775	37.759
	37	36.75	36.4	37.3	36.863		(h=0.15)	
4	3.76	3.75	3.76	3.814	3.771	1.779	0.759	37.201
	36.5	37.2	36.5	36.75	36.733		(h=0.15)	
5	3.975	3.963	4.075	4.05	4.016	1.901	0.747	36.761
	36.8	37.05	36.75	35.5	36.525		(h=0.08)	
			Ave:	(visual)	37.2326		(calculated)	37.187

APPENDIX C

DIRECT SHEAR TESTS

Table 24 Sample of Direct Shear Test Data

Direct Shear Test

FINE Sand Passing #150 and Coarse Retained #16 Sample wt(g): 83.00
speed in/r 0.052 (1.32588mm/min) Sample Thickn 0.68
Proving R #356 Diameter(in) 2.5
Top Plate 833.3 g (= 1.8374 lbs.) Area(sq in) A: 4.91
Shear τ (psi): T/A

1psi = 6.8943 kPa
1psi = 0.0703 kg/sq.cm.

(1) Fine Sand = 23.5 % Act. mix is 20% Fines
Coarse Sand = 76.5 %
Date: Oct. 23, 2002 N=(833+5618.81)g
N (lbs): 14.23 σ_{max}(3.06

Time	Vertical $1x10^{-3}$in	H.dial reading	HDeform in	Correc area A	Load dial	S.Force T (lbs)	Shear τ(psi)
00:00	0	0	0.000	4.909	0	0.000	0.000
00:15	0	15	0.015	4.871	50	7.250	1.488
00:30	2	31	0.031	4.831	63	9.135	1.891
00:45	4.5	47	0.047	4.791	71	10.295	2.149
01:00	5.5	60	0.060	4.759	80	11.600	2.438
01:15	7	73	0.073	4.726	83	12.035	2.546
01:30	6.5	83	0.083	4.701	83	12.035	2.560
01:45	6	92	0.092	4.679	85	12.325	2.634
02:00	6	102	0.102	4.654	88	12.760	2.742
02:15	6	112	0.112	4.629	87	12.615	2.725
02:30	7	132	0.132	4.579	86	12.470	2.723
02:45	8	146	0.146	4.544	84	12.180	2.680
03:00	9	165	0.165	4.497	84.5	12.253	2.725
03:15	8	182	0.182	4.454	87.5	12.688	2.848
03:30	7.5	194	0.194	4.424	89	12.905	2.917
03:45	9	212	0.212	4.379	89	12.905	2.947
04:00	7.5	225	0.225	4.347	89	12.905	2.969
04:15	8	243	0.243	4.302	89.5	12.978	3.016
04:30	8	255	0.255	4.272	89.5	12.978	3.038
04:45	7	268	0.268	4.240	89	12.905	3.044
05:00	7	283	0.283	4.203	89	12.905	3.071
05:15	6	300	0.300	4.161	89.5	12.978	3.119
05:30	5	314	0.314	4.126	88	12.760	3.093
05:45	4.5	328	0.328	4.091	88.5	12.833	3.137
06:00	4	340	0.340	4.061	91	13.195	3.249
06:15	4	352	0.352	4.032	92	13.340	3.309
06:30	2	366	0.366	3.997	91	13.195	3.301
06:45	1	382	0.382	3.957	91	13.195	3.334
07:00	0	397	0.397	3.920	91	13.195	3.366
07:15	1	412	0.412	3.883	91.5	13.268	3.416
07:30	2	427	0.427	3.846	92	13.340	3.468
07:45	1	442	0.442	3.810	91	13.195	3.464
08:00	1	458	0.458	3.770	91.5	13.268	3.519
08:15	0.5	473	0.473	3.733	91	13.195	3.534
08:30	1	490	0.490	3.692	91	13.195	3.574
08:45	1	505	0.505	3.655	91	13.195	3.610
09:00	0	520	0.520	3.618	91	13.195	3.647
09:15	-1.5	538	0.538	3.574	97	14.065	3.935
09:30	-1.5	555	0.555	3.533	98	14.210	4.022
09:45	-2	572	0.572	3.491	93	13.485	3.862
10:00	-2	583	0.583	3.465	85	12.325	3.557

(2) Fine Sand = 31.6 % Act.:33.3%
Coarse Sand = 68.4 %
Date: Oct. 24, 2002 N=(833+5618.81)g
N (lbs): 14.23 σ_{max}(p: 3.13

Time	Vertical $1x10^{-3}$in	H.dial reading	HDefo in	Correct area A	Load dial	S.Force T (lbs)	Shear τ(psi)
00:00	0	0	0	4.9087	0	0.000	0.000
00:15	0	12	0.012	4.8787	48	6.960	1.427
00:30	3	27	0.027	4.8412	66	9.570	1.977
00:45	1	45	0.045	4.7962	63.5	9.208	1.920
01:00	5	54	0.054	4.7737	69	10.005	2.096
01:15	8	63	0.063	4.7513	74	10.730	2.258
01:30	9.5	79	0.079	4.7113	78.5	11.383	2.416
01:45	10	92	0.092	4.6788	79	11.455	2.448
02:00	9	109	0.109	4.6363	79	11.455	2.471
02:15	10	135	0.135	4.5714	87	12.615	2.760
02:30	11	143	0.143	4.5514	87.5	12.688	2.788
02:45	11	157	0.157	4.5165	87	12.615	2.793
03:00	11	172	0.172	4.4791	87	12.615	2.816
03:15	9.5	186	0.186	4.4442	87	12.615	2.839
03:30	9	200	0.2	4.4093	87	12.615	2.861
03:45	8	216	0.216	4.3694	87	12.615	2.887
04:00	7	233	0.233	4.3271	87	12.615	2.915
04:15	6	247	0.247	4.2922	86	12.470	2.905
04:30	5	262	0.262	4.2549	86	12.470	2.931
04:45	5	277	0.277	4.2177	87	12.615	2.991
05:00	4	290	0.29	4.1854	87	12.615	3.014
05:15	3	305	0.305	4.1481	88	12.760	3.076
05:30	2	319	0.319	4.1134	89.5	12.978	3.155
05:45	0.5	331	0.331	4.0837	92	13.340	3.267
06:00	-2	347	0.347	4.044	90.5	13.123	3.245
06:15	-3	364	0.364	4.002	90.5	13.123	3.279
06:30	-4	377	0.377	3.9698	89.5	12.978	3.269
06:45	-3.5	390	0.39	3.9377	91.5	13.268	3.369
07:00	-4.5	406	0.406	3.8982	92	13.340	3.422
07:15	-6	422	0.422	3.8588	92	13.340	3.457
07:30	-7	437	0.437	3.8218	91.5	13.268	3.472
07:45	-9	455	0.455	3.7775	87	12.615	3.339
08:00	-11	474	0.474	3.7309	94	13.630	3.653
08:15	-12	488	0.488	3.6965	96	13.920	3.766
08:30	-13	503	0.503	3.6598	94	13.630	3.724
08:45	-13	516	0.516	3.628	95	13.775	3.797
09:00	-17	533	0.533	3.5864	95.5	13.848	3.861
09:15	-18	547	0.547	3.5522	94	13.630	3.837
09:30	-19	560	0.56	3.5205	92	13.340	3.789
09:45	-20	572	0.572	3.4913	90	13.050	3.738
10:00	-20	586	0.586	3.4573	94.5	13.703	3.963

(3) Fine Sand = 46.8 % Act.:44.4%
Coarse Sand= 53.2 %
Date: Oct. 24, 2002 N=(833+5618.81)g
N (lbs): 14.23 σ_{max}(p 3.58

Time	Vertical $1x10^{-3}$in	H.dial reading	HDefo in	Correc area A	Load dial	S.Force T (lbs)	Shear τ(psi)
00:00	0	0	0	4.909	0	0.000	0.000
00:15	0	14	0.014	4.874	38	5.510	1.131
00:30	0	30	0.03	4.834	53	7.685	1.590
00:45	0	45	0.045	4.796	60	8.700	1.814
01:00	0	60	0.06	4.759	59	8.555	1.798
01:15	0	77	0.077	4.716	61	8.845	1.875
01:30	0	93	0.093	4.676	66	9.570	2.046
01:45	0	109	0.109	4.636	68	9.860	2.127
02:00	-1	125	0.125	4.596	69	10.005	2.177
02:15	-1	137	0.137	4.566	69	10.005	2.191
02:30	-1	150	0.15	4.534	70	10.150	2.239
02:45	-2	165	0.165	4.497	70	10.150	2.257
03:00	-3.5	182	0.182	4.454	73.5	10.658	2.393
03:15	-4.5	196	0.196	4.419	72	10.440	2.362
03:30	-6.5	209	0.209	4.387	71	10.295	2.347
03:45	-8	222	0.222	4.354	69	10.005	2.298
04:00	-9	235	0.235	4.322	75	10.875	2.516
04:15	-10	250	0.25	4.285	75	10.875	2.538
04:30	-12	265	0.265	4.247	75	10.875	2.560
04:45	-13	278	0.278	4.215	75	10.875	2.580
05:00	-14	294	0.294	4.175	76.5	11.093	2.657
05:15	-15	307	0.307	4.143	77	11.165	2.695
05:30	-16	326	0.326	4.096	78	11.310	2.761
05:45	-17	340	0.34	4.061	78	11.310	2.785
06:00	-18	359	0.359	4.014	78.5	11.383	2.835
06:15	-18.5	375	0.375	3.975	81	11.745	2.955
06:30	-20	390	0.39	3.938	79.5	11.528	2.927
06:45	-21	404	0.404	3.903	79.5	11.528	2.953
07:00	-14	420	0.42	3.864	79	11.455	2.965
07:15	-16	437	0.437	3.822	82	11.890	3.111
07:30	-18	450	0.45	3.79	80.5	11.673	3.080
07:45	-19	465	0.465	3.753	56	8.120	2.164
08:00			0			0.000	
08:15			0			0.000	
08:30			0			0.000	
08:45			0			0.000	
09:00			0			0.000	
09:15			0			0.000	
09:30			0			0.000	
09:45			0			0.000	
10:00			0			0.000	

APPENDIX D

CALCULATION OF ANGLE OF FRICTION

Table 25 Sample Calculation of Interface Friction (Basal friction)

$$\tan \phi_i = \frac{\tan \beta \cos^2 \phi_m}{1 + \sin^2 \phi_m + 2\sqrt{1 - \left(\frac{\cos \phi_m}{\cos \beta}\right)^2}}$$

$Ø_m$ is always larger or equal to β

And when $Ø_m = \beta$, we have:

$$\tan \phi_i = \frac{\sin 2\phi_m}{2(1 + \sin^2 \phi_m)}$$

FOR POROUS STONE

Percentage Fines	(1) $Ø_m$	(2) β	(3) tan β	(4) cos $Ø_m$	(5) $\cos^2 Ø_m$	(6) sin $Ø_m$	(7) $\sin^2 Ø_m$	(8) cos β	(9) (E4)/(I8)	(10) $2[1-(J9)^2]^{0.5}$	(11) 1+(H7)+(K10)	(12) $\tan \beta.\cos^2 Ø_m$	(13) (M12)/(L11)	(14) Calculated $Ø_i=\tan^{-1}$(N13)	(15) Lab Results Øi
0	42.50	42.2	0.907	0.737	0.544	0.676	0.456	0.741	0.9952	0.195	1.651	0.493	0.298	16.6	29.55
15	41.30	40.8	0.863	0.751	0.564	0.660	0.436	0.757	0.9924	0.246	1.681	0.487	0.290	16.2	29.45
25	40.40	39.8	0.833	0.762	0.580	0.648	0.420	0.768	0.9912	0.264	1.684	0.483	0.287	16.0	28.95
35	39.80	39.7	0.830	0.768	0.590	0.640	0.410	0.769	0.9985	0.108	1.517	0.490	0.323	17.9	27.70
50	38.50	38.5	0.795	0.783	0.612	0.623	0.388	0.783	1.0000	0.000	1.388	0.487	0.351	19.3	25.35
65	38.05	38.1	0.783	0.787	0.620	0.616	0.380	0.787	1.0000	0.000	1.380	0.485	0.352	19.4	24.30
75	37.65	37.7	0.771	0.792	0.627	0.611	0.373	0.792	1.0000	0.000	1.373	0.484	0.352	19.4	22.00
85	37.50	37.5	0.767	0.793	0.629	0.609	0.371	0.793	1.0000	0.000	1.371	0.483	0.352	19.4	21.75
100	37.20	37.2	0.759	0.797	0.634	0.605	0.366	0.797	1.0000	0.000	1.366	0.482	0.353	19.4	21.65

FOR GLASS

Percentage Fines	(1) $Ø_m$	(2) β	(3) tan β	(4) cos $Ø_m$	(5) $\cos^2 Ø_m$	(6) sin $Ø_m$	(7) $\sin^2 Ø_m$	(8) cos β	(9) (E4)/(I8)	(10) $2[1-(J9)^2]^{0.5}$	(11) 1+(H7)+(K10)	(12) $\tan \beta.\cos^2 Ø_m$	(13) (M12)/(L11)	(14) Calculated $Ø_i=\tan^{-1}$(N13)	(15) Lab Results Øi
0	42.50	33.56	0.663	0.737	0.544	0.676	0.456	0.833	0.885	0.932	2.388	0.361	0.151	8.6	7.9
10	41.60	33.40	0.659	0.748	0.559	0.664	0.441	0.835	0.896	0.889	2.330	0.369	0.158	9.0	10.1
20	40.80	35.10	0.703	0.757	0.573	0.653	0.427	0.818	0.925	0.759	2.186	0.403	0.184	10.4	11.6
30	40.00	34.90	0.698	0.766	0.587	0.643	0.413	0.820	0.934	0.714	2.127	0.409	0.192	10.9	12.2
40	39.50	36.67	0.744	0.772	0.595	0.636	0.405	0.802	0.962	0.546	1.951	0.443	0.227	12.8	12.4
50	38.50	36.93	0.752	0.783	0.612	0.623	0.388	0.799	0.979	0.408	1.796	0.460	0.256	14.4	15.7
60	37.80	37.50	0.767	0.790	0.624	0.613	0.376	0.793	0.996	0.179	1.555	0.479	0.308	17.1	17.2
70	37.70	37.70	0.773	0.791	0.626	0.612	0.374	0.791	1.000	0.000	1.374	0.484	0.352	19.4	15.1
80	37.60	37.60	0.770	0.792	0.628	0.610	0.372	0.792	1.000	0.000	1.372	0.483	0.352	19.4	18.3
90	37.40	37.40	0.765	0.794	0.631	0.607	0.369	0.794	1.000	0.000	1.369	0.483	0.352	19.4	19.2
100	37.10	37.10	0.756	0.798	0.636	0.603	0.364	0.798	1.000	0.000	1.364	0.481	0.353	19.4	20.3

APPENDIX E

HYDRAULIC CONDUCTIVITY TEST

Table 26 Sample of Test Data for Gravel Crushed at 18.24 MPa

ANGULAR gravels:P= 12900 LBS

Date: 2-Jan-04 18:40 pm

A = $\pi D^2/4$ = 31.44161 sq.cm. = 4.873459 sq.in.
D = 2.491 in = 6.32714 cm.

Compression Load :	12900 lbs	=	5843.7 kg
Piston Load:	2035.52 g	=	2.04 kg
Maximum Crushing Load P			5845.74 kg
Stress (P/A)			1859235 kg/sq.m.
			18239100 N/sq.m.
			18.24 MPa

CRUSHING LOAD =	12900 lbs	
STRESS =	2647.0 psi	
=	18.24 MPa	

Sieve no.	wt. of sieve (g)	sieve+Agrave (g)	AngularGrave (g)	% retain	% pass 100	sieve opening 6.350	r/rL 1	FractionPass $M(R<r)/M_T$	Mean sieve size, D_i mm	Retained Mass, M_i	M_i/D_i
4	536.63	784.03	247.40	43.13	56.87	4.750	0.7480	0.5687	5.550	43.13	7.77
10	451.53	630.96	179.43	31.28	25.60	2.000	0.3150	0.2560	3.375	31.28	9.27
20	407.90	472.11	64.21	11.19	14.41	0.833	0.1312	0.1441	1.417	11.19	7.90
40	365.72	388.55	22.83	3.98	10.43	0.420	0.0661	0.1043	0.627	3.98	6.35
60	324.17	334.30	10.13	1.77	8.66	0.246	0.0387	0.0866	0.333	1.77	5.30
100	355.86	365.56	9.70	1.69	6.97	0.150	0.0236	0.0697	0.198	1.69	8.54
140	304.03	311.84	7.81	1.36	5.61	0.106	0.0167	0.0561	0.128	1.36	10.64
200	299.87	312.24	12.37	2.16	3.45	0.075	0.0118	0.0345	0.091	2.16	23.83
pan	374.80	394.60	19.80	3.45	0.00					96.55	79.60
			573.68	100.00							

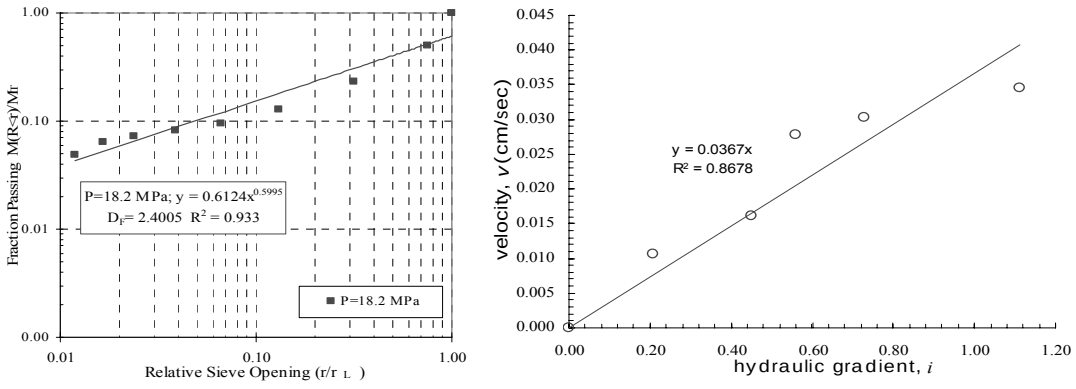

Figure 70 Fractal Fragmentation and Hydraulic Conductivity Plots

Calculation for the hydraulic conductivity:

$D_m=\Sigma Mi/\Sigma(M_i/D_i)$

D_m = 1.212993 mm 0.001213 m

take; C_s = 700 (round- 360;angular-700)

λ/θ = 1.02854 sq. mm/s at 20ºC 1.03E-06 sq. m/s

$e^3/(1+e)$= 0.064185

Therefore, k = 1.801465 /C_s m/s Equation 58.2

180.1465 /C_s cm/s ;Fundamentals of Geotechnical Analysis (ISDunn, LRAnderson, FW Kiefer, 1980)

0.2574 cm/s $k = \frac{2g}{C_s} D_m^2 \frac{\rho}{\mu} \frac{e^3}{1+e}$

D_{10} = 0.40 mm

Therefore, k = 100(D_{10})^2 Hazen

16.00 cm/s

k = 0.0576 cm/s Lab

$\gamma_d = \frac{W_s}{V} = \frac{G\gamma_w}{1+e}$ *and*

$e = \frac{G\gamma_w V}{W_s} - 1$

S.Gstones	G	2.67		
dry wt	W_s	572.65	g	
ht of stone		9.90	cm	
tube dia		6.33	cm	
x-sec area		31.442	sq.cm	
volume	V	311.27	cc	0.010992 cu.ft.
dry density	$\gamma_d=W_s/V$	1.840	g/cc	(dry unit weight)

void e	0.4535
$e^3/(1+e)$ =	0.064185

Using equation (8.3)

$$k_{V\,(equivalent)} = \frac{h}{\left(\frac{h_1}{k_{V_1}}\right)+\left(\frac{h_2}{k_{V_2}}\right)+\left(\frac{h_3}{k_{V_3}}\right)}$$

The hydraulic conductivity of the specimen k_s is obtained as 0.0576cm/s

BIBLIOGRAPHY

1. Marachi, N. D., Chan, C. K., Seed, H. B., and Duncan, J. M., Strength and Deformation Characteristics of Rockfill Materials, Report No. TE-69-5 (University of California Berkeley, Sept., 1969, 139 pp).

2. Terzaghi, K., "Discussion on Salt Springs and Lower Bear River Dams," Trans. ASCE, Vol.125 pt.2 (1960), pp. 139-148.

3. Clements, R.P., "The Deformation of Rockfill: Interparticle Behaviour, Bulk Properties and Behaviour in Dams" (unpublished Ph.D. Dissertation, Faculty of Engineering, King's College, London University, 1981).

4. Feda, J., "Notes on The Effect of Grain Crushing on the Granular Soil Behaviour," Engineering Geology, Vol. 63,(2002), pp. 93-98.

5. Transactions of The 12th International Congress on Large Dams, Volume 1, Mexico City, 1976, " Mechanical Properties of Rockfill-Soil Mixtures by Marsal, R.J., and Fuentes dela Rosa A," (Mexico City, 1976) pp. 179-209.

6. Marsal, R. J., ed., Raul J. Marsal Volume, "Rockfill for Embankment Dam by A. D. Penman" (Mexico: Sociedad Mexicana de Mecanica de Suelos, A. C., 1992), pp. 303-327.

7. Murff, J. D., "Pile Capacity in Calcareous Sands: State of The Art," Journal of Geotechnical Engineering, Vol. 113, No. 5 (May, 1987), pp. 490-507.

8. Vallejo, L. E., and Mawby, R., "Porosity Influence on The Shear Strength of Granular Material-Clay Mixtures," Engineering Geology, Vol. 58, (2000), pp. 125-136.

9. Hardin, B. O., "Crushing of Soil Particles," Journal of Geotechnical Engineering, Vol. 111, No. 10 (October, 1985), pp.1177-1192.

10. Vallejo, L. E., and Y. Zhou, "The Relationship Between The Fractal Dimension and Krumbien's Roundness Number," Soils and Foundations; (JSSMFE), Vol. 35, No. 1 (1995b), pp. 163-167.

11. Lade, P. V., Yamamuro, J. A., and Bopp, P. A., "Significance of Particle Crushing in Granular Materials," Journal of Geotechnical Engineering;(ASCE), Vol.122, No. 4 (April 1996) pp. 309-316.

12. Lee, K. L. and Farhoomand, J., "Compressibility and Crushing of Granular Soil in Anisotropic Triaxial Compresssion," Canadian Geotechnical Journal, Vol. 4, No. 1 (1967), pp. 68-86.

13. Proceedings of 15th International Conference on Soil Mechanics and Geotechnical Engineering, Istanbul, Turkey, 2001, "Model of Grain Crushing and Debonding, by Bohac, J., Feda, J. and Kuthan, B." (Istanbul: Turkish Society of Civil Engineers, 2001), Vol. 1, pp. 43-46.

14. Ramamurthy, T., "Crushing Phenomena in Granular Soils," The Journal of The Indian National Society of Soil Mechanics and Foundation Engineering, Vol. 8, No.1 (1968), pp. 67-86.

15. Oda, M., and Konishi, J., "Microscopic deformation mechanisms of granular material in simple shear," Soils and Foundations, Vol. 14, No.4 (1974), pp. 25-38.

16. Radjai, F, "Dynamique des Rotations et Frottement Collectif dans les Systemes Granulaires" (Ph.D. Thesis, Universite de Paris-Sud XI, Orsay, 1995).

17. William J. Walker Jr., "Persistance of Granular Structure During Die Compaction of Ceramic Product," Materials Research Society Proceedings, Vol. 627, (2000), pp. BB6.4.1-6.4.6.

18. Cundall, P.A., and Strack, O.D.L., "A discrete numerical model for granular assemblies," Geotechnique, Vol. 29, No. 1, (1979). pp. 47-65.

19. Proceedings of the International. Worshop on Soil Crushability, Yamaguchi, Japan, 1999, "The role of micro-mechanics in soil mechanics by Bolton, M.R.", (Yamaguchi: Japan, 1999), pp. 58-82.

20. Sowers, G., B., and Sowers, G., F, Introductory Soil Mechanics and Foundations (New York : The Macmillan Company, 1967), p. 326.

21. Cedergren, H. R., "America's Pavements: World's Longest Bathtubs," Civil Engineering , Vol. 64, No. 9 (1994), pp. 56-58.

22. Vallejo, L. E., "Fractal Assessment of The Surface Texture of Pavements," International Journal of Pavement Enginering, Vol. 2, No. 2,(2001), pp. 149-156.

23. Tyler, S. W. and Wheatcraft, S. W., "Fractal Scaling of Soil Particle-Size Distribution Analysis and Limitations," Soil Science Society of America Journal, Vol. 56, No. 2 (1992), pp. 47-67.

24. Saeed, A., Hall, J. W., and Barker, W., Performance Related Tests of Aggregates for Use in Unbound Pavement Layers (NCHRP Report 453, Transportation Research Board-National Research Council, National Academy Press, 2001)

25. Acad. Royale Sci., Paris, 1776,"Essai Sur Une Application des R'egles de Maximis et Minimis A Quelques Problemes de Statitique Relatifs A L'architecture by C. A. Coulomb," (Paris: Mem. Math. Phys.,1776), Vol. 7, pp.343-382.

26. Dunn, I. S., Anderson L. R., and Kiefer, F. W., Fundamentals of Geotechnical Analysis (New York: John Wiley and Sons 1980), pp. 164-165.

27. Costa, J. E. and Baker V. R., Surfacial Geology: Building with The Earth (Herndon, VA: John Wiley and Sons 1981), pp. 124-125.

28. Dunn, op. cit., p.168.

29. Rowe P. W., "The Stress-Dilatency Relation for Static Equilibrium on An Assembly of Particles in Contact," Pro. Roy. Soc., A269 ,(1962), pp. 500-527.

30. Annual Book of ASTM Standards, C1444-00, Standard Test Method for Measuring the Angle of Repose of Free-Flowing Mold Powders, Vol. 15.01, pp.694-695.

31. Aguirre, M., A., Calvo, A., and Ippolito, I., "Avalanche Dynamics: Influence of the Granular Packing Size,"Materials Research Society Symposium Proceedings, Vol. 627, (2000), pp. BB2.3.1-2.3.5

32. Marsal, R. J., "Large Scale of Testing of Rockfill Materials," Journal of The Soil Machanics and Foundations Division, ASCE, Vol.93 No.SM2 (1967), pp. 27-43.

33. Hyslip, J.P., and Vallejo, L. E., "Fractal Analysis of The Roughness and Size Distribution of Granular Materials," Engineering Geology, Vol. 48,(1997), pp. 231-244.

34. Brown, S. F., "Soil Mechanics in Pavement Engineering," (The Rankine Lecture - BGS) Geotechnique, Vol. 46, No. 3 (1996), pp. 383-426.

35. Loboguerrero, Sebastian, "The Elastic Moduli of Soils with Dispersed Oversize particles" (unpublished M.S. Thesis, Department of Civil and Environmental Engineering, School of Engineering, University of Pittsburgh, 2002).

36. Braja, M. D., Advanced Soil Mechanics, Tylor and Francis Publishing Company Ltd., Washington D.C., 1997, pp. 153-160.

37. Milan Vukovic and Andjelko Soro, Dertermination of Hydraulic Conductivity of Porous Media From Grain Size Composition, Water Resources Publications, Colorado, 1992.

38. Mandelbrot, B. B., "How Long is The Coast of Britain? Statistical Self-Similarity and Fractional Dimension," Science, Vol. 155 (1967), pp. 636-638.

39. Haussdorff, F., "Dimension und äußeres Mass," Mathematische Annalen, Vol. 79 (1919), pp. 157-179.

40. Turcotte, D. L., Fractals and Chaos in Geology and Geo-physics, (New York: Cambridge University Press, 1992), pp. 28-52.

41. Turcotte, D. L., "Fractals and Fragmentation," Journal of Geophysical Research, Vol.91 (1986), pp. 1921-1926.

42. Korvin, G., Fractal Models in the Earth Sciences, (Amsterdam: Elsevier Science Publishers, 1992), p. 220.

43. Ibid., pp. 191-226.

44. Fredlund, M.D., Fredlund, D.G. and Wilson, G. W., "An Equation to Represent Grain-size Distribution," Canadian Geotechnical Journal, Vol. 37,(2000), pp. 817-827.

45. Gardner, W.R., " Representation of Soil Aggregate Size Distribution by A Logarithmic-normal Distribution," Soil Science Society of America Proceedings, Vol. 20 (1956), pp. 151-153.

46. Prasher, C.L., Crushing and Grinding Process Handbook, (New York: John Wiley and Sons 1987), pp. 88-89.

47. Gutenberg, B. and Richter, C.F., Seismicity of the Earth and Associated Phenomenon, (Princeton: Princeton University Press, 1954).

48. Turcotte, Op. Cit., pp. 2-3.

49. Prasher, Op. Cit., pp. 87-88.

50. Turcotte, Op. Cit., pp. 40-41.

51. Korvin, Op. Cit., p. 212.

52. Kaye B. H., A Random Walk Through Fractal Dimensions, VCH, Weinheim, Federal Republik of Germany, 1994, p. 57.

53. Bishop, A. W., Green, G. E., Garga, V. K., Andresen, A., and Brown, J. D., "A New Ring Shear Apparatus and Its Application to the Measurement of Residual Strength," Geotechnique, Vol. 21, No. (1972), pp. 273-328.

54. Cheng Liu and Evert, J., B., Soils and Foundations, Prentice-Hall Incorporation, New Jersey, 1987.

55. Vallejo, L. E., "Interpretation of The Limits in Shear Strength in Binary Granular Mixtures," Canadian Geotechnical Journal, Vol. 38,(2001), pp. 1097-1104.

56. Saeed, Op. Cit., p. 6.

57. Pintner, R.M., Vinson, T.S. and Johnson, E.G., "Nature of Fines Produced in Aggregate Processing," Journal of Cold Regions Engineering, Vol. 1, No. 1 (1987), pp. 10-19.

58. Pintner, R.M., Vinson, T.S. and Johnson, E.G., "Quantity of Fines Produced During Crushing, Handling and Placement of Roadway Aggregates," Geotechnical Testing Journal, GTJODJ, Vol. 10, No. 4 (1987), pp. 165-172.

59. Mendelbrot, B. B., The Fractal Geometry of Nature, (San Francisco:Freeman, 1983) p 424.

60. Yoder, E.J. and Witczak, M. W., Principles of Pavement Design, John Wiley and Sons, New York, 1975.

61. Prasher, Op. Cit., pp. 24-29

62. Braja(1997), Op. Cit., pp. 399-402.

63. Lambe, T., W., Soil Testing for Engineers, John Wiley and Sons, New York, 1951.

64. Ibid., p 30.

65. Lewis, K. H. and Rojas-Gonzales, L. F, Soil Testing Manual (Pittsburgh Pa.: University of Pittsburgh, August, 1995).

66. Dunn, op. cit., pp.58-62.